

AD No. _____
DDC FILE COPY

AD610525

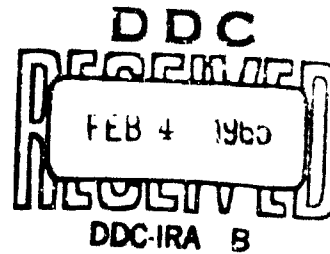
AD

USATRECOM TECHNICAL REPORT 64-70

THE COANDA EFFECT AT DEFLECTION SURFACES
WIDELY SEPARATED FROM THE JET NOZZLE

BY
S. D. BENNER

DECEMBER 1964



U. S. ARMY TRANSPORTATION RESEARCH COMMAND
FORT EUSTIS, VIRGINIA

CONTRACT DA 44-177-AMC-11(T)
UNIVERSITY OF TORONTO



COPY	2	OF	2	R
HARD COPY	\$. 3.00			
MICROFICHE	\$. 0.75			

91F

ARCHIVE COPY

**Best
Available
Copy**

DDC Availability Notice

Qualified requesters may obtain copies of this report from DDC.

This report has been furnished to the Department of Commerce for sale to the general public.

* * *

Reproduction Limitations

Reproduction of this document in whole or in part is prohibited except with permission of the Commanding Officer, USATRECOM. However, DDC is authorized to reproduce the document for United States Government purposes.

* * *

Disclaimer

The findings in this report are not to be construed as an official Department of the Army position, unless so designated by other authorized documents.

When Government drawings, specifications, or other data are used for any purpose other than in connection with a definitely related Government procurement operation, the United States Government thereby incurs no responsibility nor any obligation whatsoever; and the fact that the Government may have formulated, furnished, or in any way supplied the said drawings, specifications, or other data is not to be regarded by implication or otherwise as in any manner licensing the holder or any other person or corporation, or conveying any rights or permission, to manufacture, use, or sell any patented invention that may in any way be related thereto.

* * *

Disposition Instructions

Destroy this report when it is no longer needed. Do not return it to the originator.

HEADQUARTERS
U S ARMY TRANSPORTATION RESEARCH COMMAND
FORT EUSTIS VIRGINIA 23604

In this report, the University of Toronto, Institute for Aerospace Studies, investigated the Coanda effect in the deflection of two-dimensional jet sheets with turning surfaces located at large horizontal and vertical distances from the nozzle.

The results are used to define permissible gap sizes for practical applications of detached deflection surfaces.

This command considers the conclusions made by the contractor to be valid.

Task 1D121401A14203
Contract DA 44-177-AMC-11(T)
USATRFCOM Technical Report 64-70
December 1964

THE COANDA EFFECT AT DEFLECTION SURFACES
WIDELY SEPARATED FROM THE JET NOZZLE

UTIAS Tech. Note No. 78

Prepared by

INSTITUTE FOR AEROSPACE STUDIES
UNIVERSITY OF TORONTO
TORONTO, CANADA

for

U. S. ARMY TRANSPORTATION RESEARCH COMMAND
FORT EUSTIS, VIRGINIA

ABSTRACT

The flow phenomenon in both liquids and gases of the adherence of a jet or jet sheet to a solid surface has been named the Coanda Effect. This report discusses an experimental investigation, which has again shown that the Coanda Effect is not limited to attached deflection surfaces or to inclined single or multiple flat-plate surfaces. The horizontally ejected subsonic and overchoked jet sheets successfully bridged horizontal and vertical gaps of 32 and 10 times the nominal jet sheet thickness ($t = 1/16$ inch) respectively; for $t = 1/4$ inch, the corresponding ratios were eight and two. The vertical gap was increased until the flow detached from the deflection surface. Vertical and horizontal forces acting on three different deflection surfaces were measured with a strain gauge balance. The configurations were tested at nominal pressure ratios of 1.1, 1.2, 1.7, and 2.2, and the surface pressures were recorded.

FOREWORD

The work described in this report was accomplished by the Institute for Aerospace Studies, University of Toronto, Toronto, Canada, for the U. S. Army Transportation Research Command, Fort Eustis, Virginia. This report represents the work performed under Contract DA 44-177-AMC-11(T).

The project was conducted by the University of Toronto's Institute for Aerospace Studies, with Dr. G. K. Korbacher, Associate Professor of Aerospace Engineering Sciences, providing the technical direction. Mr. S. D. Benner, author and chief investigator, was assisted by Messrs. K. Sridhar and P. R. Stephens.

CONTENTS

	<u>Page</u>
ABSTRACT	iii
FOREWORD	v
LIST OF ILLUSTRATIONS	viii
LIST OF SYMBOLS	x
SUMMARY	1
CONCLUSIONS	2
INTRODUCTION	3
SIMPLE JET SHEET FLOW THEORY	4
TEST FACILITIES	6
TEST RIG	7
EXPERIMENTAL PROCEDURE	9
PRESENTATION OF RESULTS	12
DISCUSSION OF RESULTS	14
BIBLIOGRAPHY	75
DISTRIBUTION	76
APPENDIX I - EXACT PRESSURE RATIOS FOR PRESSURE DISTRIBUTIONS, PRESSURE COEFFICIENTS, AND MEASURED FORCES ACTING ON THE DEFLECTION SURFACES AS IN FIGURES 5 TO 33 INCLUSIVE	77
APPENDIX II - COMPARISON OF MEASURED AND INTEGRATED RESULTANT FORCES ACTING ON A DEFLEC- TION SURFACE	78

<u>Figure</u>		<u>Page</u>
26 to 27	Effect of Deflection Surface Radii on the Non-Dimensional Lift Force for Various Horizontal and Vertical Gap Sizes and Nozzle Pressure Ratios.	65 to 68
28 to 33	Contours of Constant Non-Dimensional Lift for Various Horizontal and Vertical Gap Sizes and Nozzle Pressure Ratios.	69 to 74

SYMBOLS

a	vertical distance between lower nozzle lip and leading edge of the deflection surface at their center-lines, positive in downward direction
A_N	nozzle exit area
C_p	pressure coefficient
C_{p_c}	pressure coefficient for compressible flow, thin jet sheet
C_{p_i}	pressure coefficient for incompressible flow, thin jet sheet
C_{p_i}'	pressure coefficient for incompressible flow, thick jet sheet
D	drag force acting on deflection surface, positive in outward direction
F	see "Configuration Notation" under <u>PRESENTATION OF RESULTS</u>
F_c	centrifugal force
F_p	pressure force
F_{r_i}	resultant force acting on the deflection surface and = $\int \Delta P w ds$
F_{r_m}	resultant force acting on the deflection surface and = $\sqrt{L^2 + D^2}$
l	horizontal distance between lower nozzle lip and leading edge of the deflection surface at their center lines, positive in outward direction
L	lift force acting on the deflection surface, positive in the upwards direction
I_f, I_r	vertical force restrained by the front and rear pair respectively of the horizontally mounted steel flexures
dm	mass of element of flow
P_a	atmospheric pressure
P_s	pressure at the bound surface of the jet sheet

P_T	total jet (reservoir) pressure
$\Delta P, dP$	pressure difference across the jet sheet
q_c	compressible dynamic head
q_i	incompressible dynamic head
R	radius of the jet sheet center line
R_o	radius of the Coanda surface (quadrant)
s	distance from leading edge, and measured along the deflection surface
t	nominal jet sheet thickness at nozzle exit
T_H	thrust per unit jet sheet width
V	jet sheet flow velocity
w	width of deflection surface; width of jet sheet at nozzle exit
γ	compressibility correction factor
γ	ratio of specific heats
θ	jet sheet flow turning angle
ρ	jet sheet density
χ	variable number
a/t	non-dimensional vertical gap
l/t	non-dimensional horizontal gap
$L/(P_T A_N)$	non-dimensional lift force
L. E.	leading edge
P_T/P_a	pressure ratio (\equiv P. R.)
s/t	non-dimensional distance along deflection surface
T. E.	trailing edge

SUMMARY

This experimental investigation of the deflection of two-dimensional jet sheets by means of the Coanda Effect by surfaces widely separated from the nozzle in both the horizontal and the vertical direction has again shown that the Coanda Effect is not limited to attached deflection surfaces or to inclined single or multiple flat-plate surfaces. The horizontally ejected subsonic and overchoked jet sheets successfully bridged horizontal and vertical gaps of 32 and 10 times the nominal jet sheet thickness ($t = 1/16$ -inch) respectively; for $t = 1/4$ -inch, the corresponding ratios were eight and two. The vertical gap was increased until the flow detached from the deflection surface. Vertical and horizontal forces acting on three different deflection surfaces, formed by a combination of an initial flat plate ($1/4$ -inch thick) followed by a quadrant of a circular cylinder of 2-, 3-, and 4-inch radius, were measured with a strain gauge balance. The configurations were tested at nominal pressure ratios of 1.1, 1.2, 1.7, and 2.2, and the surface pressures were recorded.

CONCLUSIONS

The conclusions which the presented experimental evidence suggests on the turning of two-dimensional subsonic and overchoked jet sheets by means of detached Coanda surfaces are as follows:

- (1) The Coanda Effect was found to function even when the deflection surface was widely separated from the nozzle.
- (2) The thicker the jet sheet at a given horizontal gap, the smaller the possible vertical gaps which the jet sheet can bridge.
- (3) The thicker the jet sheet at a given vertical gap, the larger the possible horizontal gaps which the jet sheet can bridge.
- (4) The larger the radius of the deflection surface, the larger the possible gaps.
- (5) To maintain a specific lift of a jet sheet on a deflection surface, any changes in horizontal gap size must be accompanied by related changes in vertical gap size.
- (6) For a given low-pressure ratio jet sheet, the maximum lift force occurs at rather small horizontal ($l \approx 1/4$ -inch) and vertical ($a \approx 1/8$ -inch) gaps. With increasing pressure ratio, the jet sheet can bridge larger gap distances, and the size of the vertical gap increases faster than the horizontal gap for maximum lift.

The ultimate vertical gap sizes depend on the entrainment properties of the jet sheet underside in the wedge between the jet sheet and the Coanda surface just before the jet sheet attaches itself to the surface. If the suction pressure, ΔP , at this point becomes equal to $-2(t/R)(\rho/2)V^2$, then the jet sheet will become attached and will follow the Coanda surface. Otherwise, it will not attach itself.

INTRODUCTION

The flow phenomenon in both liquids and gases of the adherence of a jet or jet sheet to a solid surface has been named the Coanda Effect. N. H. Coanda, a Roumanian inventor, discovered that when air was ejected from a rectangular nozzle, it would attach to an inclined flat plate which is connected to the nozzle exit with no gap. He deduced that the attachment was produced by a decrease in surface pressure in the separation bubble which he observed to form just downstream of the nozzle exit. Emphasizing the requirement of a sharp angle between the nozzle and the flat plate, Coanda applied this principle to a series of deflecting surfaces, each at a sharp angle with the preceding one, and succeeded in turning flows through angles as large as 180° . In this investigation, the continuous curve of the quadrant of a circular cylinder was used as the "Coanda" or deflection surface.

For investigations prior to 1961, the deflection surfaces were attached to the nozzle with no intervening gap. In References 1 and 5, the Coanda surfaces were detached for practical reasons only, and the gap between the deflection surface and nozzle was approximately 1/100-inch. It was large enough to provide flexibility in the use and location of different deflection surfaces without detrimental effects to the flow. Obviously, detached deflection surfaces are preferable for practical applications provided that the permissible gap sizes are large enough not to create mechanical problems.

The present work is a continuation of the initial investigations of detached surfaces by Dr. G. K. Korbacher (Reference 3). The test equipment was basically similar, except that the compressed air, previously piped to one side of the settling chamber, was supplied symmetrically to both sides (see Figure 4). The section of thin wall pipe downstream of the cooler was removed, and two flexible pieces of piping were located just upstream of the settling chamber; the latter was completely freed of the weight and the reaction forces of the fixed piping.

The purpose of this experimental investigation was to determine the effect of vertical and horizontal gap sizes on subsonic and overchoked jet sheets, which are produced by a rectangular convergent nozzle, as a function of the nozzle pressure ratio, the jet sheet thickness, and the radius of a smoothly-curved deflection surface. Vertical and horizontal forces acting on the deflection surfaces were to be measured by means of a strain gauge balance. Also, center-line surface pressure distributions were to be recorded for comparison with pressure coefficients predicted by a simple theory.

SIMPLE JET SHEET FLOW THEORY

The fundamental theory of jet sheet bending, offered in References 3 and 5, is summarized here for convenience. The bending of a jet sheet with one free and one bound surface (Coanda deflected jet sheet) is produced by a pressure difference across it. The pressure at the bound surface, P_s , is less than the pressure at the free surface, P_a , which is assumed to be atmospheric. This pressure difference, ΔP , is the result of a suction pressure along the solid surface, and is due to viscous effects which entrain the air trapped between the surface and the jet sheet into the jet sheet.

Consider an element of flow, dm , in a thin jet sheet of high aspect ratio (defined as w/t) and assume that $t \ll R_0$, that the jet momentum along the sheet is constant, and that the pressure gradient across the jet sheet is negligible (see Figure 2). In addition, the flow is considered to be loss-free and two-dimensional.

The centrifugal force, F_c , and the pressure force, F_p , acting on the flow element are in radial equilibrium, and are given by

$$\rho R d\theta dR \frac{v^2}{R} = R d\theta dP. \quad (1)$$

The pressure difference across the curved jet sheet follows then as

$$\Delta P = (P_s - P_a) = -\rho \frac{t}{R} v^2 = -\frac{2t}{R} \cdot \frac{\rho}{2} v^2. \quad (2)$$

Since the thrust per unit jet sheet width is

$$T_H = \rho t v^2 \quad (3)$$

" ΔP " can also be expressed as

$$\Delta P = -\frac{T_H}{R} \quad (4)$$

Let us now define a pressure coefficient as

$$C_p = \frac{\Delta P}{\frac{\rho}{2} v^2} \quad (5)$$

which, after substitution of equation (2) into equation (5), becomes

$$C_p = -\frac{2t}{R}. \quad (6)$$

This pressure coefficient, for a given jet sheet thickness and Coanda surface radius, is a constant and independent of pressure ratio.

For incompressible flow, the pressure difference across the curved jet sheet can be expressed, using Bernoulli's theorem -

$$\frac{\rho}{2} v^2 = (P_T - P_a), \quad (7)$$

as

$$\Delta P = -\frac{2t}{R} (P_T - P_a) \quad (8)$$

or

$$\frac{\Delta P}{(P_T - P_a)} = -\frac{2t}{R} = C_{pi} \quad (9)$$

For compressible flow, however,

$$\Delta P = -\frac{2t}{R} \cdot \frac{\rho}{2} \cdot v^2 \quad \text{must be used.}$$

Therefore,

$$\frac{\Delta P}{(P_T - P_a)} = -\frac{2t}{R} \cdot \frac{\frac{\rho}{2} \cdot v^2}{(P_T - P_a)} = -\frac{2t}{R} \cdot Y \quad (10)$$

Since, for compressible flow, the dynamic head pressure is given by

$$\frac{\rho}{2} v^2 = \frac{\gamma}{\gamma-1} \left[P_T \left(\frac{P_a}{P_T} \right)^{\frac{1}{\gamma}} - P_a \right] \quad (11)$$

"Y" follows as

$$Y = \frac{\gamma}{\gamma-1} \cdot \frac{\left[\left(\frac{P_T}{P_a} \right)^{\frac{\gamma-1}{\gamma}} - 1 \right]}{(P_T/P_a - 1)} \quad (12)$$

and, therefore,

$$\frac{\Delta P}{(P_T - P_a)} \cdot \frac{1}{Y} = C_{pc} = -\frac{2t}{R} \quad (13)$$

Roderick (Reference 5) has developed an expression for the theoretical pressure coefficient of a thick jet sheet ($t \ll R_0$, but of the same order of magnitude) bending over a curved deflection surface. From his assumptions that the flow is loss-free and two-dimensional, and that the pressure gradient across the jet sheet is not negligible, the following incompressible pressure coefficient has been derived:

$$C_{pi}' = \frac{2t}{R} \left[1 + \frac{t}{2R} \right] = C_{pi} \left[1 + \frac{t}{2R} \right]. \quad (14)$$

These simple expressions are very useful for a physical interpretation and understanding of some of the characteristics of curved jet sheets with a free surface on one side.

TEST FACILITIES

Compressed air was produced by a small gas turbine air bleed engine. The compressor was able to deliver a maximum weight flow of 2.7 pounds per second and to achieve a maximum pressure ratio of 3.7. The engine was supported on a simple box frame and mounted in a small soundproof room. Intake and cooling air for the engine and engine room respectively was obtained through a window open to the outside of the laboratory, and the engine's exhaust gases were ducted outside to a vertically mounted muffler. Additional information about the compressed air system and turbine installation can be found in References 2 and 4. The air pressure and mass flow were remotely controlled at an instrument panel outside of the engine room.

After leaving the engine, the hot compressed air was diffused to an 8-inch diameter pipe, and then passed through a cooler which utilized the main water supply. As the temperature of the bleed air could be as high as 230°C, a large water cooler, which is able to reduce it to approximately 15°C, was used.

Immediately downstream of the cooler, an immersed glass thermometer was located to record the temperature of the compressed air. Next, a gate valve was located, since two other test rigs were supplied from the same compressed air source. Farther downstream was a mass flow orifice measuring section with its two pressure taps connected to a water U-tube manometer. Beyond this, the 8 inch piping was divided into two branches of 6-inch diameter piping. Two pieces of corrugated double-walled flexible piping, each followed by a 6-inch by 8-inch diffuser, completed the air passage from the compressor to the symmetrical inlets of the settling chamber.

TEST RIG

The air entered a 24-inch diameter, horizontally mounted, settling chamber. The chamber had two flat ends; one was solid, the other had an opening into which a bell-mouth collector was fitted (see Figure 2). The purpose of the collector and settling chamber was to provide good flow characteristics to the interchangeable nozzle attached to the downstream end of the collector.

The rectangular convergent nozzles which were used in this experiment were installed by bolting them to the flanged end of the bell mouth or contraction section mounted in the end of the settling chamber. The nominal exit heights of these nozzles were 1/16-inch and 1/4-inch. Since each nozzle was made from four machined-steel sections which were welded together, warping resulted and the exit heights were not uniform across the span of the nozzle. The average exit heights were measured as 0.0674-inch and 0.2560-inch respectively.

The settling chamber was supported by four aircraft cable flexures attached to a steel framework, which is bolted to the concrete floor. These flexures were to permit frictionless fore and aft movement of the settling chamber, which was separated by means of the previously mentioned flexible piping from the rigid piping.

The leading edge of the deflection surface had to be adjusted in such a way as to maintain its relative position with respect to the nozzle lip under all load conditions. A camera was used to record the multitube manometer readings of the pressures along the Coaxia surface. The total head pressure, total air temperature, and mass flow readings were also taken.

Instrumentation

The basic instrumentation consisted of a multitube mercury manometer (fifty 45-inch tubes with individual reservoirs), a total head mercury manometer with a range of 85 inches, a U-tube manometer for mass flow measurement, and a two-component strain gauge balance. Due to the delayed delivery of a multitube water manometer, mercury had to be used as a manometer fluid for all pressure ratios. At a nominal pressure ratio of 1.1 and a jet sheet thickness of 1/16-inch, the surface pressure measurements in inches of mercury were unreliable.

The multitube manometer was connected to the surface pressure taps drilled along the center line of the deflection surface (see Figure 1b). The total head manometer was connected to the parallel section of the bell mouth just upstream of the nozzle attachment flange. The orifice plate was located in the 8-inch piping, upstream of the settling chamber (see Figure 4). The two pressure taps, located in the piping at specified distances from the orifice plate, were connected to a U-tube manometer. The flow temperature was measured just downstream of the water cooler.

An SR-4 strain indicator was used in combination with a multi-deck switch. Hence, it was possible to read all the strain increments with one meter and without too much time delay.

The effects of pressure fluctuations on pressure readings were minimized by photographing the multitube manometer which recorded the pressure distributions along the deflection surfaces. The camera produced 4- by 5-inch plate negatives.

Due to the high noise level of the jet sheet, normal voice communication between the operators was impossible. Carbon throat microphones and soundproof earphones which were connected to an aircraft inter-communication amplifier provided satisfactory voice contact.

Force Balance and Deflection Surfaces

It had been the practice in earlier Coanda Effect investigations, to attach the deflection surface rigidly to the nozzle. In this study the deflection surface was not rigidly attached to the nozzle exit. The two main advantages of detached deflection surfaces are as follows: 1) allowance for greater flexibility in the testing of different surfaces, 2) design of the force balance exclusively for the forces acting on the deflection surfaces and independent of the dead weight of the piping system.

The general layout of the force balance and deflection surface mounting is shown in Figure 3. The deflection surface being tested is attached to the mounting plate by two bolts. Figure 3 also shows that the deflection surface mounting column and its adjustment screws are attached to a base plate. The base plate is connected to the horizontal and vertical force measuring beams by six rigid pin-jointed links.

In the ends of these links are small needle roller bearings which keep friction forces at a minimum. With the assumption that the balance system experiences small rotations only, the vertical links transmit the vertically applied force, and the horizontal links rotate without transmitting any force; conversely for a horizontally applied force. Sidesway of the system is prevented by two wire braces, which do not introduce any constraints in the vertical or horizontal directions.

The curved surfaces tested were circular arcs in shape (quadrants) machined from solid aluminum blocks. A series of static pressure holes, located on the center-line of these surfaces, were provided to measure the surface pressure distribution. Each surface was fitted with Plexiglas side plates (see Figure 1b) to eliminate flow separation and flow entrainment from the side. These side plates were made at least as high as the maximum nozzle exit height used in this investigation. The quadrant could be moved vertically and horizontally with respect to the nozzle to obtain any practical gap size desired.

EXPERIMENTAL PROCEDURE

Test Objective

The purpose of this experimental investigation was to explore the effect of gap size - both vertical and horizontal, between deflection surface and nozzle - on the proficiency of flow turning. The basic test variables were the nozzle pressure ratio, the deflection surface radius, and the jet slot thickness for two-dimensional convergent nozzles.

Balance Calibration

The lift force sensing elements which consisted of four steel flexures mounted horizontally, and joined to the base plate by means of the vertical links, restrained vertical forces acting on the deflection surface (see Figure 3). The fore and aft movement of the deflection surface was restrained by two vertically mounted steel flexures. The horizontal flexures, which have a strain gauge bonded on both the top and bottom surfaces, are mounted in two pairs, and their strain is read as "lift front" and "lift rear". The total lift force acting on the deflection surface is equal to the algebraic sum of the loads restrained by the front and rear pair of flexures. The "drag" strain is measured by means of the strain gauges on each side of the vertically mounted flexures.

This two-component balance was calibrated by applying loads incrementally to the deflection surface mounting plate atop of the supporting pylon. First, a vertical load was applied, and the "lift front", "lift rear", and "drag"-strain readings were recorded. This load was increased slowly to approximately 62 pounds, then removed in a similar manner. The strain readings were recorded during the increasing and decreasing of the applied load to ascertain the amount, if any, of hysteresis in the balance system. The resulting calibrations indicated a negligible amount of stored energy for the range of applied loads. Second, the loading process was repeated for a horizontally applied load. From these measurements, the flexure spring constants were obtained. By applying a pure lift or drag load separately, it was determined that there was negligible interaction between the vertical and horizontal sensing units, at least for small rotations of the base plate.

During the course of the experiment, two strain gauges began to separate from the flexures due to the deterioration of the bonding agent caused by high frequency, vibratory loads on the steel flexures. These faulty gauges were removed, and replaced with new ones. Calibration of the balance was repeated after each gauge installation to verify that the calibration factors were not affected by the removal of the steel flexures from the balance.

At the time of the initial test runs at high pressure ratios, it was discovered that a small portion of the deflected jet sheet was impinging on the plate which supports the deflection surface pylon, and produced an error in the strain reading, especially for the "lift front". For this impingement to

occur, a part of the jet sheet must have experienced a turning angle in excess of 90° . The piece of dexion cross-support which is parallel to the deflection surface (see Figure 1b) is actually well under and behind the trailing edge of the deflection surface so as to avoid interference with the jet sheet. It was used to support a thin sheet of steel which was installed to make sure that under no circumstances could the deflected jet sheet hit the balance platform.

The lower end of this curved piece of steel rested on a thick sheet of plywood which was attached by hinges at its top to the framework supporting the settling chamber; the floor supported the other end of the plywood sheet.

Testing

The tests were conducted in two parts. The first part employed a rectangular convergent nozzle of $t = 1.16$ -inch (8 inches wide), which was operated at nominal nozzle pressure ratios of 1.1, 1.2, 1.7, and 2.2. The horizontal gap, L , between the nozzle and the leading edge of the deflection surface was varied from $L/t = 0$ to $L/t = 32$. The vertical displacement, a , of the deflection surface normal to the jet was varied from $a/t = 0$, - equivalent to proper alignment of the surface leading edge with the lower lip of the nozzle - to flow separation at approximately $a/t = 8$. The deflection surfaces were combinations of a 1/4-inch-thick flat plate, at zero-degree angle of attack, followed by quadrants of $R_o = 2$ -, 3-, and 4-inch radius. Side-plates were installed on the 8-inch-wide deflection surfaces to simulate two-dimensional flow. Horizontal and vertical forces due to the jet acting on the deflection surface were recorded by means of a strain gauge balance. Static pressure distributions on the deflection surface were also recorded, except for a pressure ratio of 1.1, because a multitube water manometer could not be made available in time for the tests.

The second part, similar to the first, was conducted with a convergent nozzle of $t = 1/4$ -inch. The variation of " L/t " was from zero to eight, and that of " a/t " from zero to flow separation, at approximately two. Nominal pressure ratios for these tests were confined to 1.1, 1.2, and 1.7. An attempt to operate at a pressure ratio of 2.2 had to be discontinued due to extremely high noise levels generated by the high velocity air blowing over the sharp edge of the flat surface which precedes the quadrants. No effort was made to determine the magnitude of this aerodynamic noise, as it was considered to be beyond the range of the available measuring equipment. The noise level was estimated in excess of 150 decibels.

Surface pressure distributions and forces acting on the deflection surface were also recorded. The jet sheet temperature was kept at approximately 15°C .

Using one particular nozzle-deflection surface combination and keeping both the nominal pressure ratio and horizontal gap constant, the vertical gap was varied from the zero position to flow separation in incre-

ments of 1/16-inch. This procedure was repeated for the other three pressure ratios. The horizontal gap was then changed, and the tests were repeated as outlined above. After five horizontal gaps (0 inch to 2 inches in 1/2-inch increments) had been tested, the second nozzle was installed, and the complete test program was performed again. Two other deflection surfaces were used in similar series of tests.

Although the forces - lift (vertical) and drag (horizontal) - acting on the deflection surfaces were measured by the strain gauge balance, they could also be obtained by integrating the surface pressure distribution over the deflection surface. The Ames dial (see Figure 1b) rigidly mounted to the settling chamber at the nozzle attachment flange, was located so that it could measure the vertical travel of the leading edge of the deflection surface from the zero position. The spindle was always raised and locked to prevent its interference with the jet sheet as well as the force measurement during a run.

Accuracy

The pressure distributions on the deflection surface were obtained from the photographs of the multitube manometer. The photo negatives were projected, and could be read with reasonable accuracy to the nearest 1/100 inch of mercury. Since the pressure values at the lower pressure ratios in combination with the nozzle exit height of $t = 1/16$ inch averaged 1/4 inch of mercury, an error of 4 percent in the surface pressure is possible at the lower pressure ratios. However, the error decreases with increasing pressure ratio to less than 1 percent. The total head pressure (measured in the parallel section of the bell mouth just upstream of the nozzle attachment flange) was read in all cases with an accuracy of 1 percent or less. Hence, the measured pressure coefficients, uncorrected for flow compressibility, have an accuracy of approximately 5 percent. The accuracy of the lift and drag force measurements decreased with increasing pressure ratio, because at large horizontal gaps (1 inch to 2 inches) the deflection surface experienced a vibratory motion, the amplitude of which increased in proportion to the total head pressure. This load fluctuation made the strain readings rather difficult to obtain. However, a 5 percent error in the force measurements is considered to be somewhat conservative.

Another cause for variation in the results was found to be their sensitivity to the relative position of the leading edge of the deflection surface to the lip of the nozzle. Proper level alignment was difficult since the nozzle slots were not perfectly uniform in height, and alignment was subject to correction with changing forces on the deflection surface. The effect of improper alignment is examined in more detail in the DISCUSSION OF RESULTS.

PRESENTATION OF RESULTS

The majority of the experimental results which are presented in this report consist of the surface pressure distributions and pressure coefficients. The pressure distributions are plotted in two ways. For a particular nozzle and deflection surface combination, the variation of the pressure distribution along the Coanda surface with pressure ratio for various gap sizes is demonstrated. Using the same data but replotting for a constant pressure ratio, the variation in surface pressure distribution with deflection surface radius is shown. This method of data presentation was repeated for the pressure coefficients which are corrected for flow compressibility.

Since this experiment involved the use of five different parameters which were also varied (4-P.R.'s, 2-t's, 3- R_0 's, 5- L 's, and approximately 8-a's) nearly 1000 separate tests were performed. Hence only a small, but significant, portion of the test results have been presented. All measurements taken for $L=1.5$ inches have been omitted except those of the lift forces in Figures 28 to 33 inclusive. In selecting the cases to demonstrate the effects of the vertical gaps, four values were chosen. These consisted of zero vertical gap, two values between $1/16$ and $1/4$ inch inclusive (depending on the jet sheet thickness), and a vertical gap just before the flow detached from the deflection surface.

The vertical (lift) and horizontal (drag) forces acting on the deflection surface were calculated from the strain gauge readings. Some of these values were plotted for $R_0 = 3$ inches to show how the lift and drag forces are affected by the size of the vertical gap. However, all of the values of the measured lift forces were non-dimensionalized by the product of the total head pressure and nozzle exit area. These values were then plotted to demonstrate how the lift force varied with the radius of the deflection surface; the pressure ratio was selected as the parameter. The composite set of graphs were arranged to show conveniently the effects of both the vertical and horizontal gap sizes. The non-dimensional lift forces were also plotted against vertical gap size for two horizontal gaps and three quadrants. Again, the pressure ratio was chosen as the parameter. Further, to assist in the understanding of the effect of gap size on the lift force, the non-dimensional lift forces were multiplied by 100, and the values were plotted at a point on a grid which represented the size of the gap. Contours of isolift lines were drawn. The sign convention used with these forces is shown in Figure 2.

In plotting the pressure coefficients, no attempt was made to connect the points of a constant pressure. The addition of such lines would complicate the display and tend to show that the compressible pressure coefficients are dependent on pressure ratio even when allowance is made for experimental errors in the readings (see Figures 14b, $a/t = 0$, and 17d, $a/t = 3/4$).

In non-dimensionalizing "a", "L", and "s", the nominal value of "t" was used. For ease of comparison, the numerical value of the theoretical pressure coefficients ($-2t/R$) shown in Figures 13 to 19 was determined from the nominal value of "t" and the radius of the deflection surface, R_0 .

When the graphs were initially plotted, a point was used as the symbol for $P.R. \approx 1.2$. During the final preparation of the graphs, the points were made larger and appear as solid circles - the same size as the open circles used for $P.R. \approx 1.7$. In the case where the plotted values for $P.R. \approx 1.2$ and $P.R. \approx 1.7$ are approximately equal, only the solid circle is visible. Appendix I gives the exact pressure ratios used during the particular tests. The figures state the nominal pressure ratio. It was intended to show the theoretical pressure coefficient line ($-2t/R$) on all graphs on which the measured pressure coefficients are shown. But, due to insufficient space, several graphs had to be cropped so that the data for four vertical gap sizes could be displayed on one page. Hence, the theoretical curve is shown only where space permits.

Configuration Notation

The nozzle and deflection surface combinations are summarized by a notation which is shown in the following example:

$t\ 1/16 - F\ 1/4 - R_0\ 2.0$

This presentation is interpreted, left to right, as the order in which the jet sheet travels from the nozzle to the trailing edge of the deflection surface; that is, the jet sheet emerges from

$t\ 1/16$ is the rectangular convergent nozzle which has an exit height of 1/16-inch;

then, with or without an air gap separating the nozzle and deflection surface, it crosses

$F\ 1/4$ is an initial flat plate surface of 1/4-inch width followed by a quadrant

$R_0\ 2.0$ is of 2-inch radius.

DISCUSSION OF RESULTS

(a) Pressure Distribution

(i) Figures 5 to 10

Figures 5 to 10 inclusive present the change in pressure, ΔP , along the curved jet sheet and are plotted against the non-dimensional distance, s/t , from the leading edge of the deflection surface. P_T/P_a , the nozzle pressure ratio, is the parameter. Four combinations of vertical and horizontal gap sizes were selected for each figure to show the effect of the gap size on the pressure distribution for a particular nozzle and deflection surface combination. In plots of large vertical gap sizes (e. g., Figure 5 (iii) various "a/t" values had to be shown since the ultimate "a/t" changed with pressure ratio. In these cases, the gap closest to the one prior to flow detachment was then plotted.

From any of these graphs, it is evident that two regions of flow adjustment exist. In between these two regions, the flow follows the constant curvature of the quadrant.

In general, the first region of flow adjustment was found to extend approximately one inch downstream from the leading edge of the deflection surface, and to be independent of the configuration tested. The length of the subsequent attached flow region increased, of course, with increasing radius of the deflection surface, but decreased with increasing size of the vertical gap. The length of the second region of flow adjustment (the region between the attached flow and the trailing edge of the deflection surface where the flow has adjusted itself to the atmospheric pressure) indicated a similar variation with " R_0 " and "a". Further, this variation due to "a" was enhanced when " l " was increased. It is believed that the reduction in the length of the attached flow region is caused by the growth in thickness and decrease in momentum of the jet sheet, caused by entrainment on the lower side of the jet, and resulting in a reduction (i. e., less negative) in " ΔP " across the jet sheet.

In Figure 5(i), for example, the first static pressure tap in the centre of the 1/4-inch-wide initial flat plate shows a $\Delta P \approx 0$ for P. R. ≈ 1.1 , but for P. R. ≈ 1.7 and 2.2, " ΔP " is positive. This indicates that high velocity air from the jet sheet was entering the pressure tap. It is the result of improper alignment of the nozzle lip with the leading edge of the deflection surface, that is, $a/t < 0$. In Figure 5(ii), this same pressure tap measured an extremely large negative " ΔP " for high-pressure ratios as a result of the underside entrained air ahead of the deflection surface being forced around the sharp corner of the leading edge, thus lowering the static pressure further.

Figures 8 to 10 inclusive are pressure plots for the $t = 1/4$ -inch nozzle. Due to the thicker jet, the pressure force required to bend the jet

sheet is greater, and the ultimate vertical gap sizes are smaller than for $t = 1/16$ inch.

The scatter in the pressure readings, especially for configuration $t 1/4 - F 1/4 - R_0 3.0$, is caused by imperfect flushness of the pressure taps in the quadrant.

(ii) Figures 11 and 12

Figures 11 and 12 show " ΔP " for $l = 1/2$ -inch and various " a/t ", as a function of the deflection surface radius, R_0 . The theoretical relationship given by equation (4) stating that " ΔP " at constant jet sheet thrust is inversely proportional to the jet sheet radius, R , is qualitatively verified in these two figures. Also, this relationship suggests that the integrated pressure force on the deflection surface is independent of " R "; and hence, both the lift and drag forces should be independent of " R " or " R_0 ". This latter hypothesis was also confirmed and is illustrated in Figures 26 and 27.

(iii) Figure 13

Korbacher in Figure 4a of Reference 3 demonstrated that when his $C_{pi} = \Delta P / (P_T - P_a)$ values are plotted for four different pressure ratios, they do not collapse - at least in the attached flow region where the flow follows the quadrant curvature - into the predicted single horizontal line for incompressible or compressible flow, given by $C_{pi} = -2t/R$, (see equation (9)). If, however, equation (13), which accounts for compressibility, is used, Korbacher in Figure 4b of the same Reference illustrated that the pressure coefficient for compressible and incompressible flows, $C_p = -2t/R$, is independent of pressure ratio.

In Figure 13 the values of " ΔP " along with the corresponding values of " C_{pc} " are plotted to demonstrate again that the pressure coefficients corrected for compressibility effects are independent of pressure ratio. Even for a thick jet ($t = 1/4$ inch), agreement between Korbacher's theory and the experimental results is quite satisfactory in the attached flow region where the jet sheet follows the curvature of the deflection surface. If the simple theory would also include the viscous losses in the flow, agreement between the theoretical line and the experimental values in the attached region would be still better.

(b) Pressure Coefficients

(i) Figures 14 to 21

The pressure coefficients plotted in these figures have all been corrected for flow compressibility. The graphs of one figure, Figure 14a for example, are plotted to show the effect of the vertical gap, keeping the horizontal gap constant. At $a/t = 0$, the static pressure tap in the centre of the $1/4$ -inch-wide initial flat plate measured near atmospheric pressure.

As " a/t " was increased, the " ΔP " measured at this tap became negative, and approached a constant value. Subsequent pressure taps show increasing suction pressures on the deflection surface and, therefore, indicate a stronger bending of the jet sheet with increasing vertical gap. This phenomenon is observed more easily in these figures than in those which show the " ΔP 's", since two more vertical gap sizes are shown for a constant " l/t ".

In Figure 14a, for $a/t = 2$ and 4, the suction pressure is smaller (less negative) at the end of the first region of flow adjustment than it is for $a/t = 0$. As the vertical gap increases, the suction pressure in this region increases, and the depression in the curves widens and becomes more shallow. Just before the flow detaches ($a/t > 6$), no evidence of this depression is visible.

If the suction pressure increases by increasing the size of vertical gaps, then this behaviour should result in an increase of the lift force exerted on the quadrant by the curved jet sheet flow. This prediction is observed in Figures 22 to 33 inclusive.

The effect of increasing " l/t " is shown by comparing Figures 14b, c, and d with 14a for a constant " a/t ". Since the radius of curvature of the flow between the nozzle exit and attachment to the deflection surface increases with increasing horizontal gap, the suction pressure, ΔP , becomes less negative, and the point of flow attachment to the deflection surface moves toward the leading edge of the deflection surface.

The effect of the horizontal gap size on the pressure distribution, and hence, C_p , was small for values of " l " equal to one inch or less; for larger values, the effect was more pronounced and " ΔP " became less negative. The measured lift and drag forces acting on the deflection surface experienced this same effect of horizontal gap size, and are shown in Figures 22 to 25 inclusive.

The relationship between the theoretical and measured pressure coefficients shows good agreement in the region of the attached flow for small vertical and horizontal gaps. As the size of the gap increases, the measured values become less negative in comparison with the theoretical values. This variation between the two values which is caused mostly with increasing horizontal gap is primarily due to the assumption that the jet sheet has one free and one bound surface. This is not the case, especially for $l = R_0 = 2.0$ inches, because the jet sheet actually starts with two free surfaces and then, upon bending over the quadrant, the lower surface becomes bound. Also, the losses due to viscous effects are greater for a jet with two free surfaces.

Probing the jet sheet would be most beneficial in explaining the effect which the gap size has on the pressure distribution and measured forces acting on the deflection surface. It would also be interesting to see the behaviour of the mixing cone in the jet sheet as a function of gap size. Since the length of the mixing cone is proportional to the nozzle exit height, thicker jet sheets can bridge larger horizontal gaps. For the same reason, thin jet sheets can bridge larger vertical gaps.

The pressure coefficients for the other two quadrants and the 1/16-inch nozzle are shown along with the same three quadrants and the 1/4-inch nozzle. Figures 20 and 21 are plots of the pressure coefficients determined from the " ΔP 's" shown in Figures 11 and 12 respectively.

(c) Measured Lift and Drag Forces

(i) Figures 22 and 23

In Figure 22a, the vertical gap is varied, keeping " P_T/P_a " and " L/t " constant, to show its effect on the measured lift and drag forces acting on a deflection surface. It is quite evident that the measured drag forces were influenced by the size of the vertical gap, the drag decreasing with increasing " a/t ". The drag force measured is the resultant horizontal force acting on the quadrant. Flow which was entrained by the underside of the jet sheet created a suction force that acted on the back of the quadrant and opposed the suction force on the deflection surface itself.

The lift force initially increased and then decreased when " a/t " was increased until the jet sheet detached from the quadrant; both lift and drag then fell off to zero. As the horizontal gap is increased from $L/t = 0$ for $a/t = 0$ and constant, some of the jet sheet flow is peeled off by the leading edge of the quadrant, and results in a pressure force on the back of the quadrant. This pressure force, when added to the integrated horizontal pressure force acting on the deflection surface, produced a drag force larger than the lift force (see Figures 22a and 22b). As the vertical gap was increased for a constant " L/t ", this pressure force became a suction force and the net drag force experienced a reduction.

In Figure 22b for $L/t = 16$, the peculiar shape of the lift and drag curve for $P.R. = 1.7$ and 3.2 is unexplainable, especially since it occurred for both $R_0 = 2$ and 4 inches. However, it did not occur at all for $t = 1/4$ inch (see Figures 23a and 23b).

No attempt was made to show the ultimate value of " a/t " at which the flow broke away from the deflection surfaces. It may be mentioned, however, that the " a/t " at which the flow separated increased with increasing values of " R_0 ". This is seen in Figures 26 and 27. The difference between the lift and drag forces for a constant " a/t ", was proportional to the pressure ratio.

Since the measured drag force represented the net horizontal force on the quadrant rather than the horizontal force acting on the deflection surface, no further analysis of the drag force was considered.

From Figures 7 and 10, the areas under the pressure curves for $P. R. \approx 1.2$ and 1.7 were determined with a planimeter, and the resultant forces, F_{R_i} , acting on the deflection surfaces were calculated. From the measured lift and drag forces, corresponding resultant forces, F_{R_m} , were determined. These resultant forces are compared for various gap sizes in Appendix II.

For $a/t = 0$ and $l = 1/2$ inch, " F_{R_m} " is greater than " F_{R_i} " because " D " is composed of two forces which are additive. If, then, the vertical gap is increased, " F_{R_i} " becomes greater than " F_{R_m} " since the "secondary" drag force (acting on the back of the quadrant) now acts opposite to the positive drag direction. For $l = 2.0$ inches, the difference between the resultant forces is still larger.

(d) Non-Dimensional Lift

(i) Figures 24 and 25

The measured lift forces were non-dimensionalized by dividing them by " P_{TAN} ", and then were plotted in these two Figures for two horizontal gaps. Note that the thicker the jet sheet, the smaller the vertical gap the jet sheet can bridge before it detaches from the deflection surface. This behavior is due to the fact that a thicker jet sheet requires a stronger " ΔP " to bend it around a given curvature. However, " ΔP " can be made more negative only as long as the suction pressure in the wedge between the deflection surface and the curved jet sheet prior to its attachment can be increased; this criterion is a function of the jet sheet entrainment and wedge angle. Therefore, the thick jet sheet detaches when its optimum possible " ΔP " in the wedge is smaller than that required to bend the jet sheet enough to attach itself to the deflection surface. The thin jet sheet detaches when the mixing has penetrated to the jet sheet's center, thereby limiting further entrainment and higher suction pressures.

Increasing the radius of the deflection surface reduces " ΔP " and has the same effect as decreasing the jet sheet thickness. It enables, therefore, the jet sheet to bridge larger gaps before the flow detaches.

(ii) Figures 26 and 27

It was noted in Figures 11 and 12 that the integrated pressure forces on the deflection surface in both the lift and drag direction should be independent of " R_0 ". To verify this observation, the non-dimensional lift forces were plotted versus the three deflection surface radii for a constant " l/t " and " a/t ". In general, the variation of " $L/(P_{TAN})$ " with " R_0 " is negligible, but the results show a considerable amount of scatter. However, if the values

are compared for a constant " P_T/P_a " and either a constant " L " or " a ", they exhibit the expected trend. It is evident from these graphs that an increase in the horizontal gap results in an appreciable decrease in the lift force. But, by increasing the vertical gap, the lift force approaches a constant value and then reduces to zero when the flow detaches.

In several of the graphs, the lift curves are shown partly by a broken line to indicate that since no measured value was available, the line was simply extrapolated. The results of the 1/4-inch nozzle are shown in Figure 27.

(e) Isolift Lines

(i) Figures 28 to 33

The non-dimensional lift forces were multiplied by 100, to convert all ratios into integers, and then plotted for a constant pressure ratio (see Figure 28). The horizontal and vertical axes are " L/t " and " a/t " respectively, and are positive in the direction shown.

The maximum lift force occurs for a horizontal gap ranging from zero to 1/4 inch. As the pressure ratio is increased, this maximum lift force shifts to larger values of " a/t ". For $P_T/P_a = \text{constant}$, corresponding isolift lines are displaced toward larger " L/t " values if the radius of the deflection surface is increased.

It is apparent from these figures for constant " P_T/P_a " and " L/t " that two values of " a/t " provide the same lift force. Therefore, one particular " a/t " and " L/t " combination will give a maximum lift force. The locus of these points forms the gap size required for optimum lift. As " L/t " increases for a constant "P. R.", the ultimate lift force occurs for larger " a/t ". For overchoked jet sheets ($t = 1/16$ -inch), the shape of the optimum lift line was affected more by " a/t " than for subsonic jet sheets (see Figure 32). A boundary line which separates the region of attached and detached flow can be considered to be located at the bottom of each set of graphs in these figures. If " a/t " is made larger than the vertical gap which corresponds to the limiting lift line, the flow will detach. Similarly, if " L/t " is increased, a horizontal gap will be reached for which the jet sheet contains insufficient momentum and will not attach itself to the deflection surface, because the " ΔP " required to deflect the jet sheet will not be possible to achieve. Hence, the limiting lift line must, then, turn back on itself, in the same manner of the isolift lines.

Comparing the effect of jet sheet thickness for constant " R_0 " and "P. R.", it is seen that the optimum lift line occurs for larger " a/t " when " t " is decreased. Again, it is illustrated that thicker jet sheets have a smaller range of vertical gap sizes if the flow is to be deflected by the Coanda surface.



(a) GENERAL VIEW



(b) CLOSE-UP VIEW OF THE TEST SECTION

FIGURE 1. TEST RIG FOR DETACHED COANDA SURFACES.

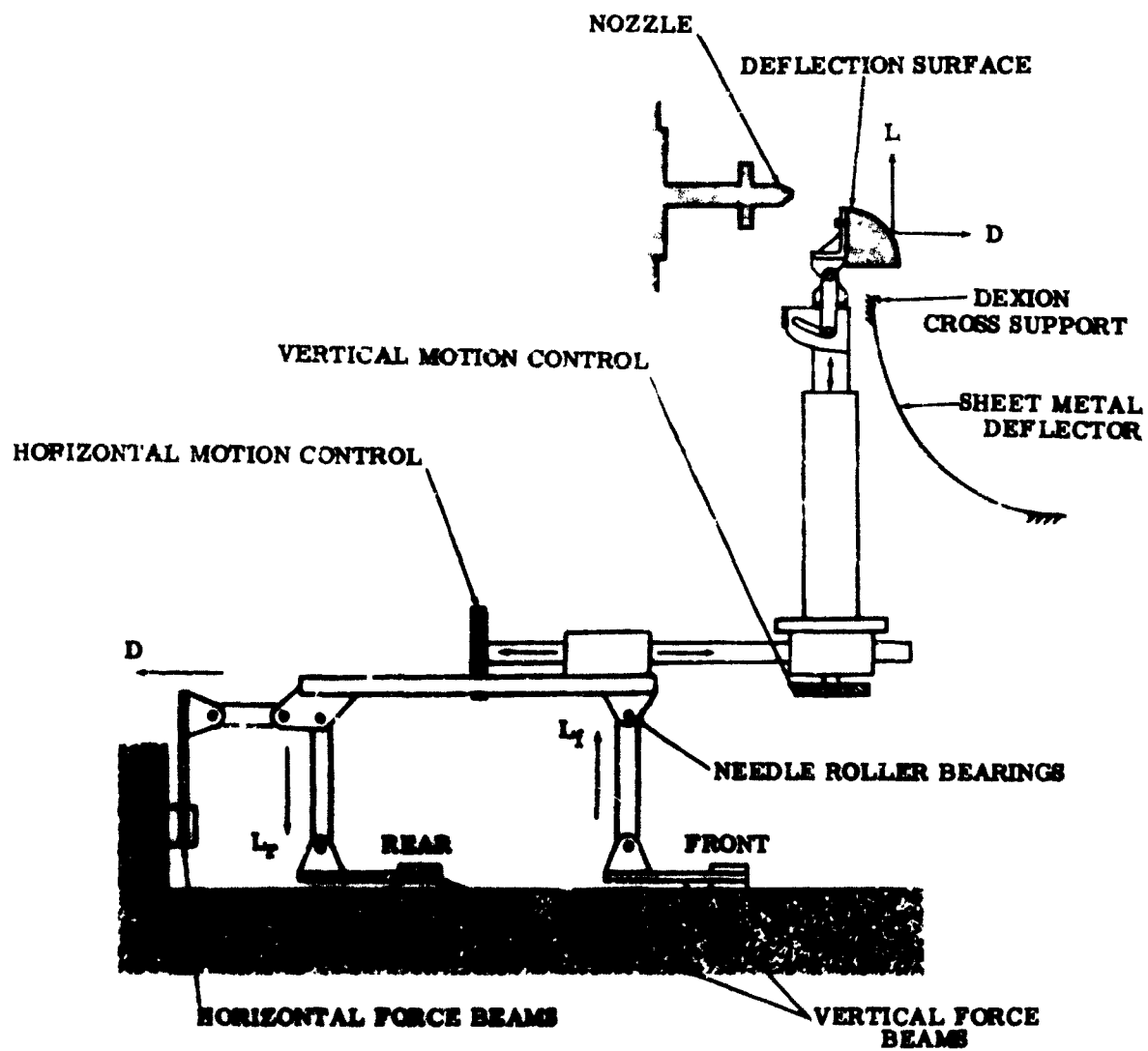


FIGURE 3. SCHEMATIC DETAIL OF THE STRAIN GAUGE BALANCE FOR MEASURING FORCES ACTING ON THE DEFLECTION SURFACE.

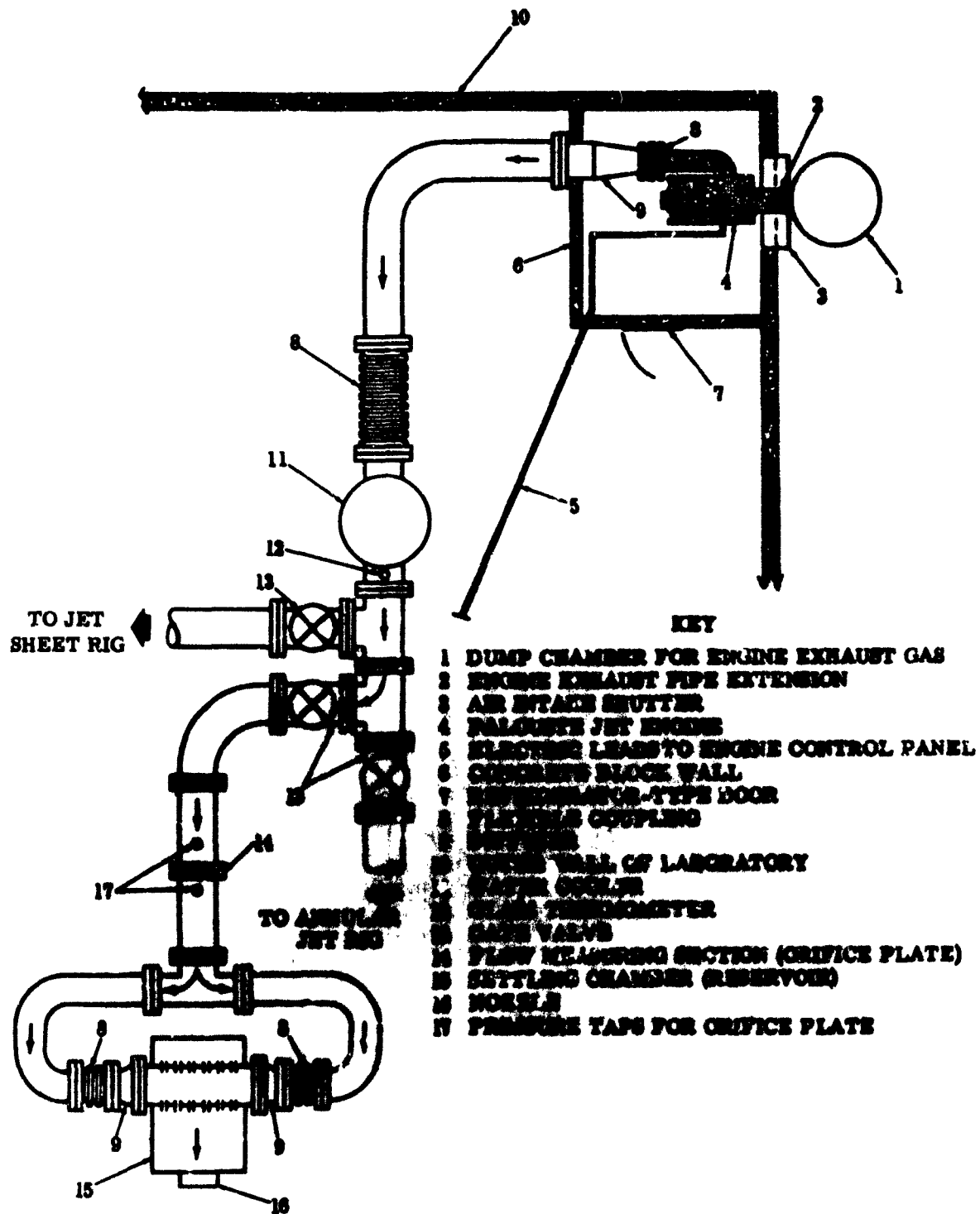


FIGURE 4.

SCHEMATIC LAYOUT OF THE COMPRESSED AIR SUPPLY TO THE TEST RIG.

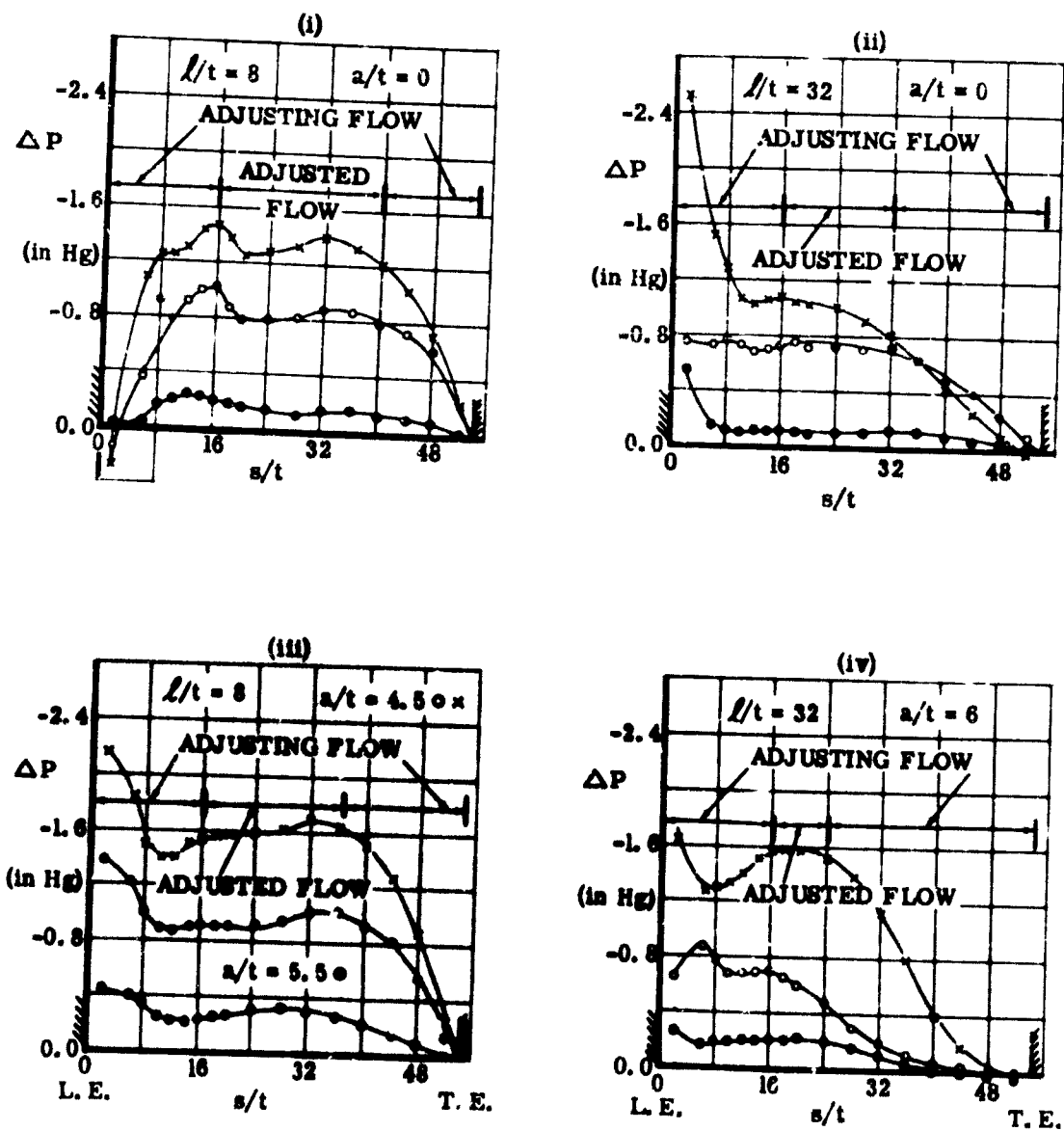


FIGURE 5. EFFECT OF HORIZONTAL AND VERTICAL GAP SIZES ON THE PRESSURE DISTRIBUTIONS ALONG A DEFLECTION SURFACE AT VARIOUS NOZZLE PRESSURE RATIOS.

W/16 - F/4 - R₀3.0

P.R. ≈ L2 ●
L7 ○
2.2 X

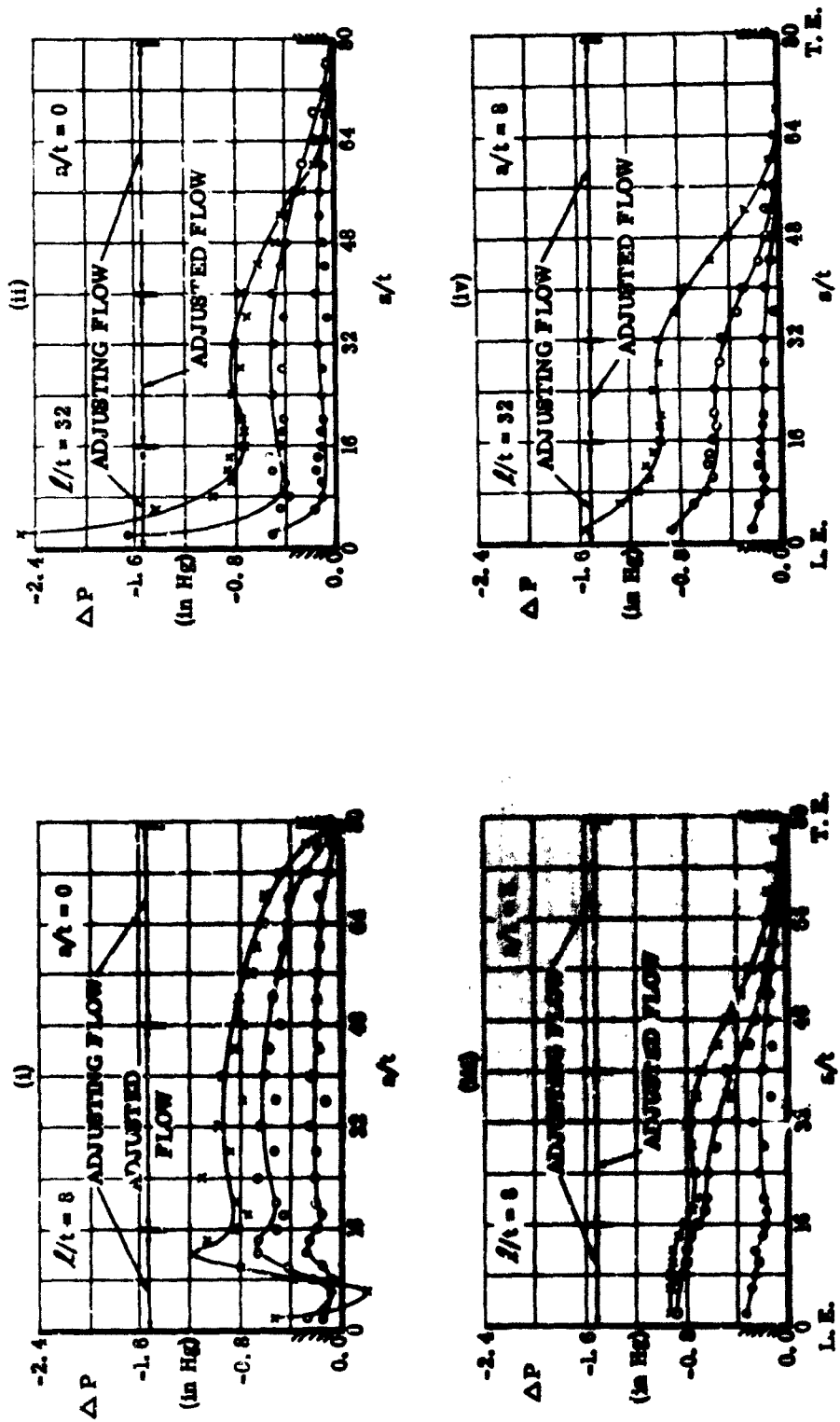


FIGURE 8. EFFECT OF HORIZONTAL AND VERTICAL GAP SIZES ON THE PRESSURE DISTRIBUTIONS ALONG A DEFLECTION SURFACE AT VARIOUS NOZZLE PRESSURE RATIOS.

P. R. \approx 1.2 ●
 1.7 ○
 2.2 x

11/16 - F/4 - R₀ 4.0

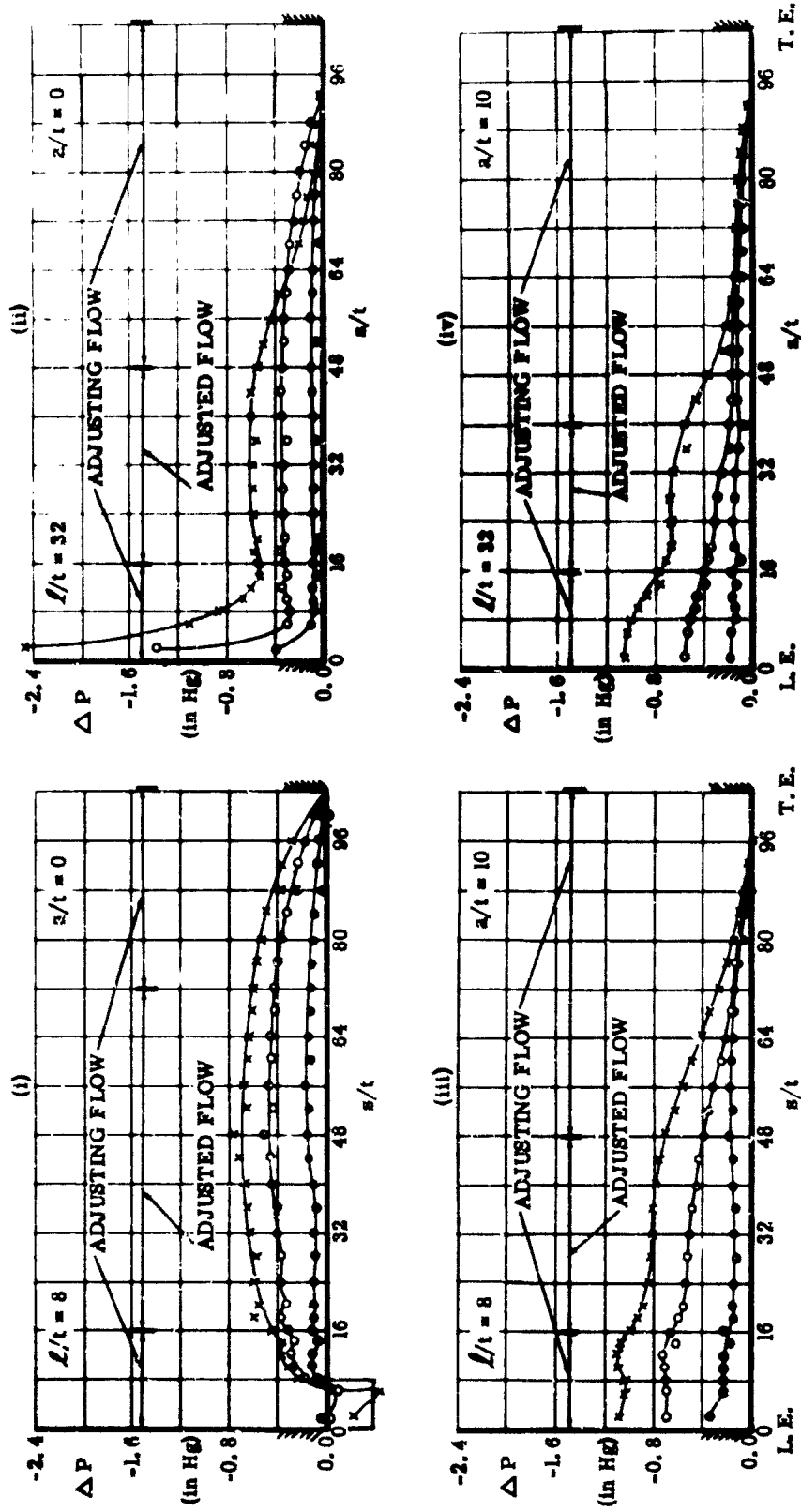
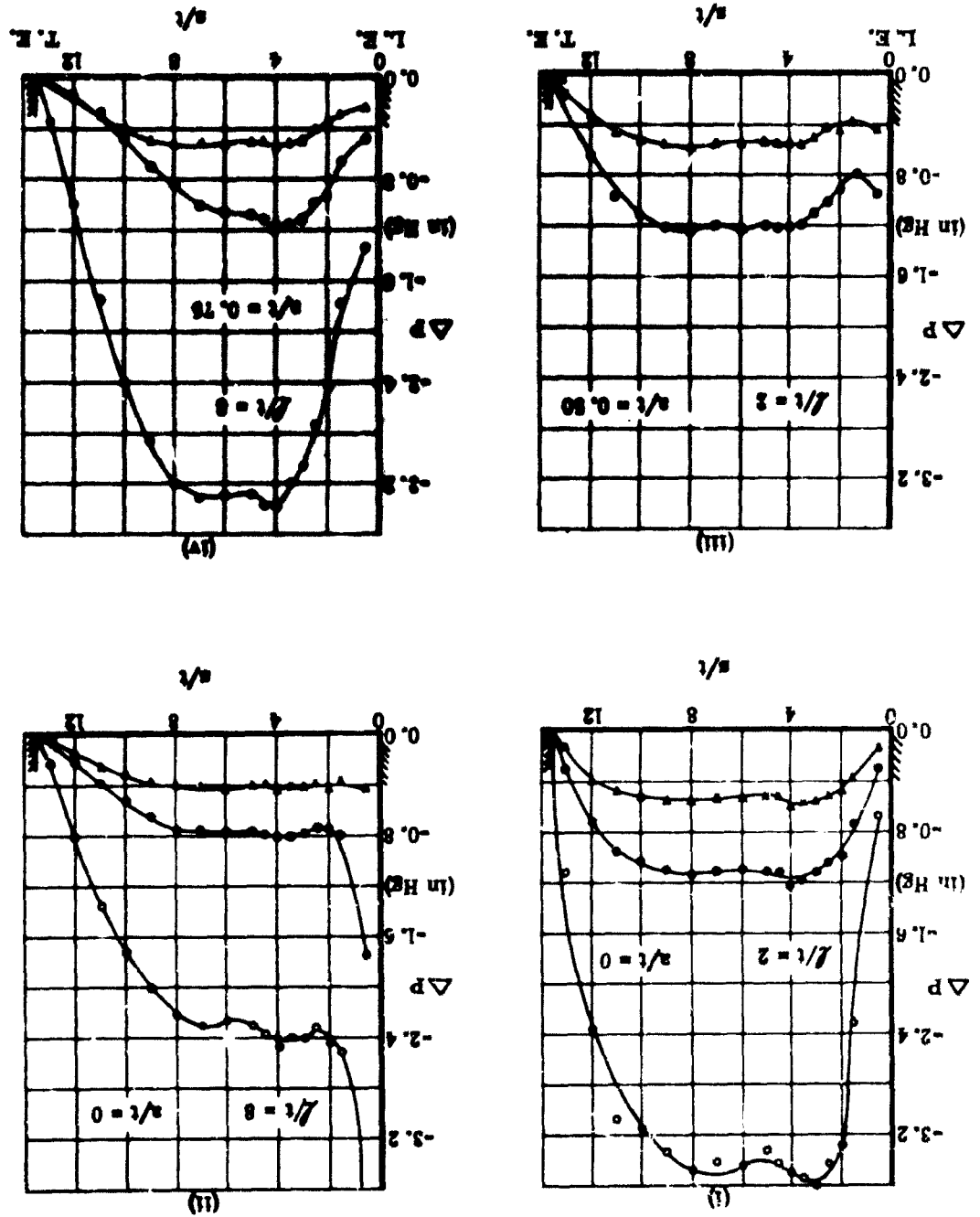


FIGURE 7. EFFECT OF HORIZONTAL AND VERTICAL GAP SIZES ON THE PRESSURE DISTRIBUTIONS ALONG A DEFLECTION SURFACE AT VARIOUS NOZZLE PRESSURE RATIOS.

FIGURE 8. EFFECT OF HORIZONTAL AND VERTICAL GAP SIZES ON THE PRESSURE DISTRIBUTIONS ALONG A DEFLECTION SURFACE AT VARIOUS NOZZLE PRESSURE RATIOS.



U/4 - F/4 - R₀2.0

P.R. = L14
L30
L70

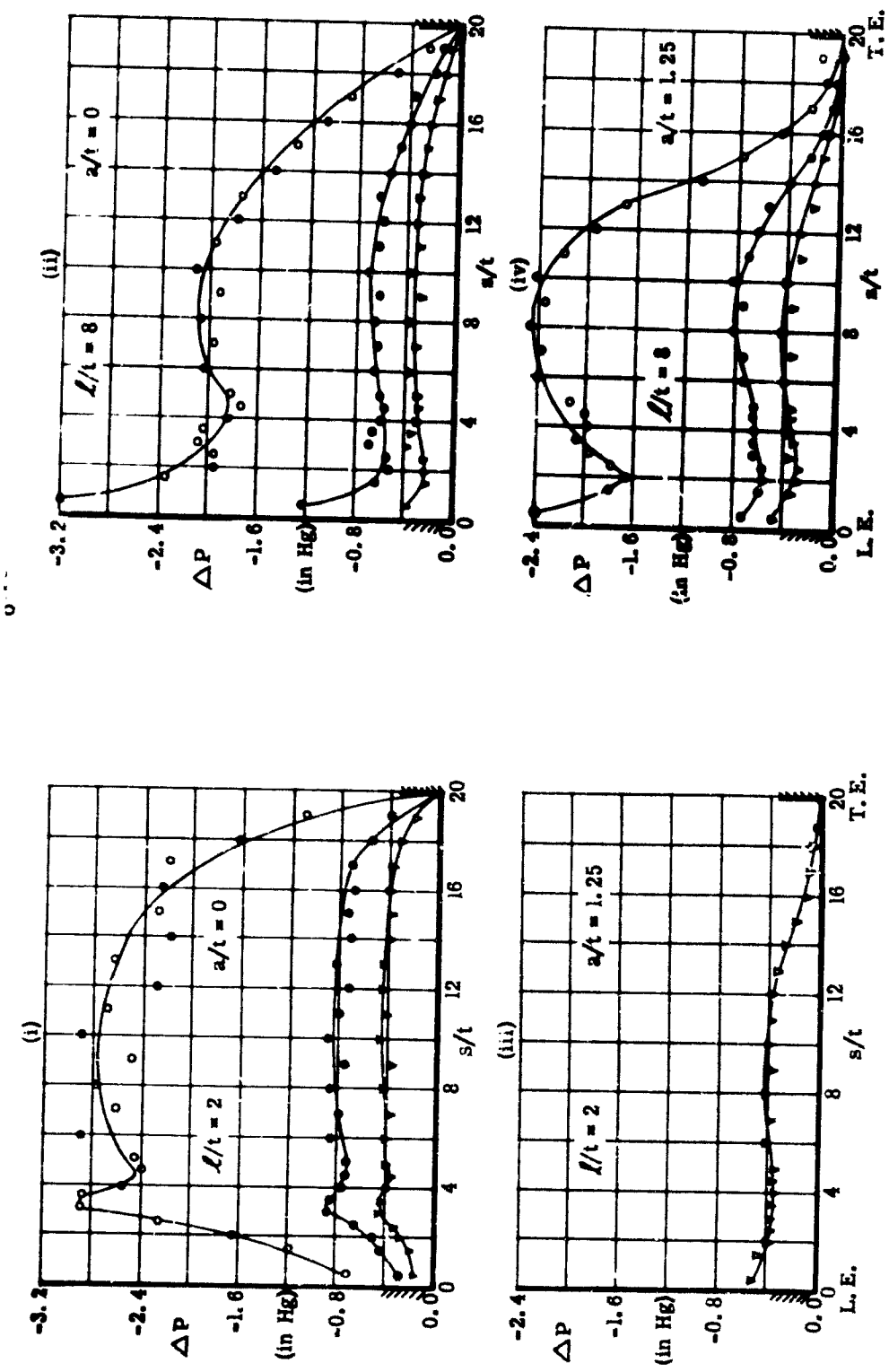


FIGURE 9. EFFECT OF HORIZONTAL AND VERTICAL GAP SIZES ON THE PRESSURE DISTRIBUTIONS ALONG A DEFLECTION SURFACE AT VARIOUS NOZZLE PRESSURE RATIOS.

P. R. 117
L. 20
L. 70

W/4 - FV/4 - R₀ = 0

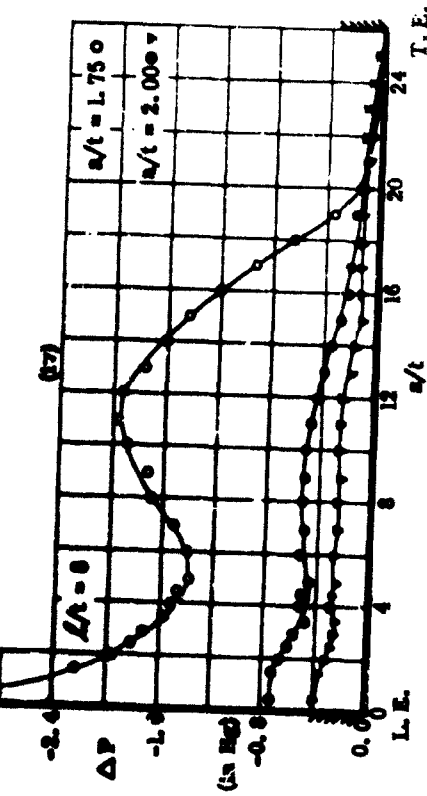
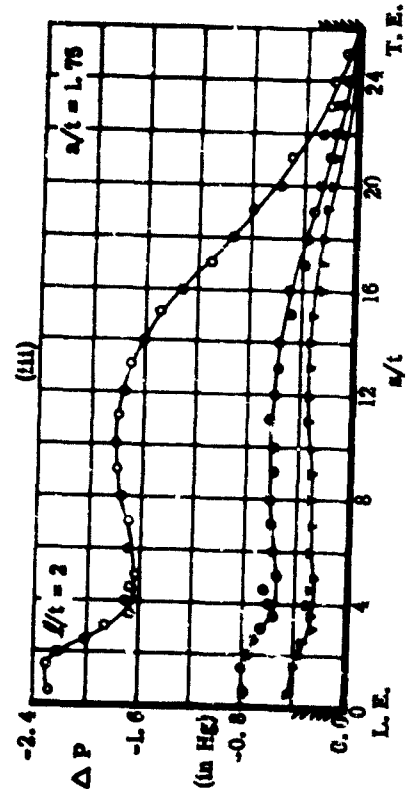
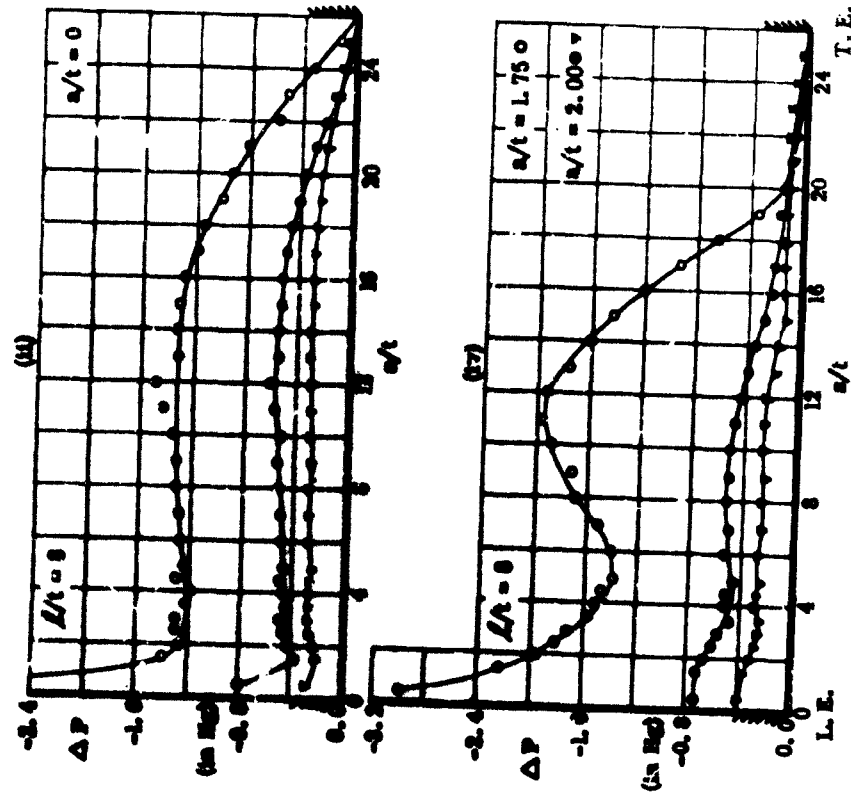
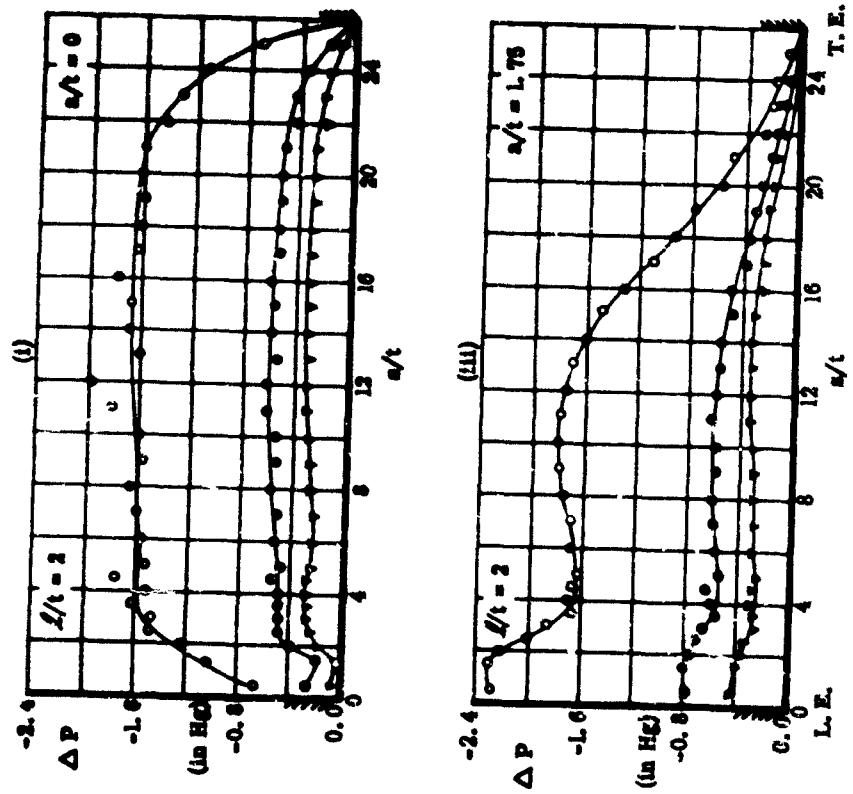


FIGURE 10. EFFECT OF HORIZONTAL AND VERTICAL GAP SIZES ON THE PRESSURE DISTRIBUTIONS ALONG A DEFLECTION SURFACE AT VARIOUS NOZZLE PRESSURE RATIOS.

$$W' = l/4 - R_0 X$$

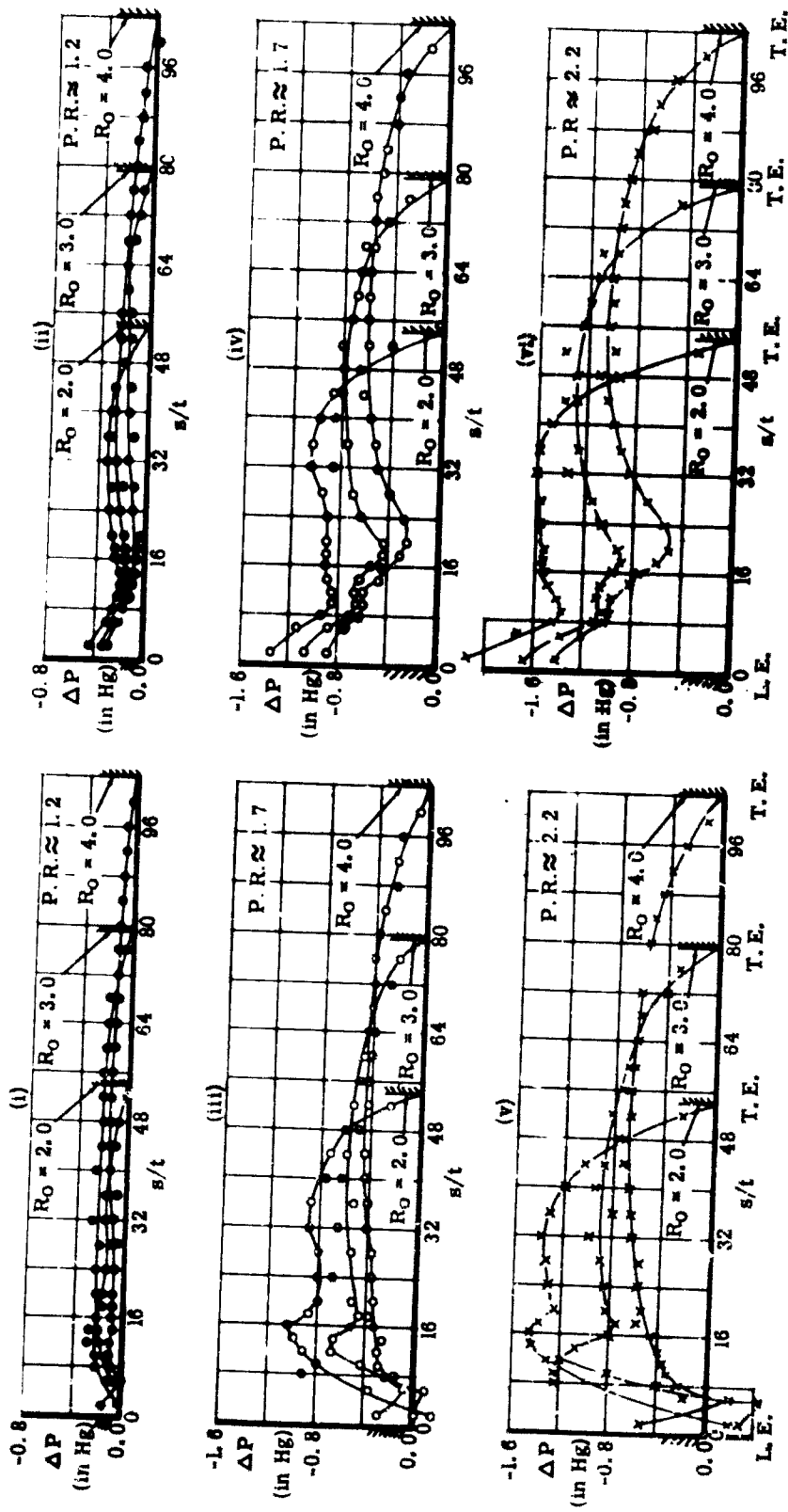
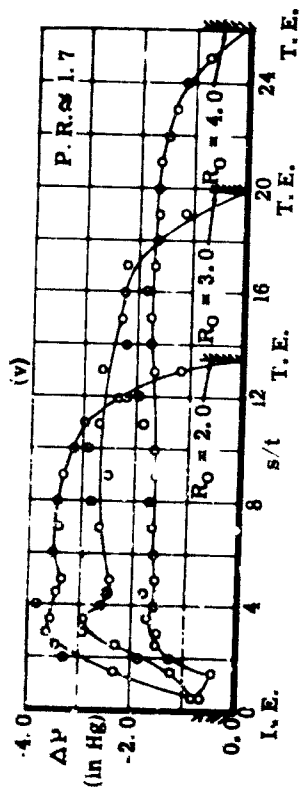
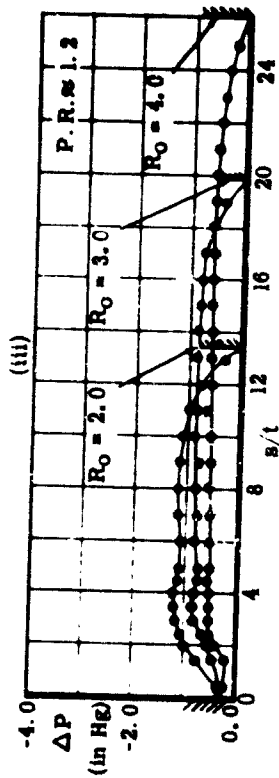
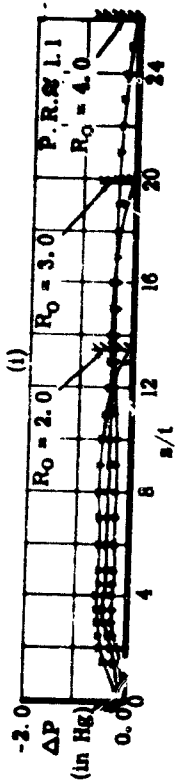
 $L/t = 8$
 $a/t = 0$
 $a/t = 4.0$


FIGURE II. EFFECT OF THE VERTICAL GAP SIZE ON THE PRESSURE DISTRIBUTIONS ALONG THE SURFACE FOR DIFFERENT DEFLECTION SURFACE RADII AT VARIOUS NOZZLE PRESSURE RATIOS.

$$1/4 - FV/4 - R_0^2$$

$$L/t = 2$$

$$s/t = 1.5$$



$$L/t = 2$$

$$s/t = 0.5$$

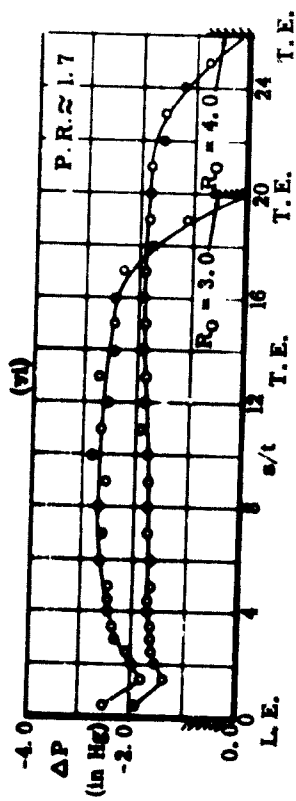
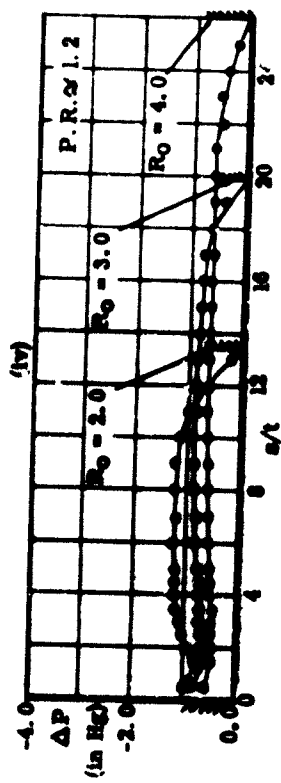
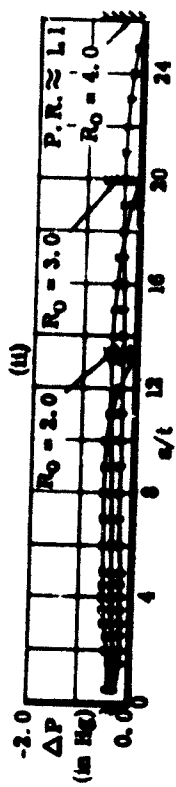


FIGURE 12. EFFECT OF THE VERTICAL GAP SIZE ON THE PRESSURE DISTRIBUTIONS ALONG THE SURFACE FOR DIFFERENT DEFLECTION SURFACE RADII AT VARIOUS NOZZLE PRESSURE RATIOS.

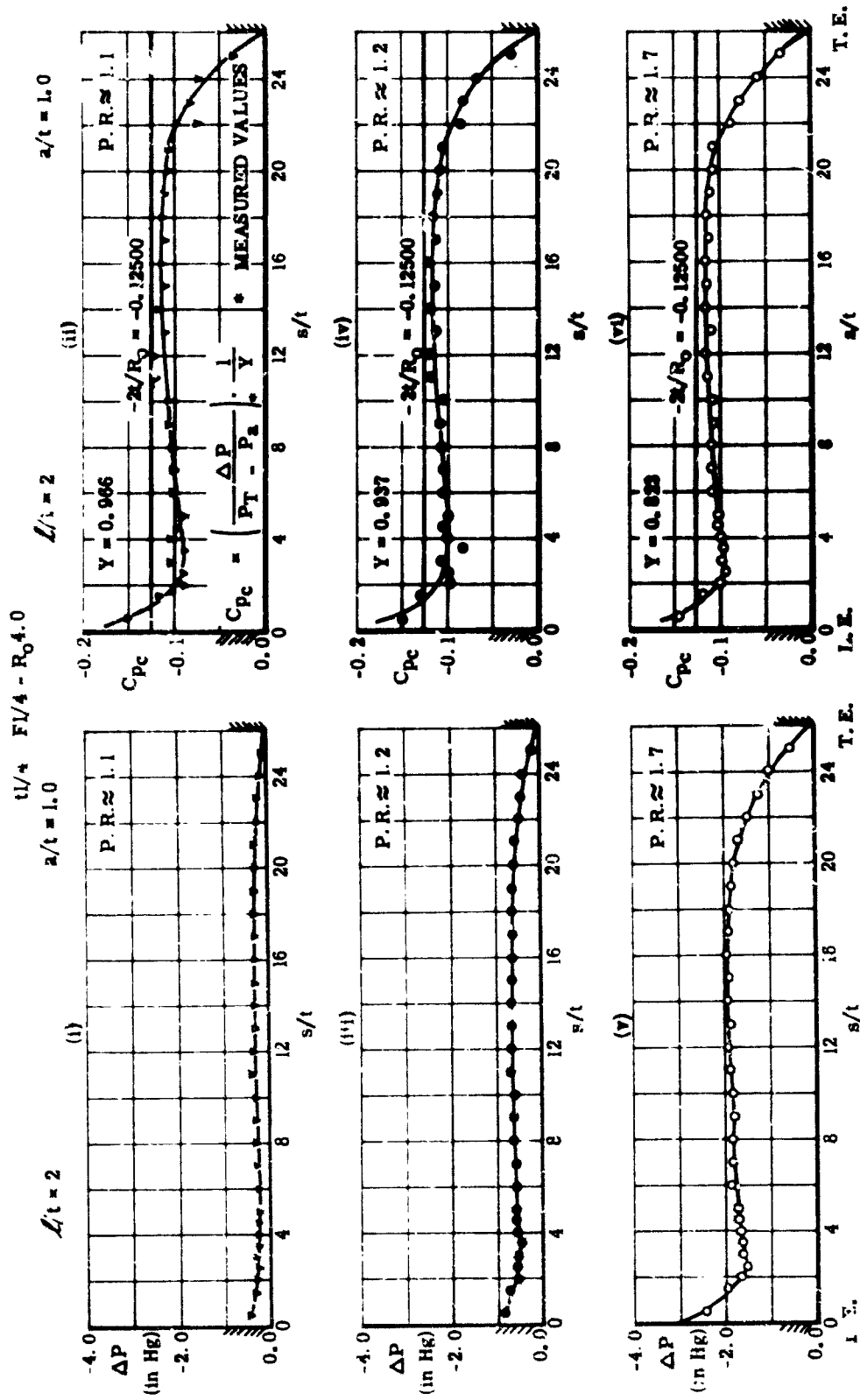


FIGURE 13. RELATIONSHIP BETWEEN PRESSURE COEFFICIENTS CORRECTED FOR
FLOW COMPRESSIBILITY AND MEASURED PRESSURE DISTRIBUTIONS.

$t_1/b = F/4 - R_0 2.0$

P. R. ≈ 1.20
L. T. ≈ 1.70
2.24

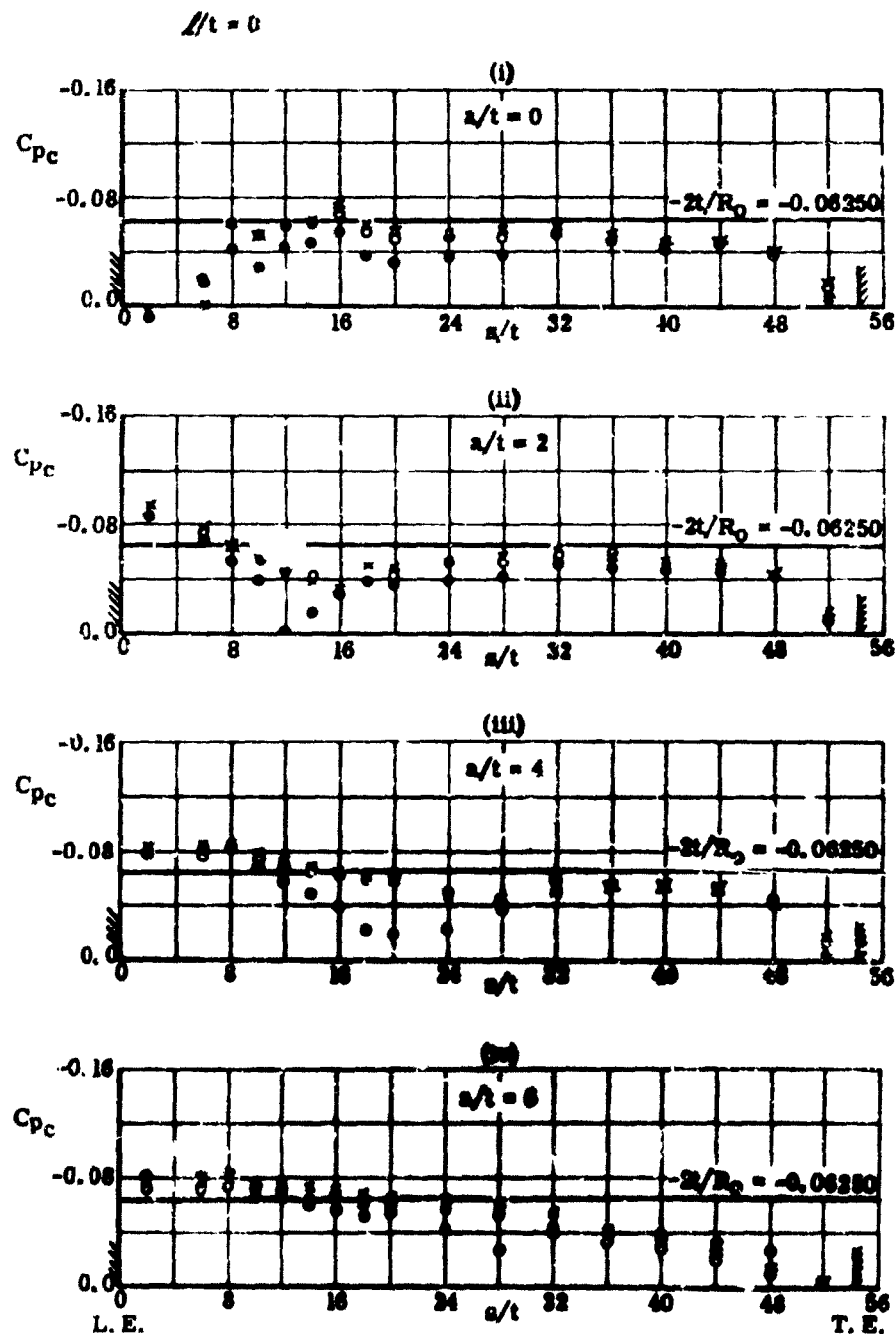


FIGURE 14a. EFFECT OF THE VERTICAL GAP SIZE ON THE PRESSURE COEFFICIENTS CORRECTED FOR FLOW COMPRESSIBILITY AT VARIOUS NOZZLE PRESSURE RATIOS

$1/16 - F_1/4 - R_0 2.0$

P. R. \approx 1.3 \bullet
1.7 \circ
2.2 \times

$L/t = 3$

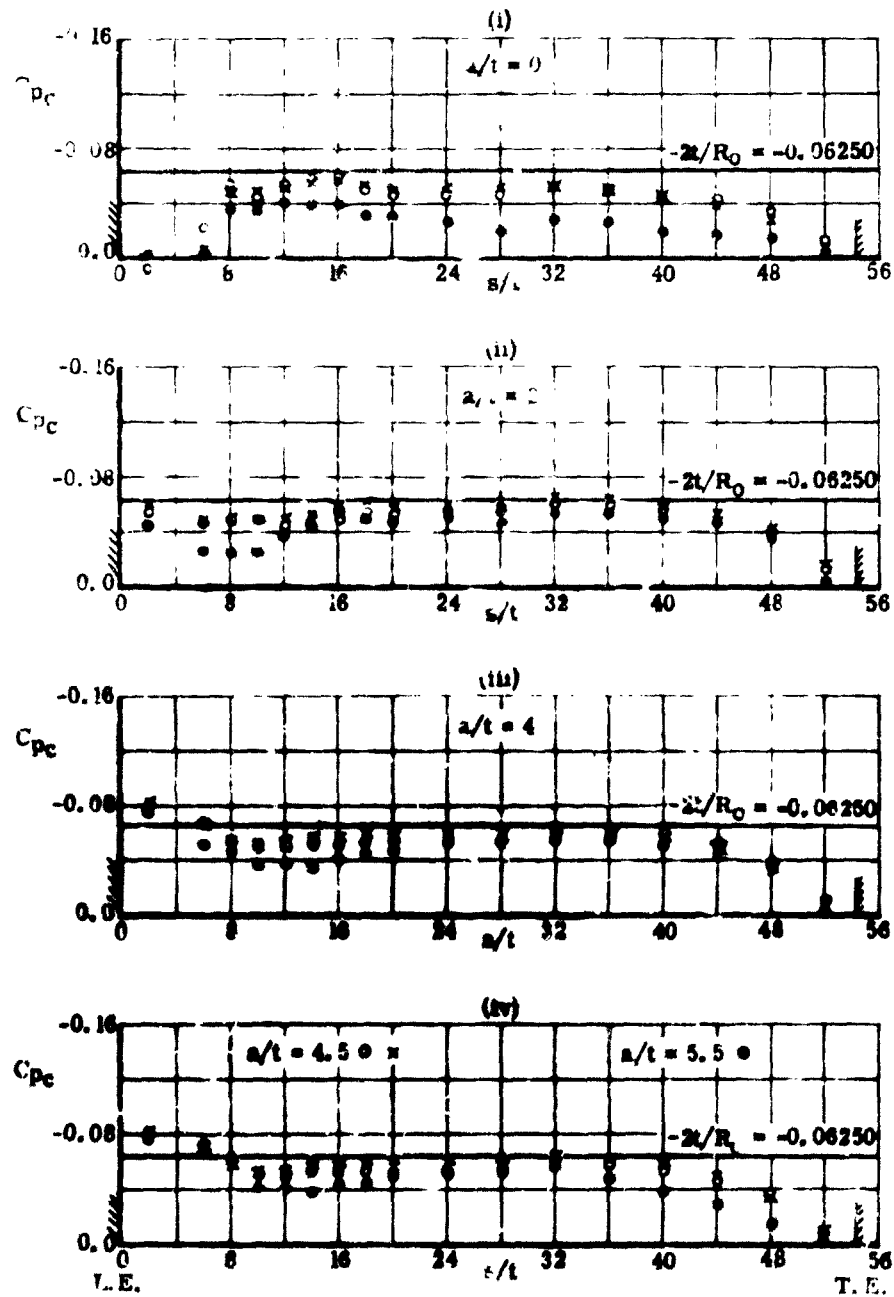
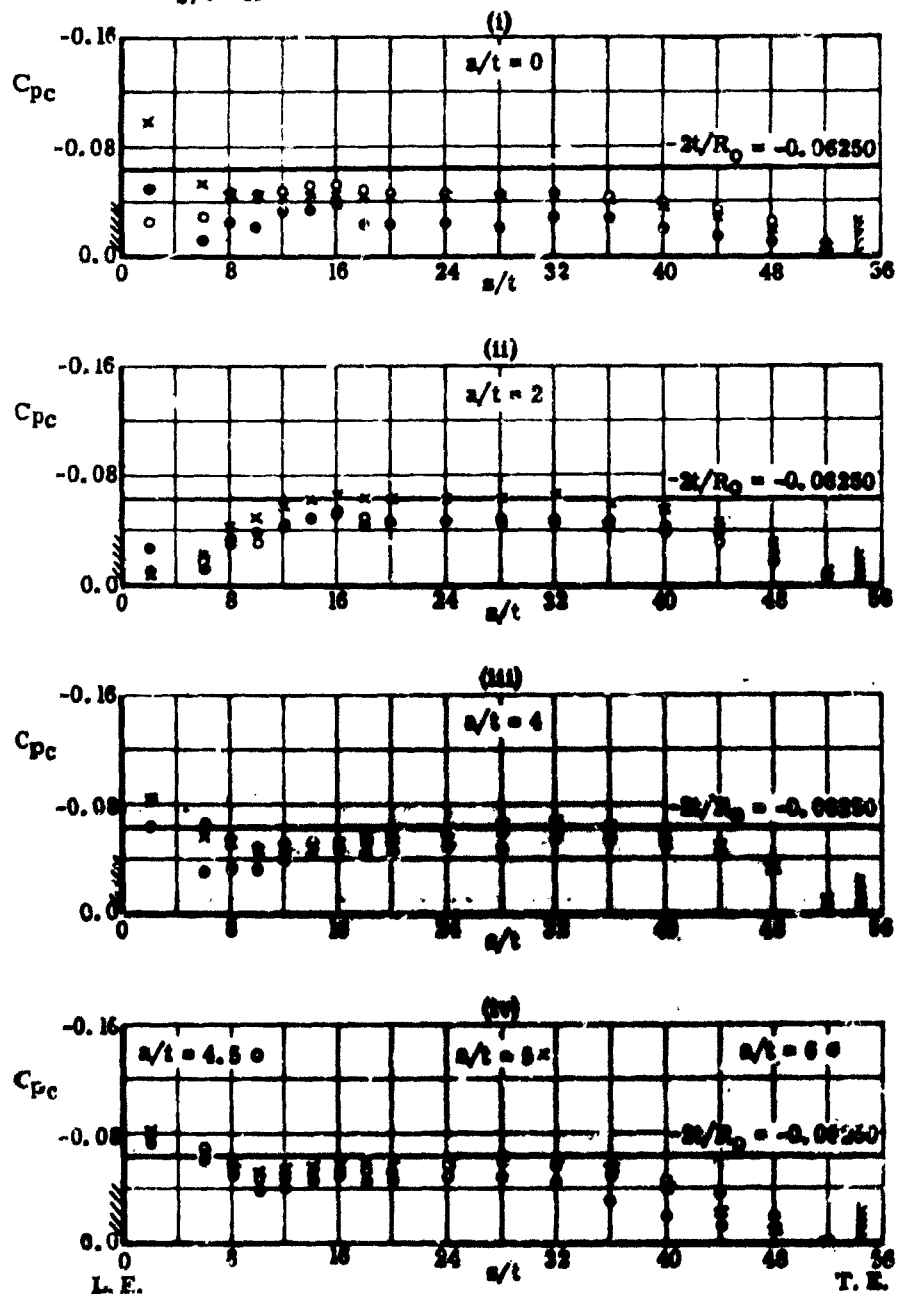


FIGURE 14b. EFFECT OF THE VERTICAL GAP SIZE ON THE PRESSURE COEFFICIENTS CORRECTED FOR FLOW COMPRESSIBILITY AT VARIOUS NOZZLE PRESSURE RATIOS.

$t_1/16 - F/4 - R_0 2.0$

P. R. = 1.2 ○
1.7 ○
2.2 x

$l/t = 16$



—E 14c. EFFECT OF THE VERTICAL GAP SIZE ON THE PRESSURE COEFFICIENTS CORRECTED FOR FLOW COMPRESSIBILITY AT VARIOUS NOZZLE PRESSURE RATIOS.

$l/16 - F1/4 - R_0 2.0$

P. R. = 1.2 ○
1.7 ○
2.2 ×

$l/t = 32$

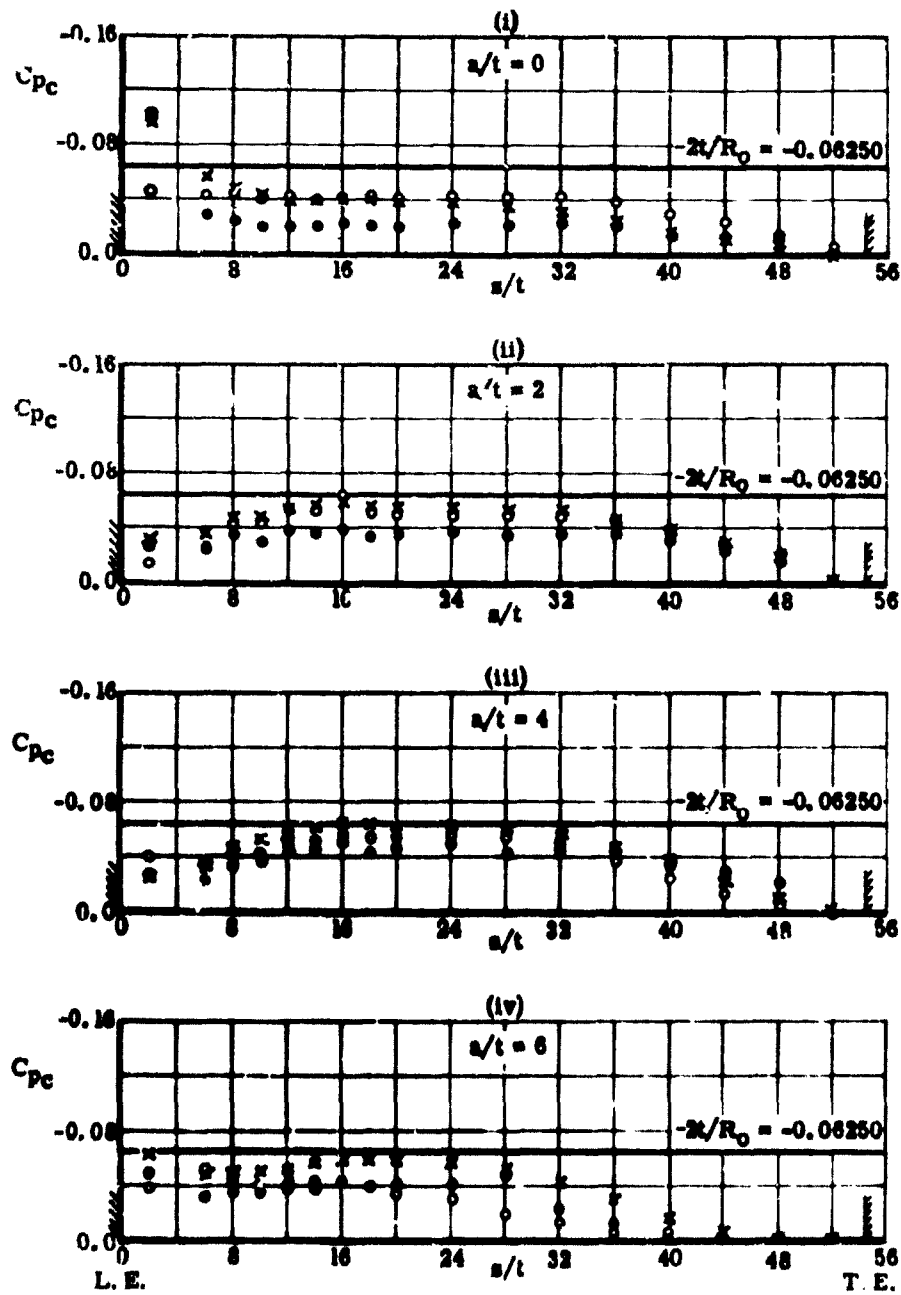


FIGURE 14d. EFFECT OF THE VERTICAL GAP SIZE ON THE PRESSURE COEFFICIENTS CORRECTED FOR FLOW COMPRESSIBILITY AT VARIOUS NOZZLE PRESSURE RATIOS.

P.R. = L20
 L70
 2.2x

$1/16 - F1/4 - R_c 3.0$

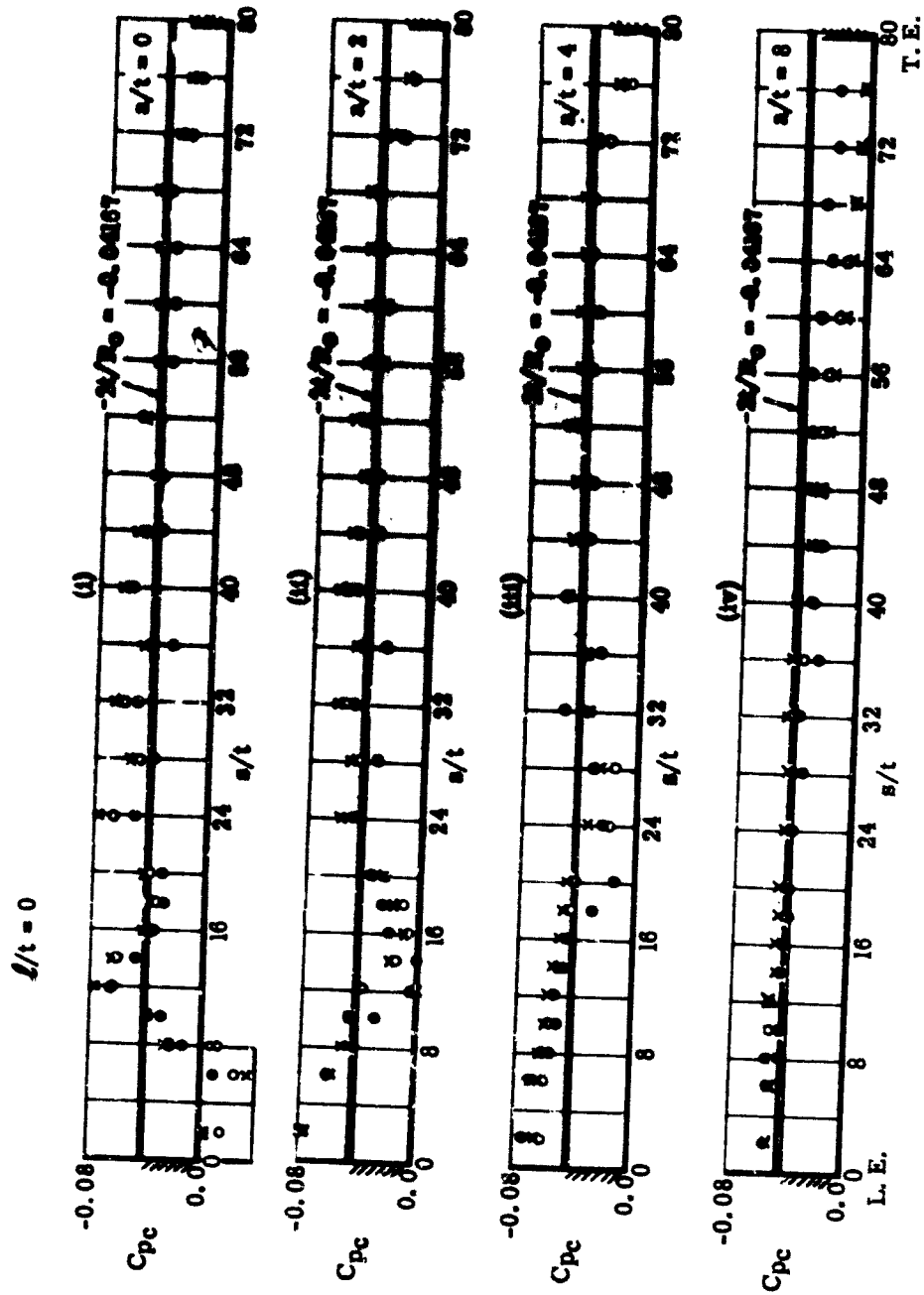


FIGURE 15a.
 EFFECT OF THE VERTICAL GAP SIZE ON THE PRESSURE COEFFICIENTS
 CORRECTED FOR FLOW COMPRESSIBILITY AT VARIOUS NOZZLE PRESSURE
 RATIOS.

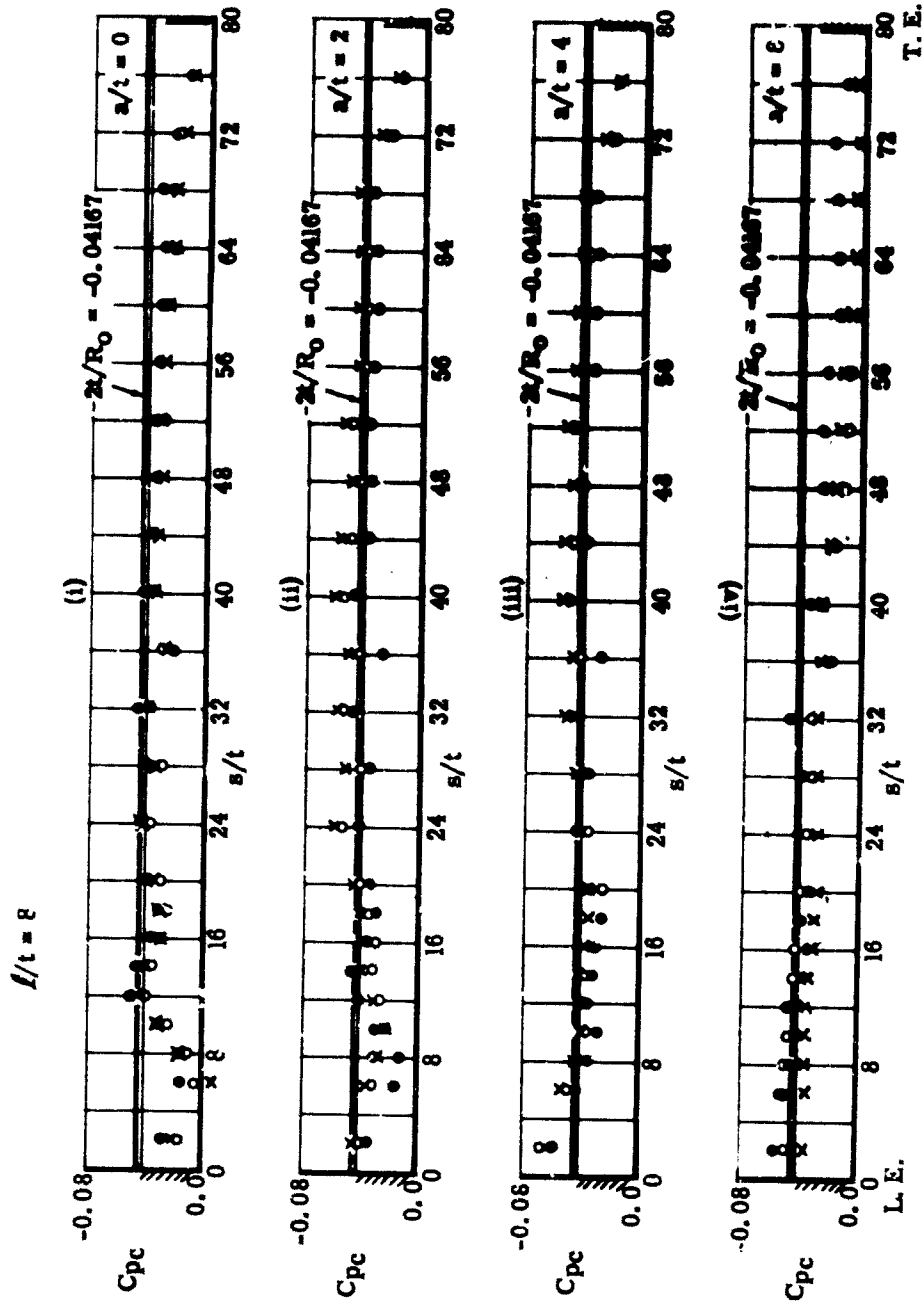


FIGURE 15b. EFFECT OF THE VERTICAL GAP SIZE ON THE PRESSURE COEFFICIENTS CORRECTED FOR FLOW COMPRESSIBILITY AT VARIOUS NOZZLE PRESSURE RATIOS. T. E.

P. R. # L20
L70
2.2x

$u/16 - FV/4 - R_0 3.0$

$l/t = 16$

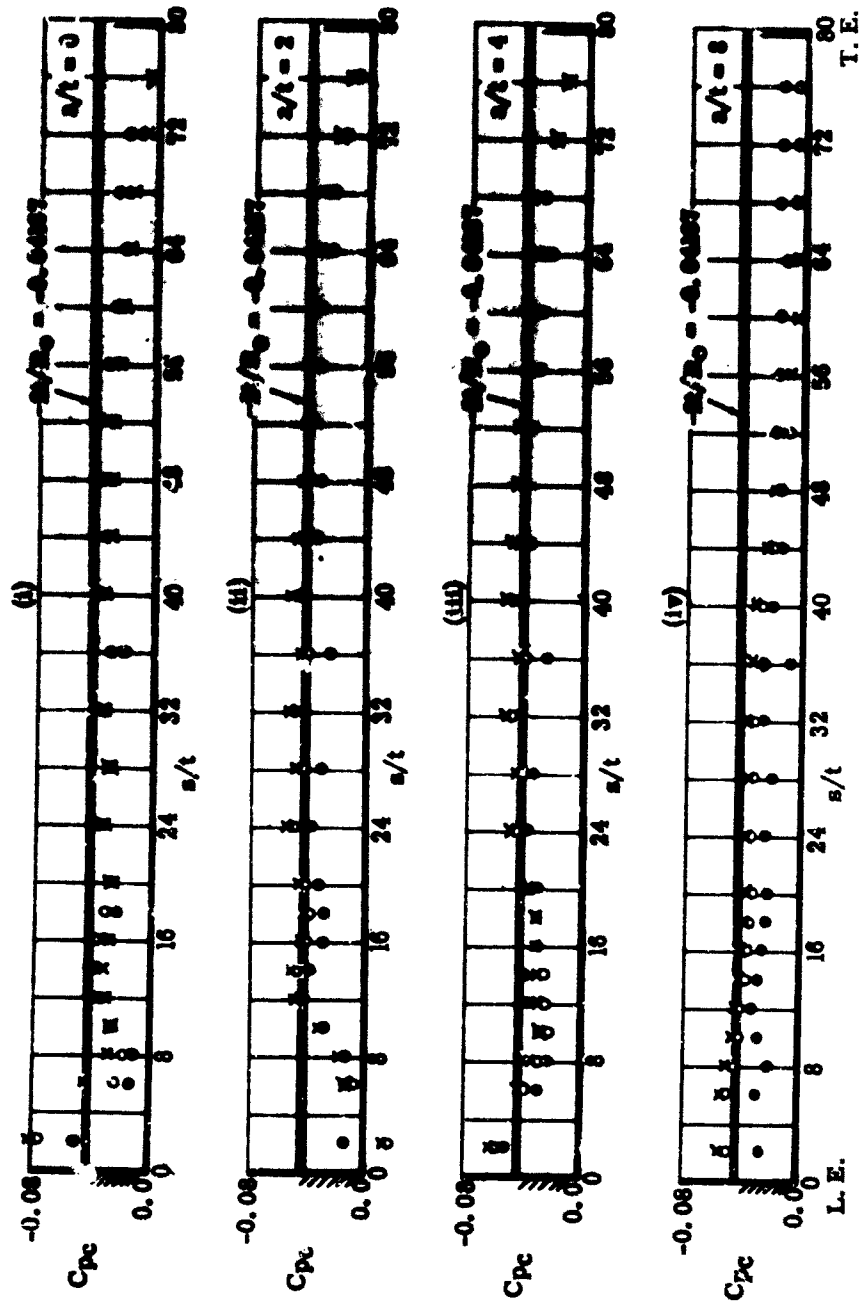


FIGURE 15c. EFFECT OF THE VERTICAL GAP SIZE ON THE PRESSURE COEFFICIENTS CORRECTED FOR FLOW COMPRESSIBILITY AT VARIOUS NOZZLE PRESSURE RATIOS.

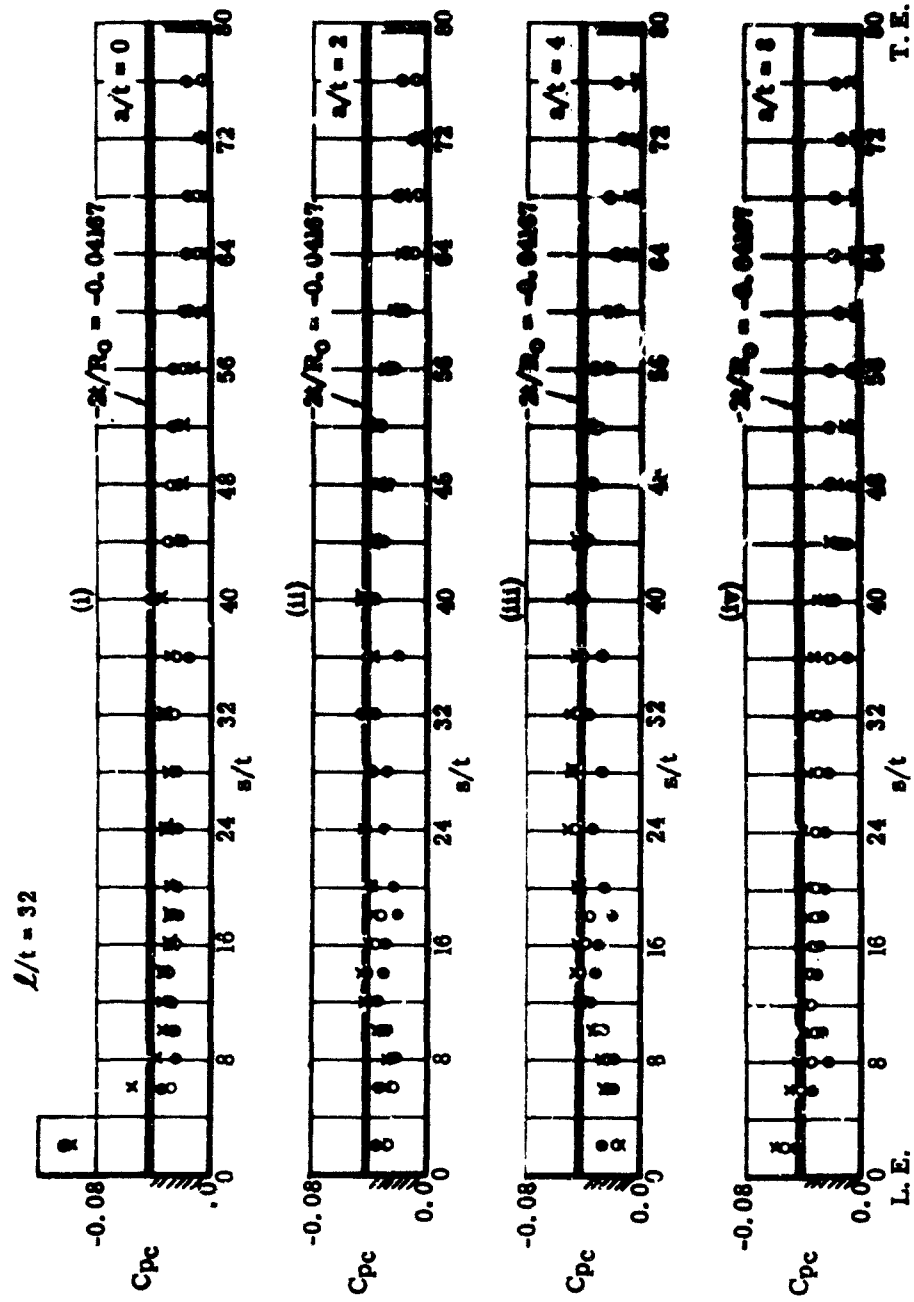


FIGURE 15d. EFFECT OF THE VERTICAL GAP SIZE ON THE PRESSURE COEFFICIENTS CORRECTED FOR FLOW COMPRESSIBILITY AT VARIOUS NOZZLE PRESSURE RATIOS.

P.R. ≈ L.2 ●
 L.7 ○
 2.2 x

11/16 - F1/4 - R₀ 4.0

L/t = 0

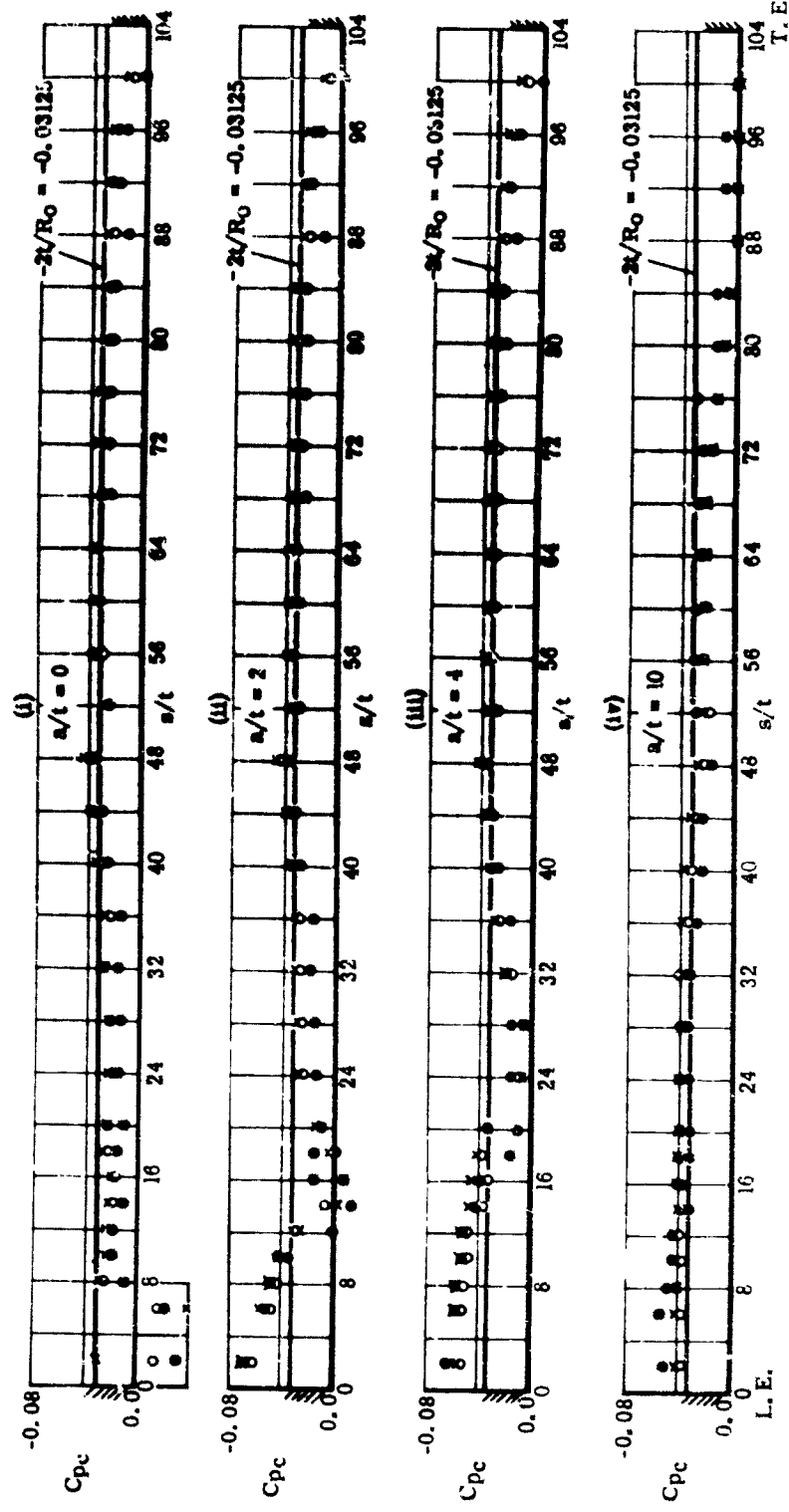


FIGURE 16a. EFFECT OF THE VERTICAL GAP SIZE ON THE PRESSURE COEFFICIENTS CORRECTED FOR FLOW COMPRESSIBILITY AT VARIOUS NOZZLE PRESSURE RATIOS

P. R. \approx 1.2 ●
 1.7 ○
 2.2 x

$U/55 = F_{L, 7} - R_0 A_0$

$A/t = b$

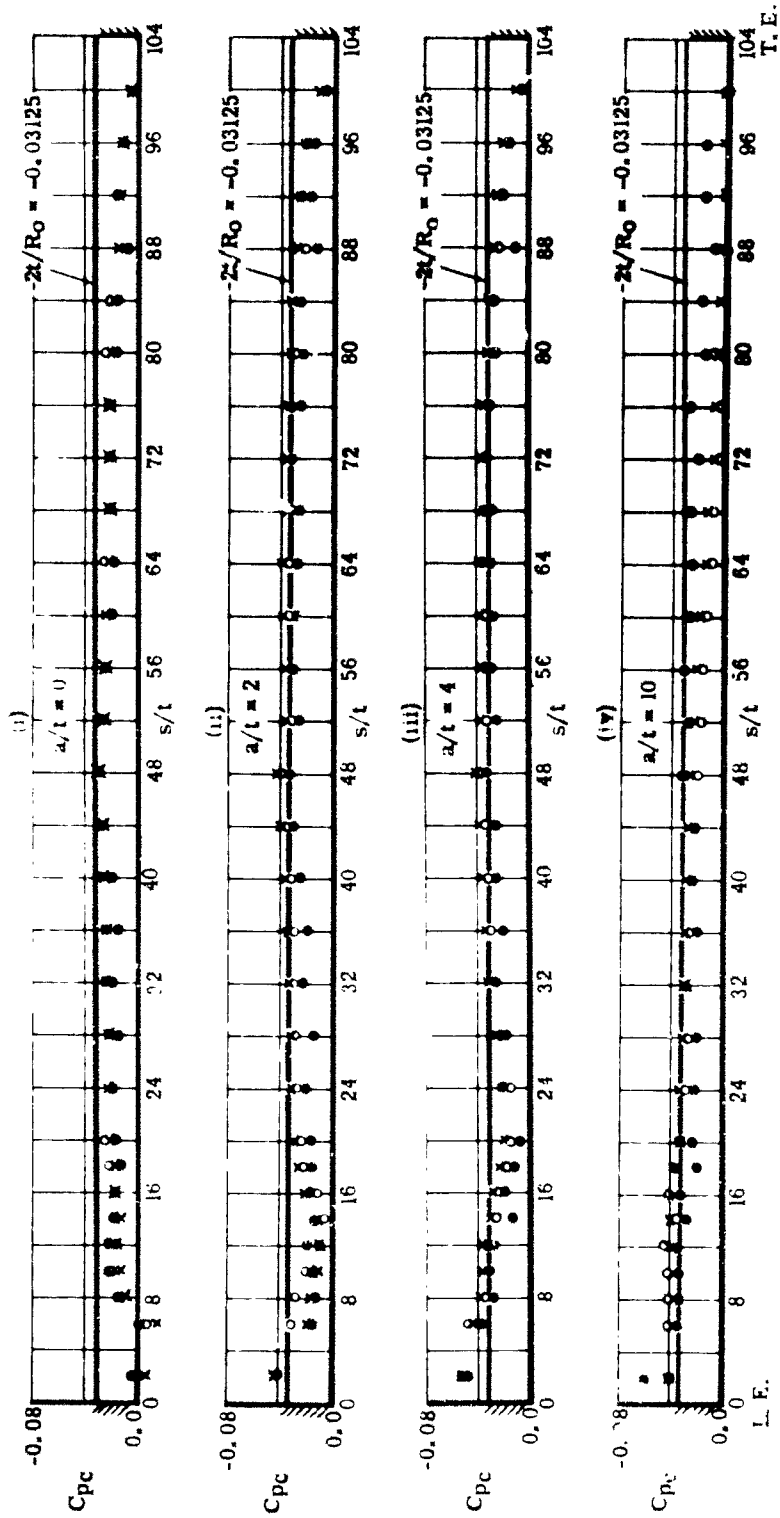


FIGURE 16d. EFFECT OF THE VERICAL GAP SIZE ON THE PRESSURE COEFFICIENTS CORRECTED FOR FLOW COMPRESSIBILITY AT VARIOUS NOZZLE PRESSURE RATIOS.

P.R. ≈ 1.2 ●
 1.7 ○
 2.2 x

$t/16 = FV/4 - R_0 4.0$

$L/t = 16$

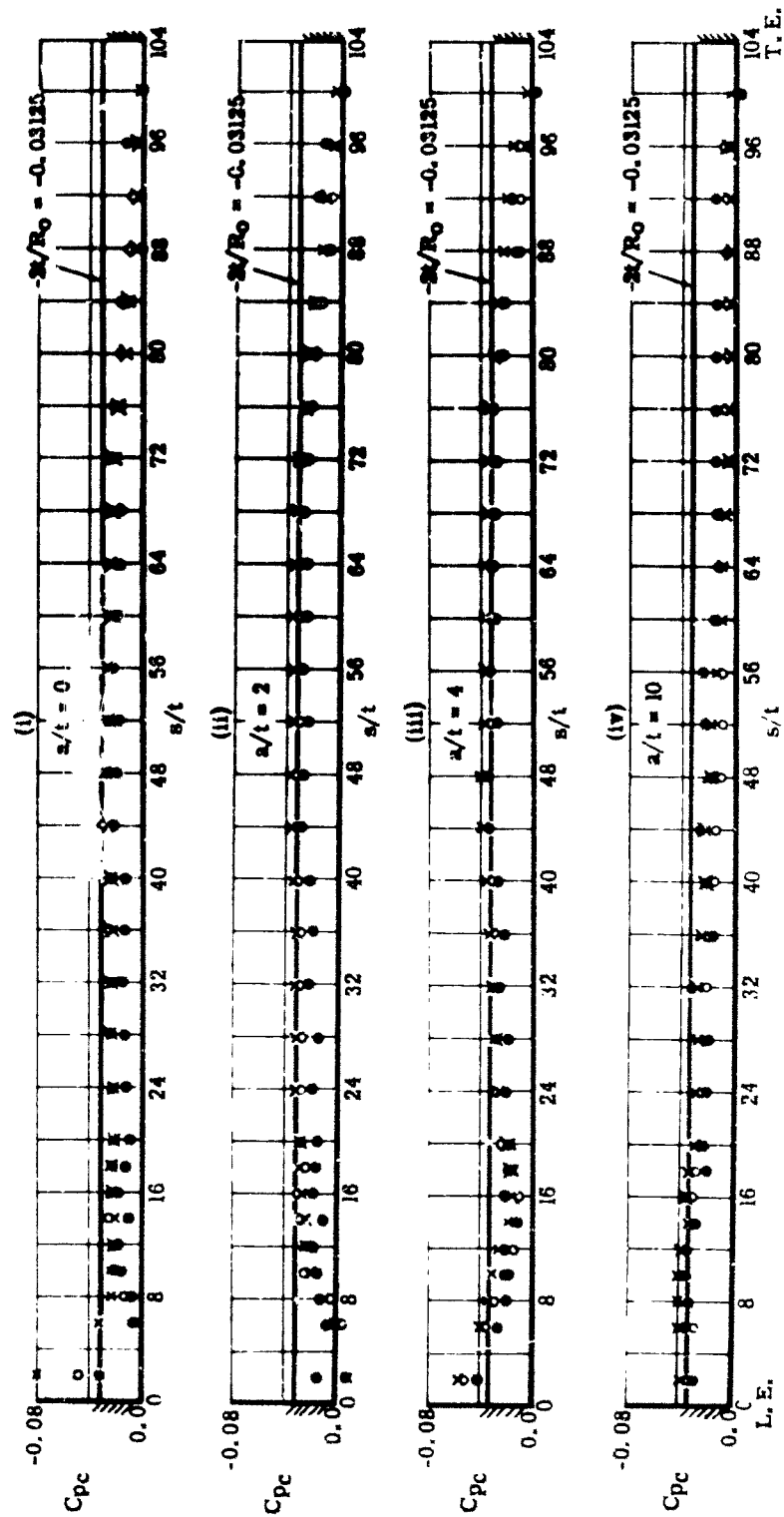


FIGURE 16c. EFFECT OF THE VERTICAL GAP SIZE ON THE PRESSURE COEFFICIENTS CORRECTED FOR FLOW COMPRESSIBILITY AT VARIOUS NOZZLE PRESSURE RATIOS.

P. R. \approx 1.2 \bullet
 L. 7 \circ
 2.2 \times

$$1\sqrt{16} - F\sqrt{4} - R_0 4.0$$

$$l/t = 32$$

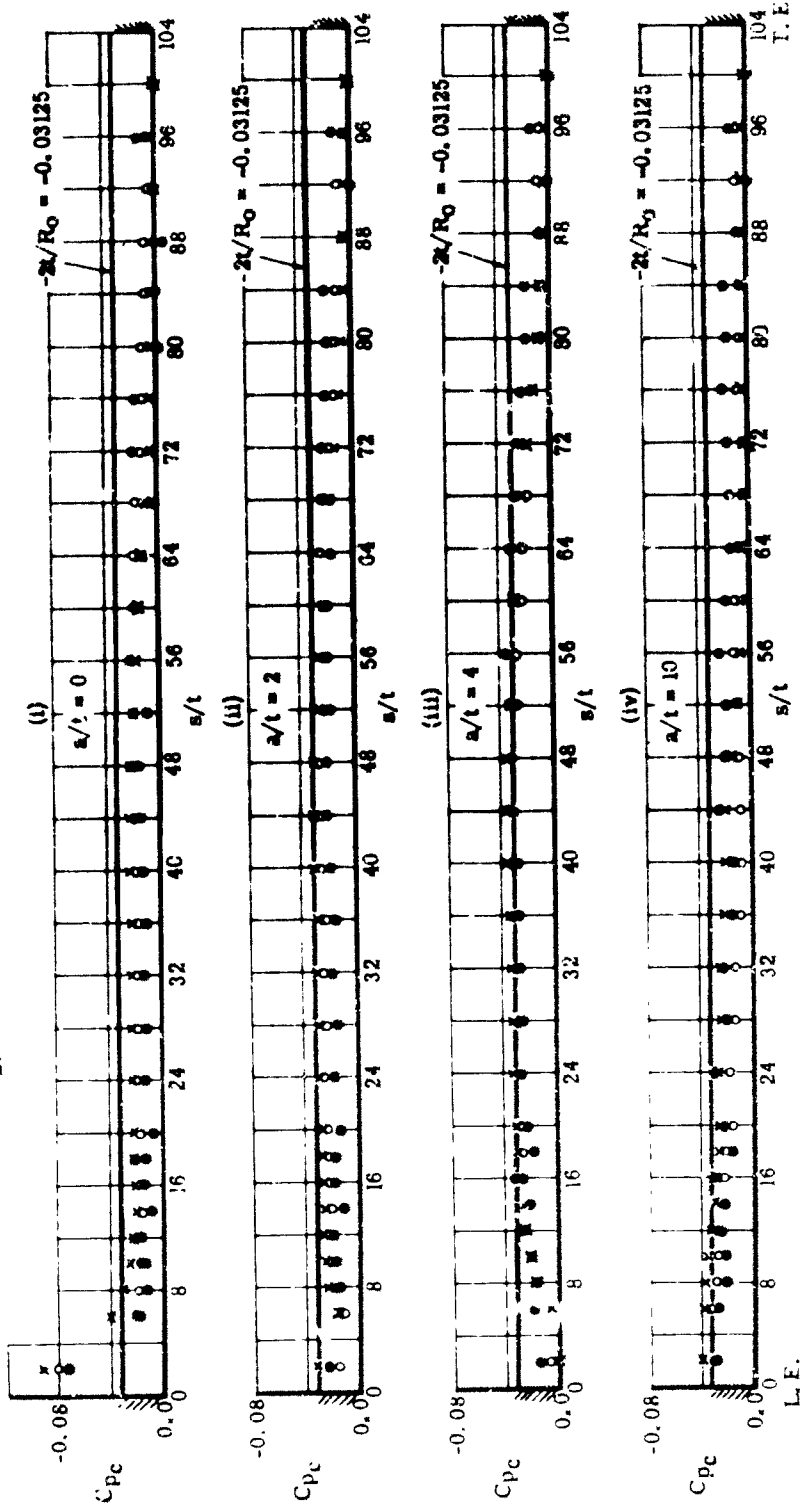


FIGURE 16d. EFFECT OF THE VERTICAL GAP SIZE ON THE PRESSURE COEFFICIENTS CORRECTED FOR FLOW COMPRESSIBILITY AT VARIOUS NOZZLE PRESSURE RATIOS.

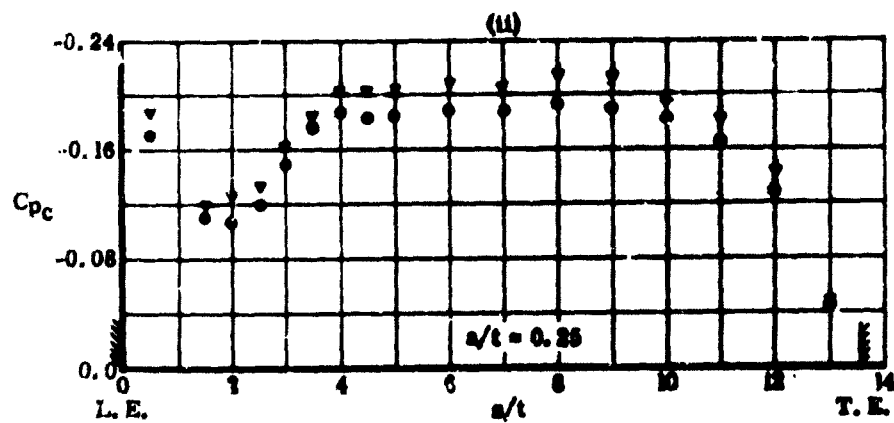
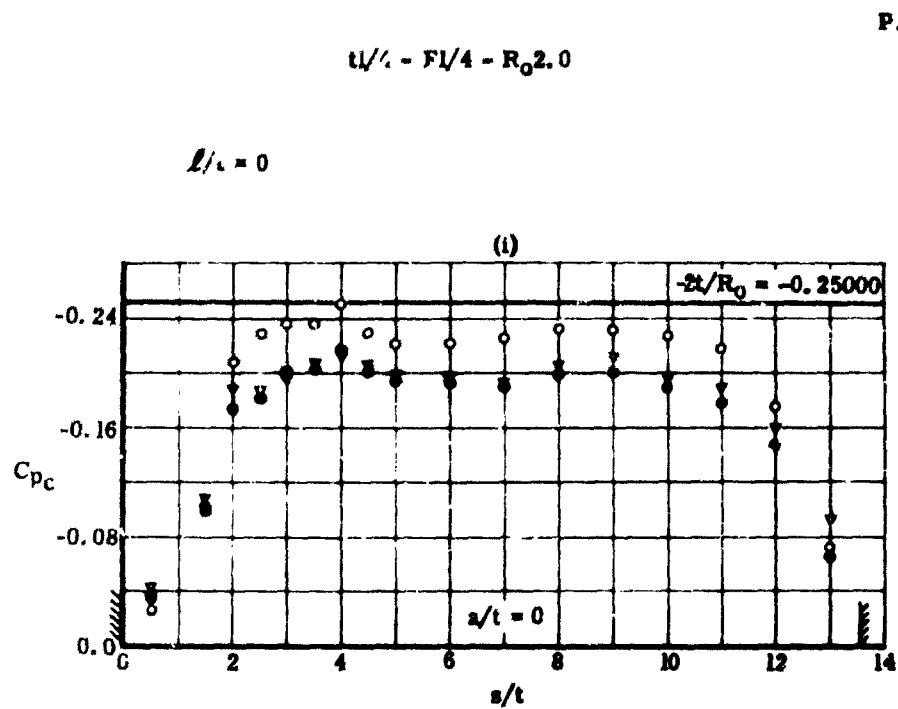


FIGURE 17a. EFFECT OF THE VERTICAL GAP SIZE ON THE PRESSURE COEFFICIENTS CORRECTED FOR FLOW COMPRESSIBILITY AT VARIOUS NOZZLE PRESSURE RATIOS.

$t/4 - F/4 - R_0 2.0$

P. R. \approx L1 ∇
L2 \bullet
L7 \circ

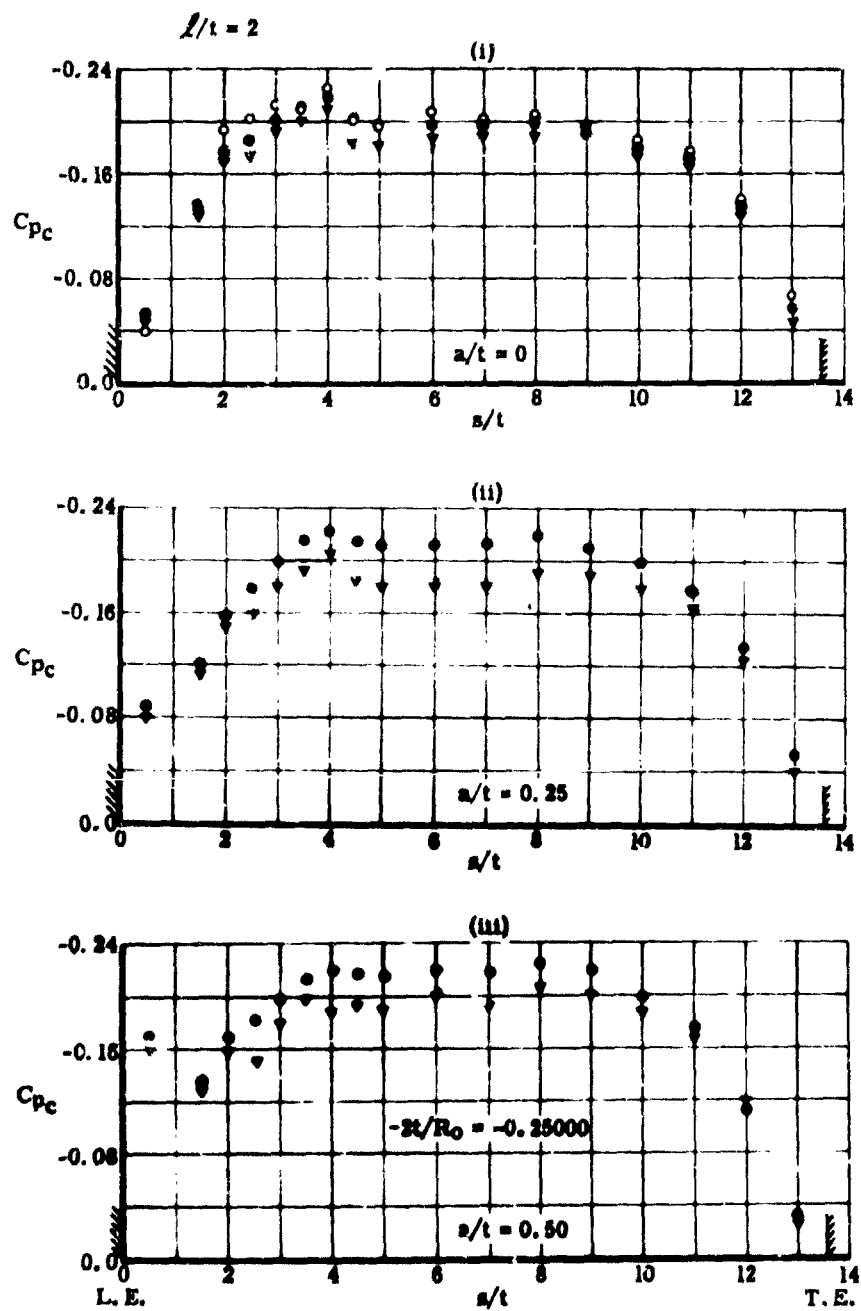


FIGURE 17b. EFFECT OF THE VERTICAL GAP SIZE ON THE PRESSURE COEFFICIENTS CORRECTED FOR FLOW COMPRESSIBILITY AT VARIOUS NOZZLE PRESSURE RATIOS.

FIGU

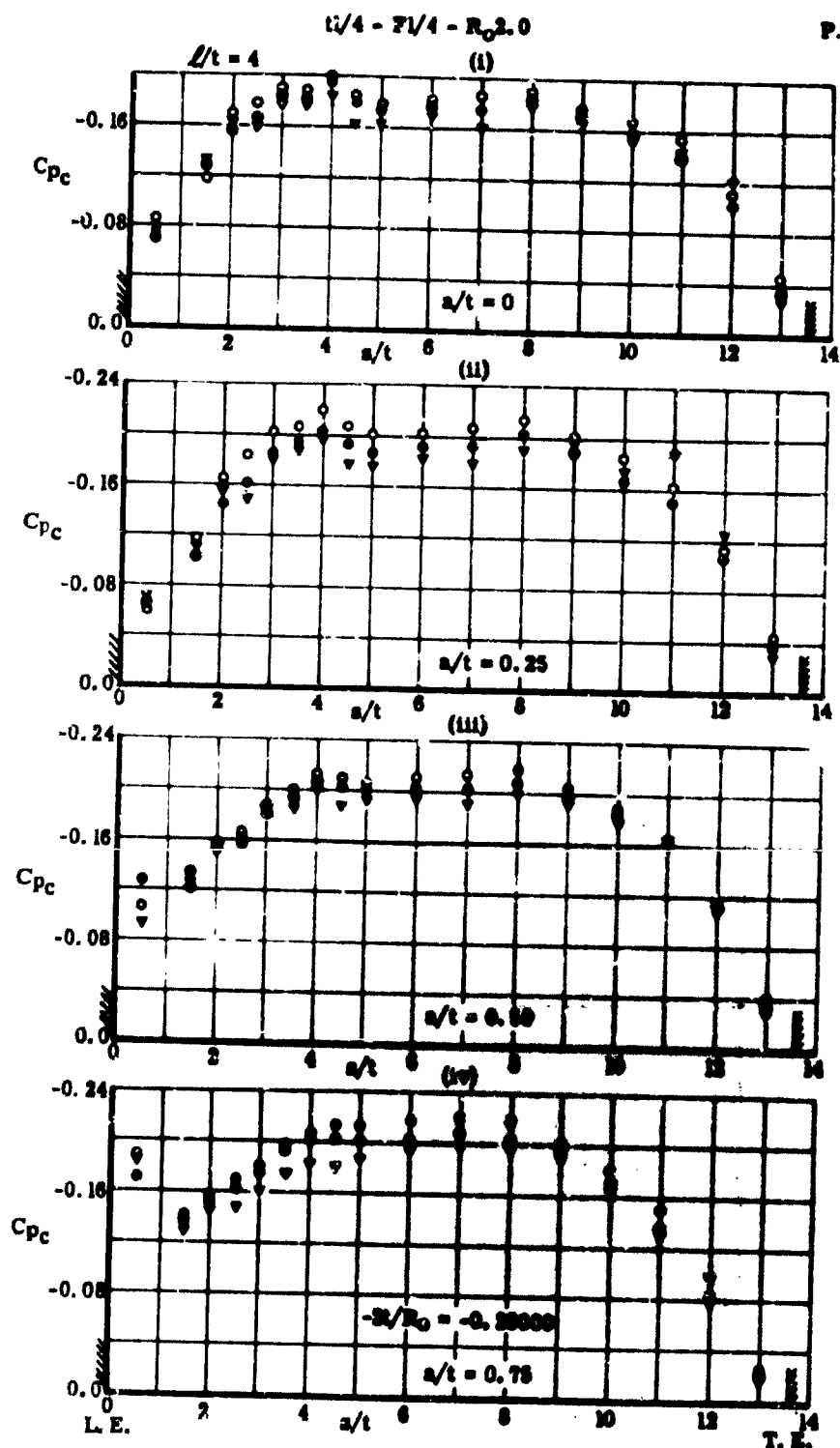


FIGURE 17c. EFFECT OF THE VERTICAL GAP SIZE ON THE PRESSURE COEFFICIENTS CORRECTED FOR FLOW COMPRESSIBILITY AT VARIOUS NOZZLE PRESSURE RATIOS.

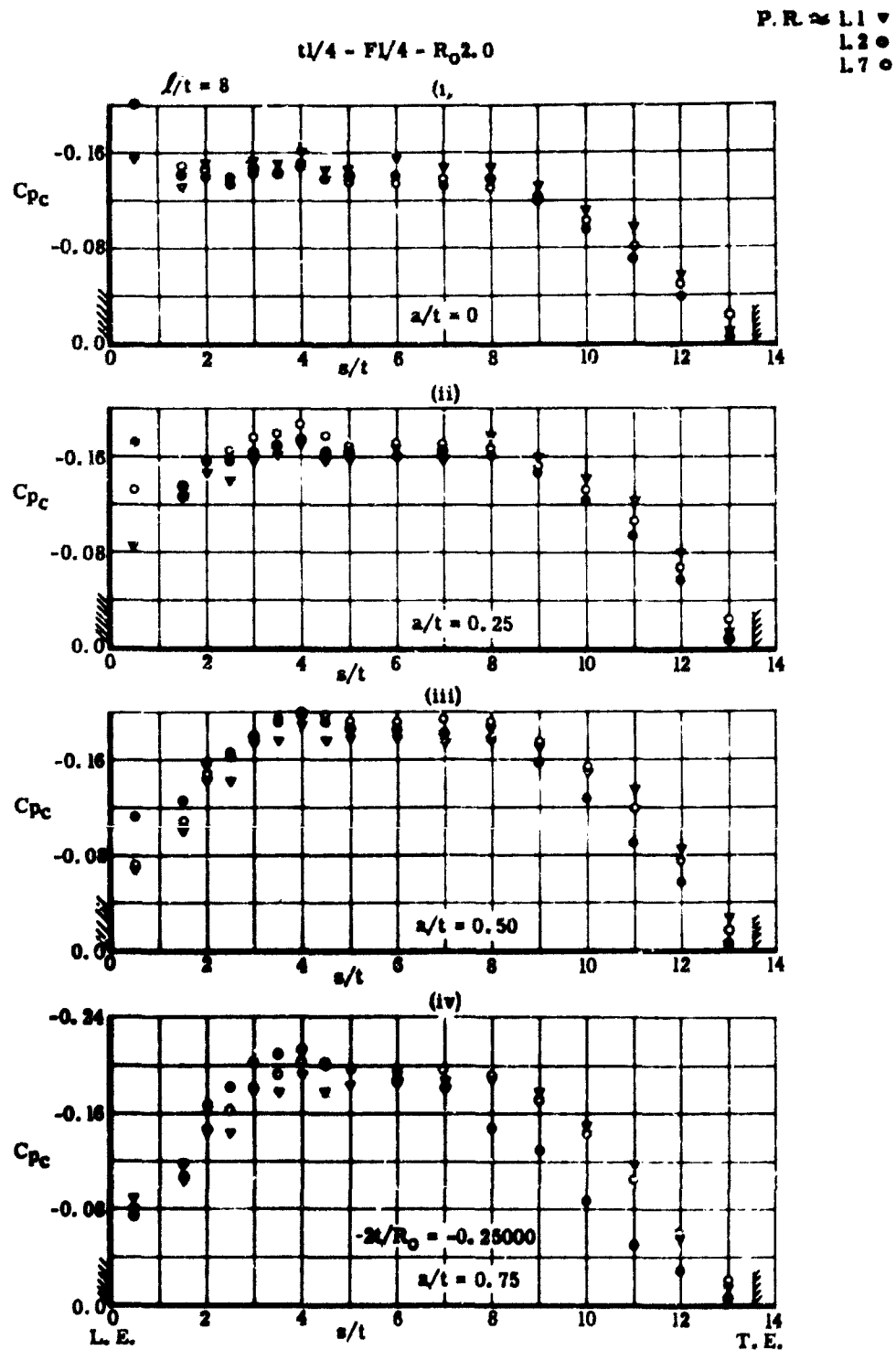


FIGURE 17d. EFFECT OF THE VERTICAL GAP SIZE ON THE PRESSURE COEFFICIENTS CORRECTED FOR FLOW COMPRESSIBILITY AT VARIOUS NOZZLE PRESSURE RATIOS.

1/4 - F1/4 - R₀3.0

P.R. ≈ L1 ▽
L2 ●
L7 ○

$\beta/t = 0$

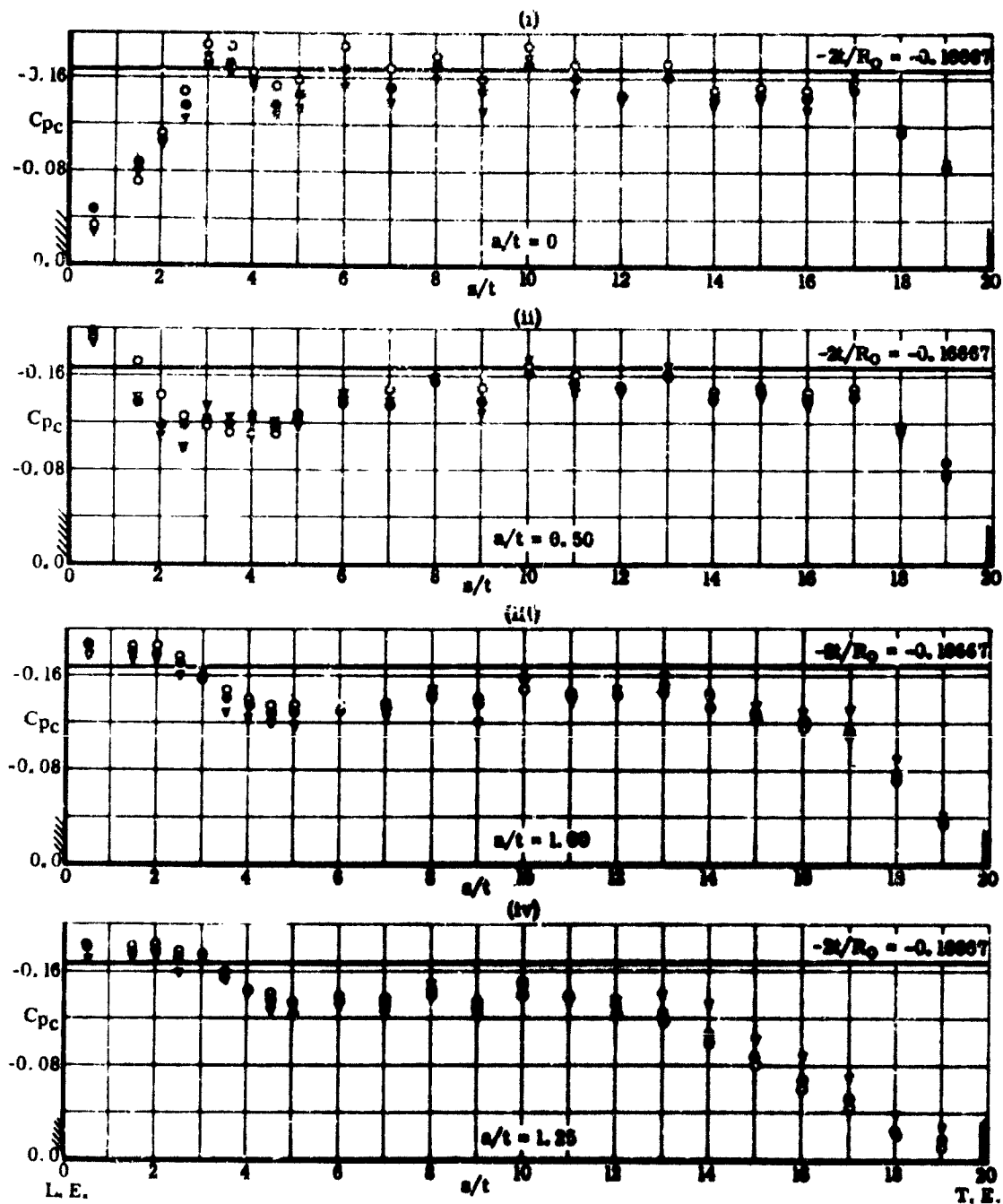


FIGURE 18a. EFFECT OF THE VERTICAL GAP SIZE ON THE PRESSURE COEFFICIENTS CORRECTED FOR FLOW COMPRESSIBILITY AT VARIOUS NOZZLE PRESSURE RATIOS.

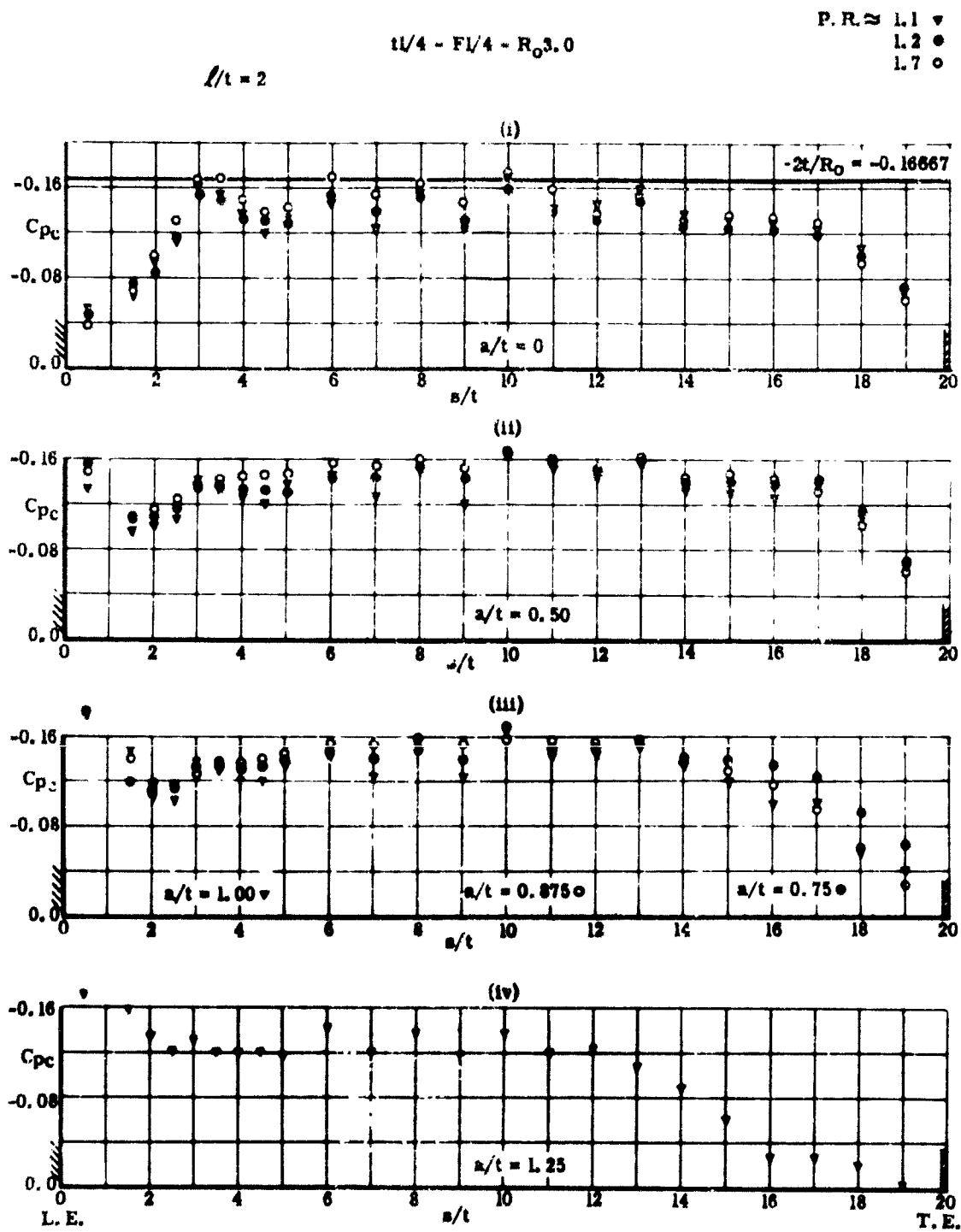


FIGURE 18b. EFFECT OF THE VERTICAL GAP SIZE ON THE PRESSURE COEFFICIENTS CORRECTED FOR FLOW COMPRESSIBILITY AT VARIOUS NOZZLE PRESSURE RATIOS.

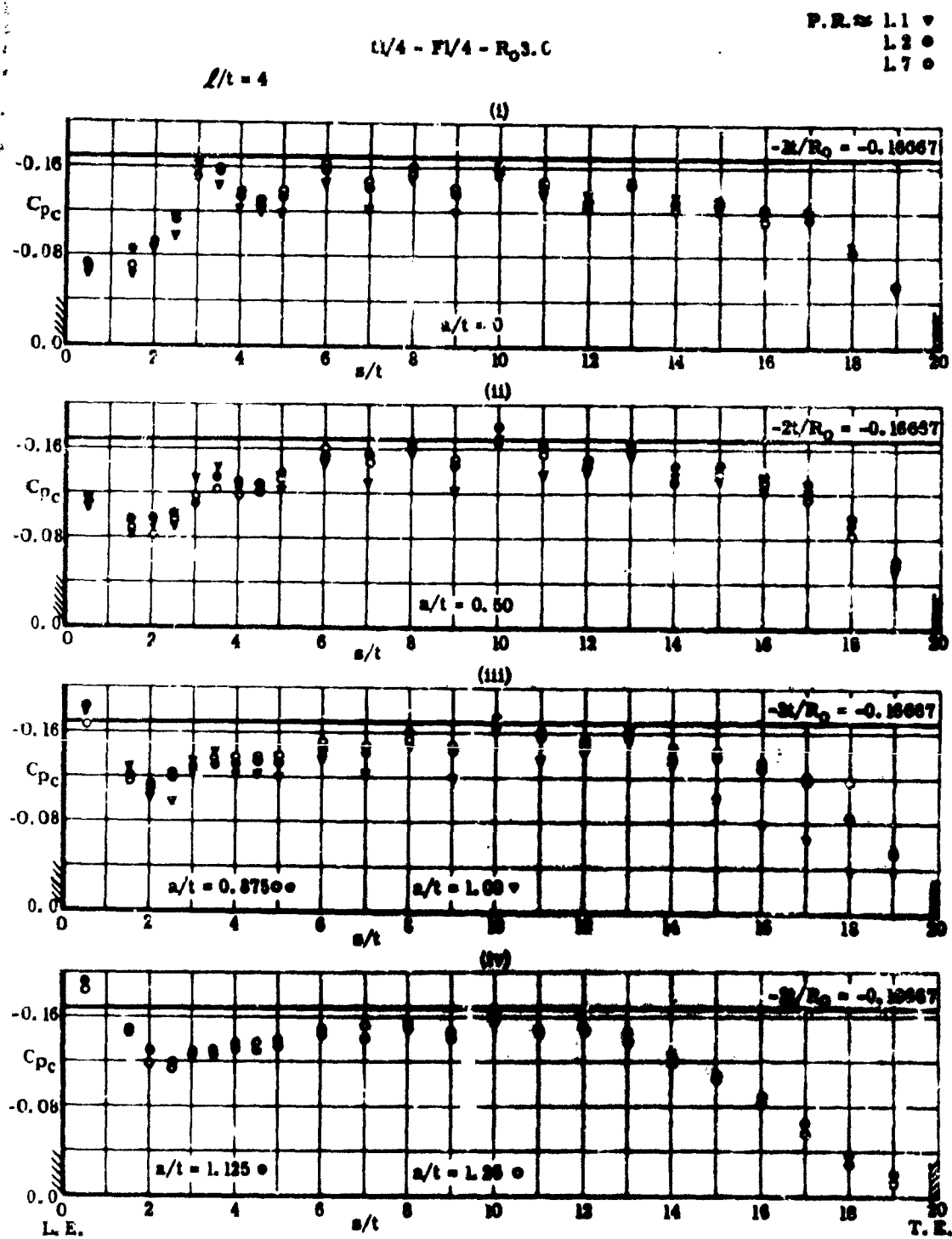


FIGURE 18c. EFFECT OF THE VERTICAL GAP SIZE ON THE PRESSURE COEFFICIENTS CORRECTED FOR FLOW COMPRESSIBILITY AT VARIOUS NOZZLE PRESSURE RATIOS.

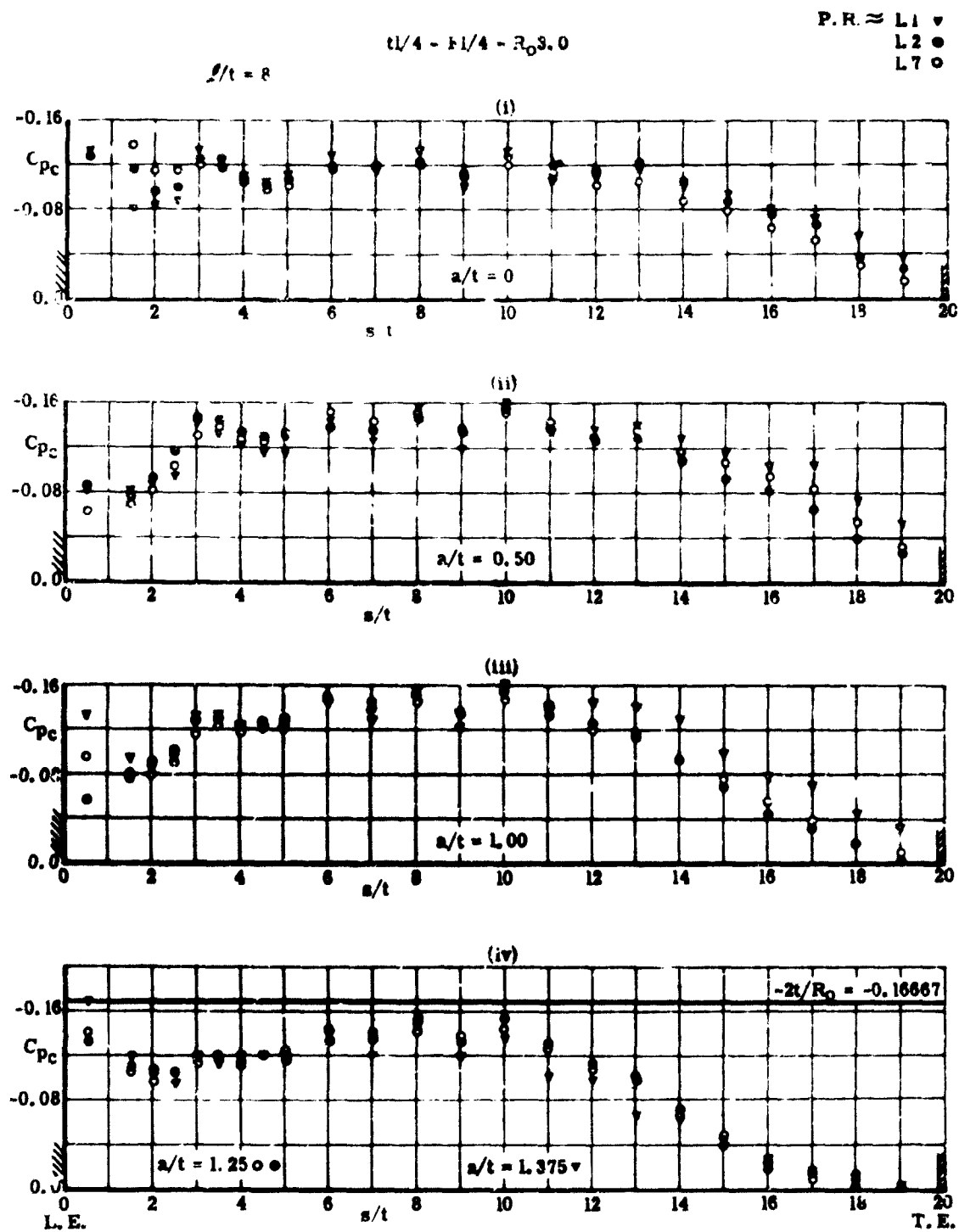


FIGURE 18d. EFFECT OF THE VERTICAL GAP SIZE ON THE PRESSURE COEFFICIENTS CORRECTED FOR FLOW COMPRESSIBILITY AT VARIOUS NOZZLE PRESSURE RATIOS.

P. R. 20
L11 v
L20
L70

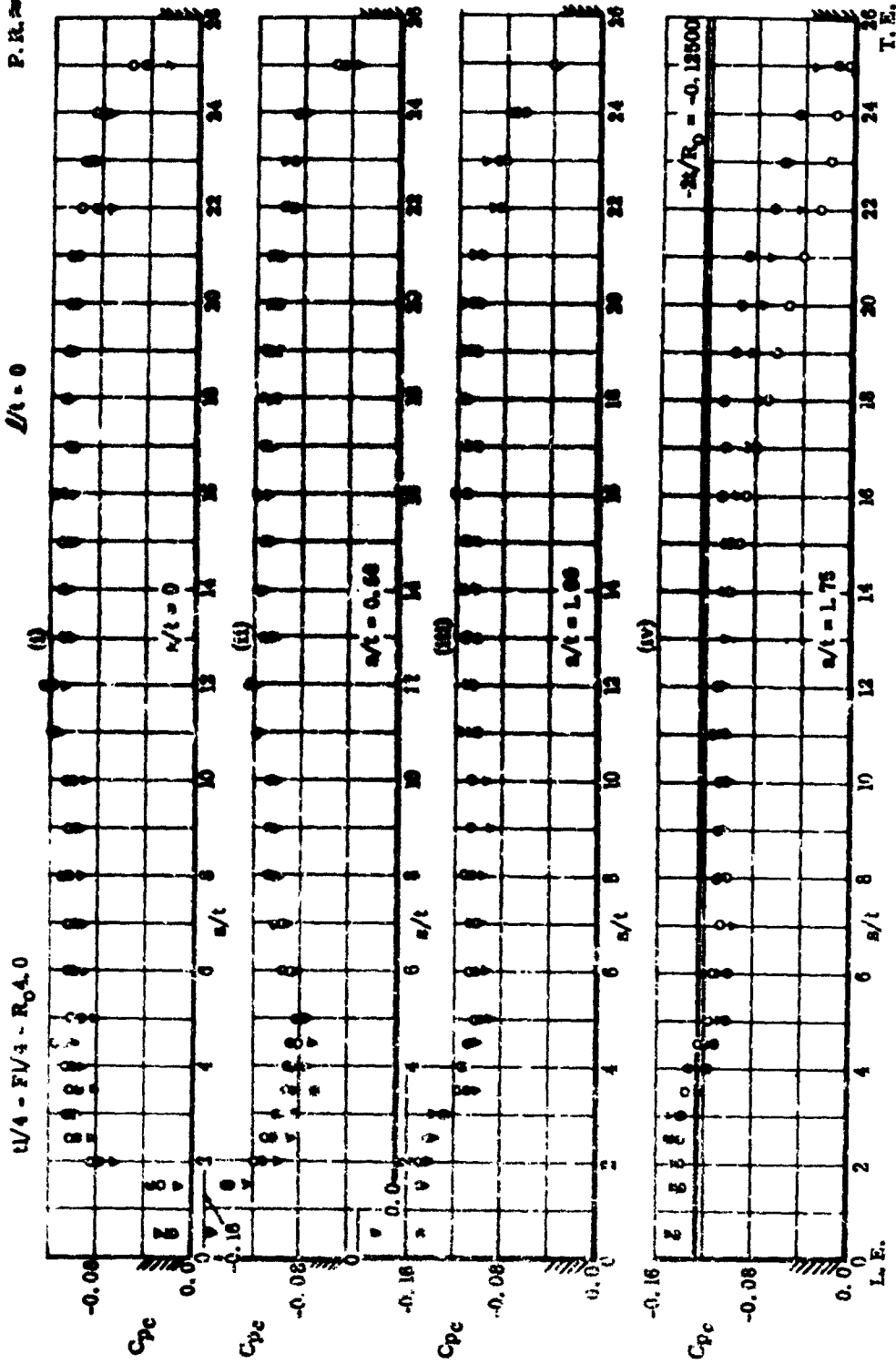


FIGURE 19a.
EFFECT OF THE VERTICAL GAP SIZE ON THE PRESSURE COEFFICIENTS
CORRECTED FOR FLOW COMPRESSIBILITY AT VARIOUS NOZZLE PRESSURE
RATIOS.

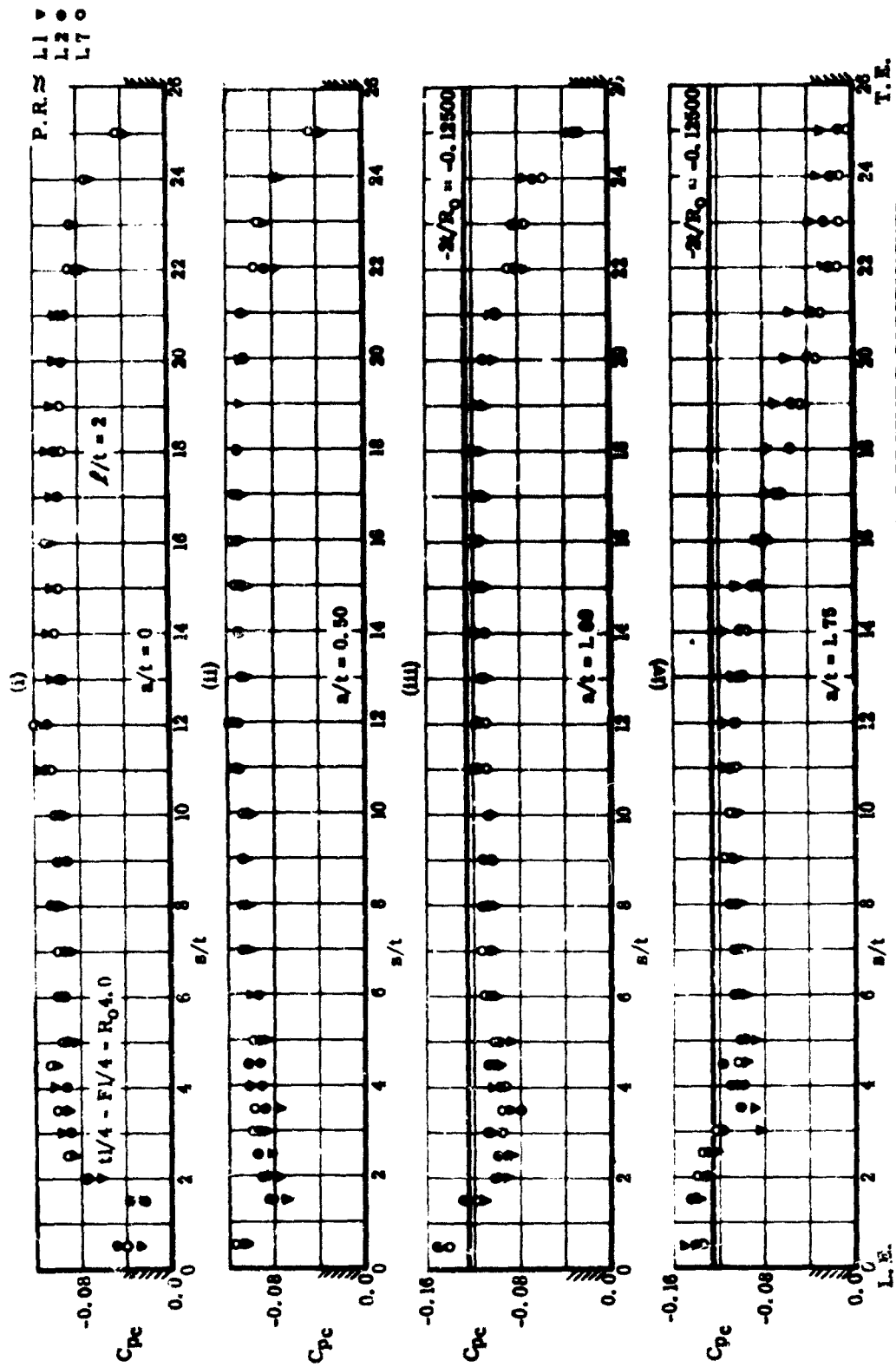


FIGURE 19b.
EFFECT OF THE VERTICAL GAP SIZE ON THE PRESSURE COEFFICIENTS
CORRECTED FOR FLOW COMPRESSIBILITY AT VARIOUS NOZZLE PRESSURE
RATIOS.

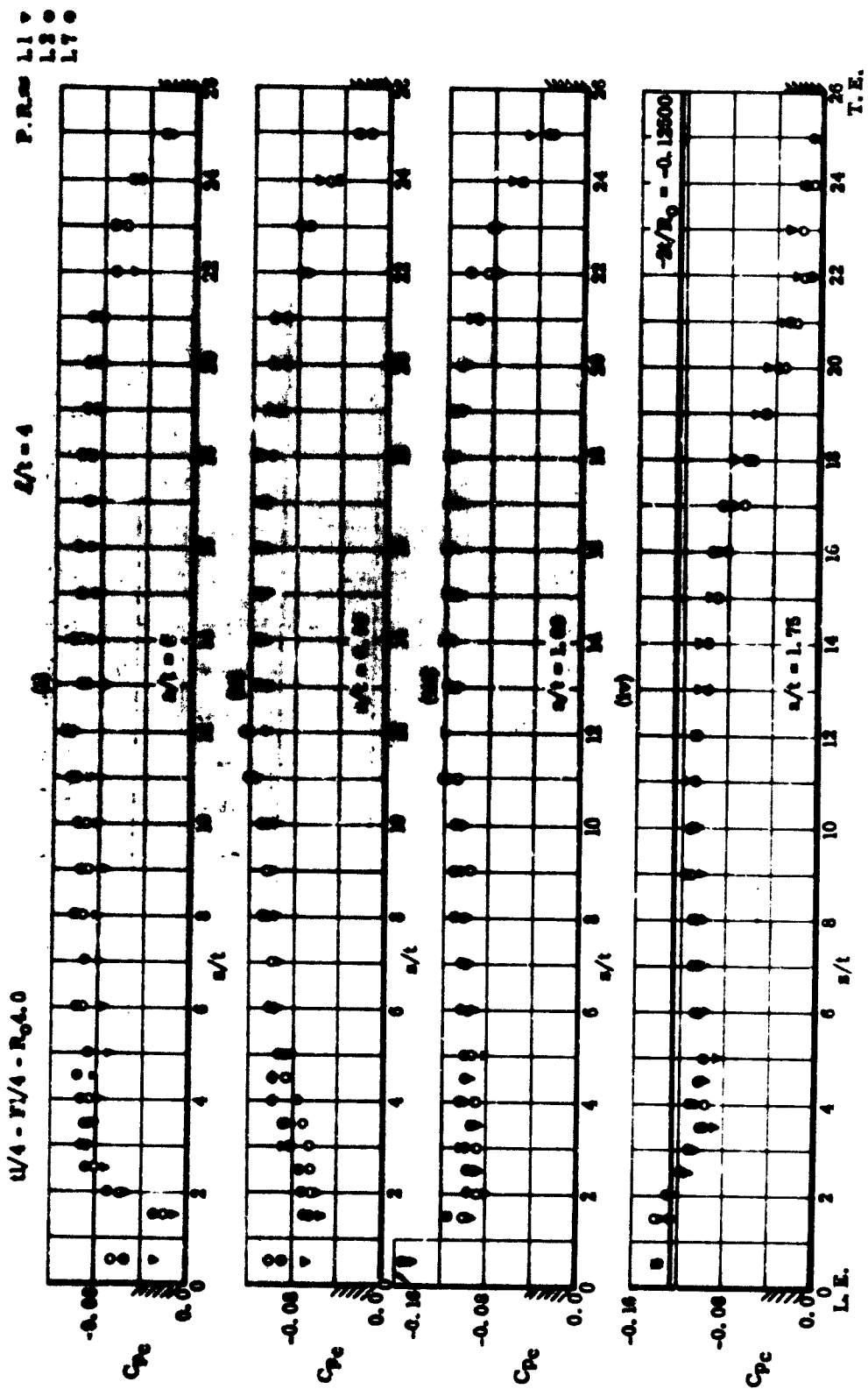


FIGURE 19c. EFFECT OF THE VERTICAL GAP SIZE ON THE PRESSURE COEFFICIENTS CORRECTED FOR FLOW COMPRESSIBILITY AT VARIOUS NOZZLE PRESSURE RATIOS.

$\Gamma.R. \approx$ L.1 ∇
 L.2 \bullet
 L.7 \circ

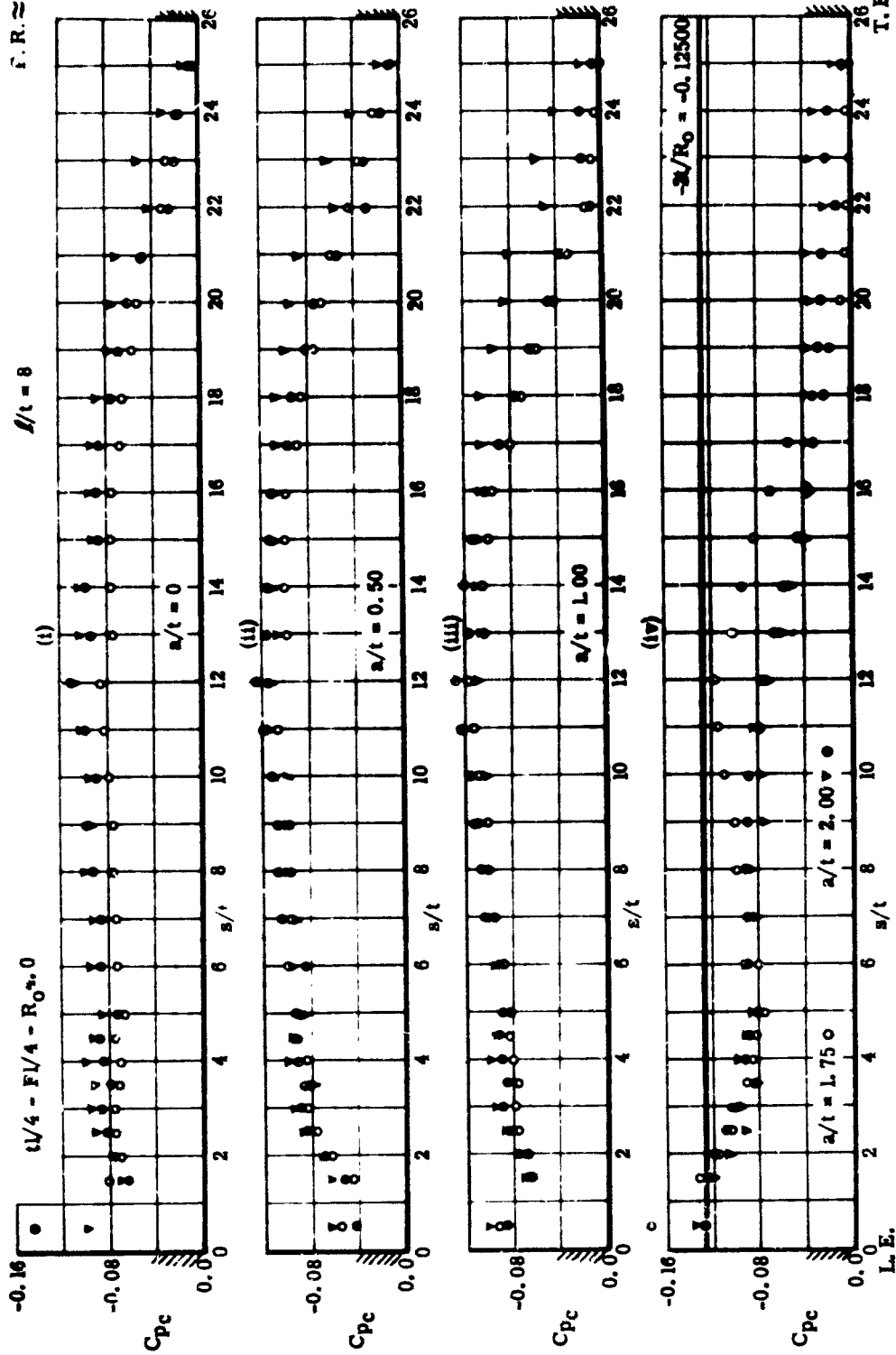


FIGURE 19d. EFFECT OF THE VERTICAL GAP SIZE ON THE PRESSURE COEFFICIENTS CORRECTED FOR FLOW COMPRESSIBILITY AT VARIOUS NOZZLE PRESSURE RATIOS.

$$t/16 - P/4 - R_0 X$$

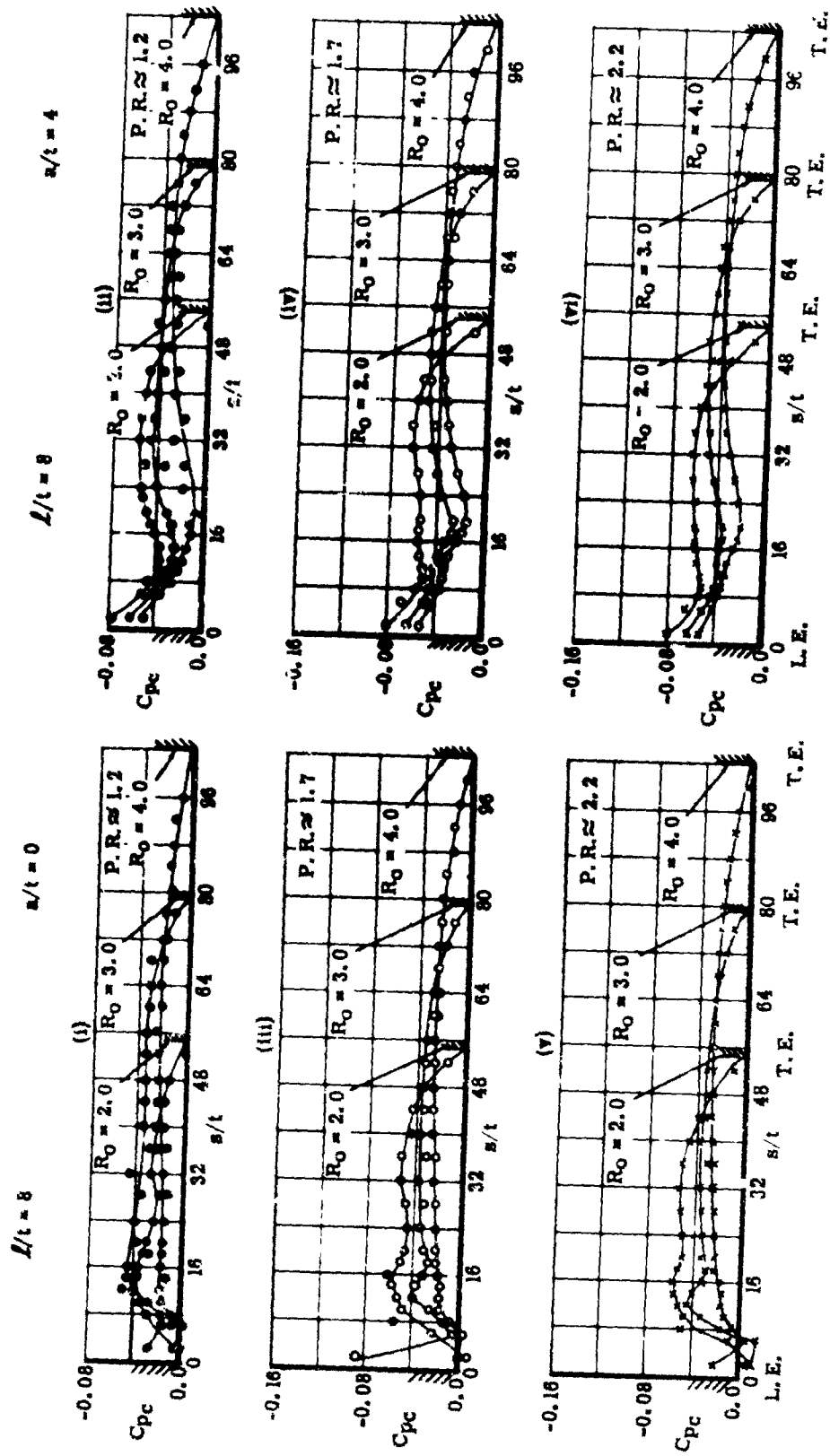


FIGURE 20.
EFFECT OF THE VERTICAL GAP SIZE ON THE PRESSURE COEFFICIENTS
CORRECTED FOR FLOW COMPRESSIBILITY FOR DIFFERENT DEFLECTION
SURFACE RADII AT VARIOUS NOZZLE PRESSURE RATIOS.

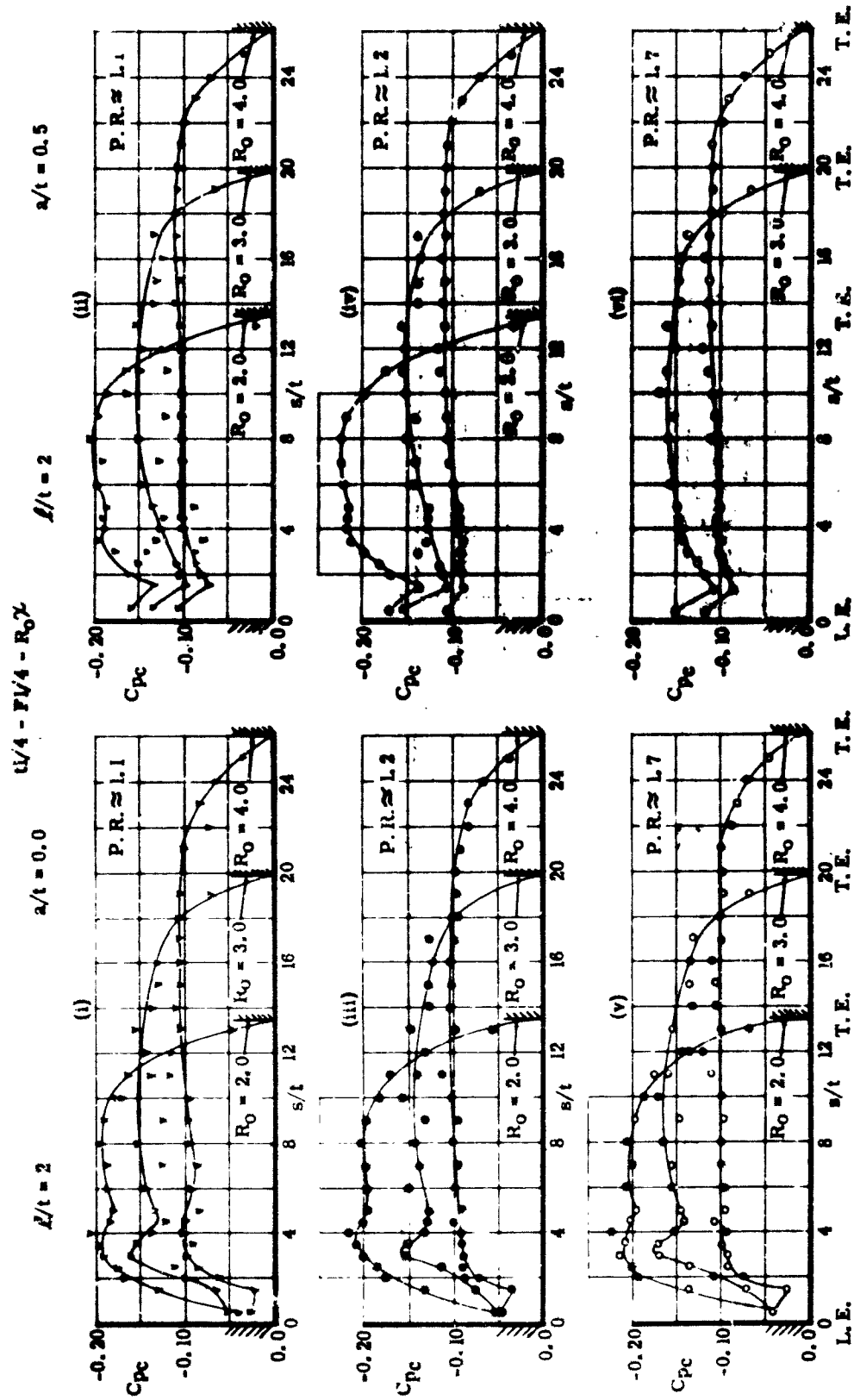


FIGURE 2L
EFFECT OF THE VERTICAL GAP SIZE ON THE PRESSURE COEFFICIENTS
CORRECTED FOR FLOW COMPRESSIBILITY FOR DIFFERENT DEFLECTION
SURFACE RADII AT VARIOUS NOZZLE PRESSURE RATIOS.

$t/16 - F/4 - R_0 3.0$

P.R. \approx L D
 1.1 $\nabla \nabla$
 1.2 $\circ \circ$
 1.7 $\circ \circ$
 2.2 $\times \bullet$

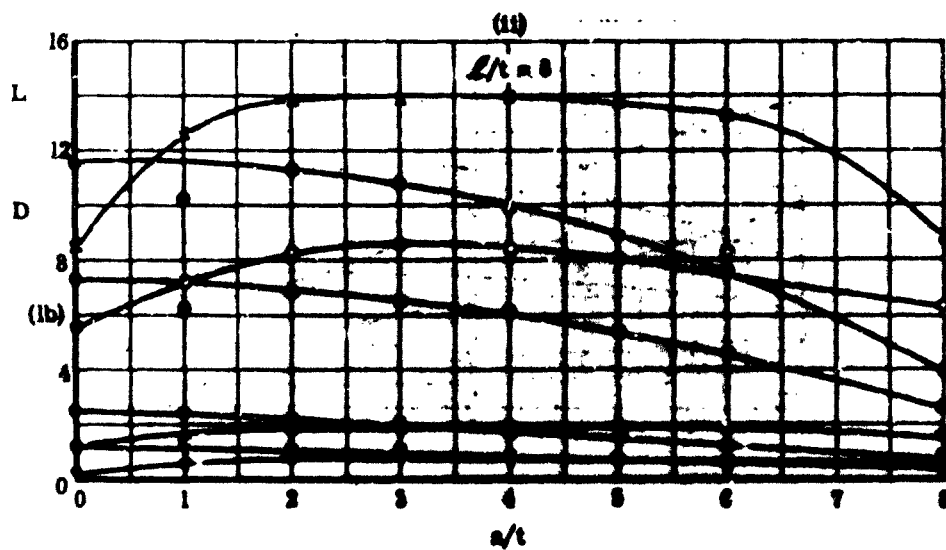
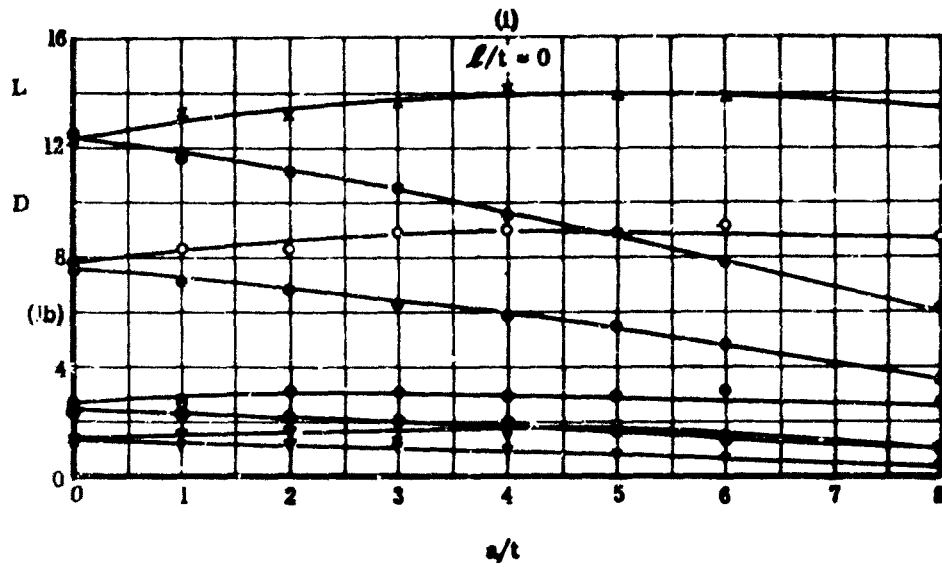


FIGURE 22a. EFFECT OF THE VERTICAL GAP SIZE ON THE MEASURED LIFT AND DRAG FORCES ACTING ON THE DEFLECTION SURFACE AT VARIOUS NOZZLE PRESSURE RATIOS.

$t/l/16 - F1/4 - R_0 3 0$

P. R. \approx L D
 1.1 ∇ ∇
 1.2 \bullet \bullet
 1.7 \circ \bullet
 2.2 \times \bullet

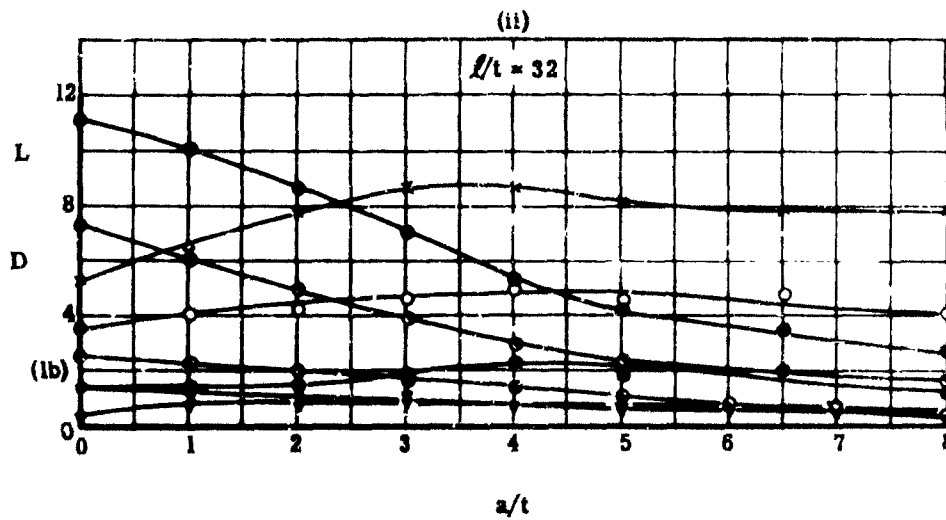
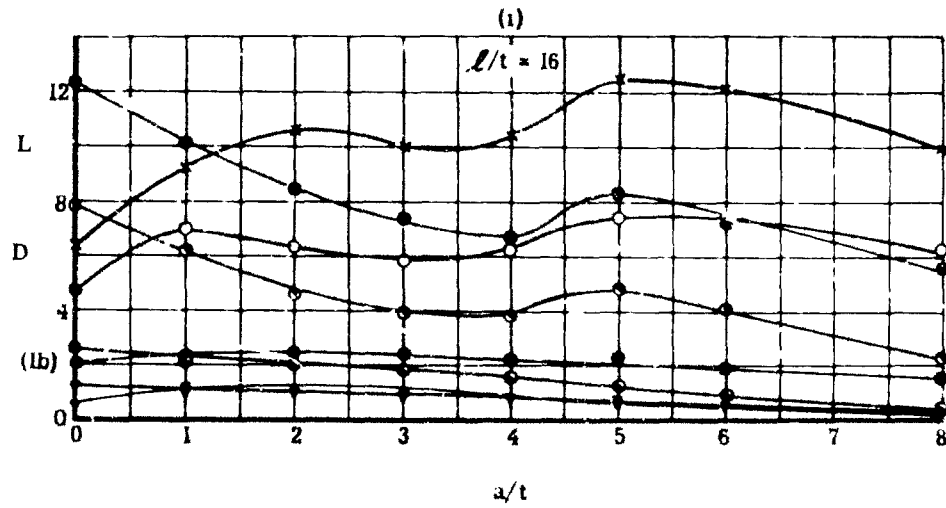


FIGURE 22b. EFFECT OF THE VERTICAL GAP SIZE ON THE MEASURED LIFT AND DRAG FORCES ACTING ON THE DEFLECTION SURFACE AT VARIOUS NOZZLE PRESSURE RATIOS.

$t/4 - F/4 - R_0 3.0$

P. R. \approx L D
 1.1 ∇ ∇
 1.2 \bullet \bullet
 1.7 \circ \bullet

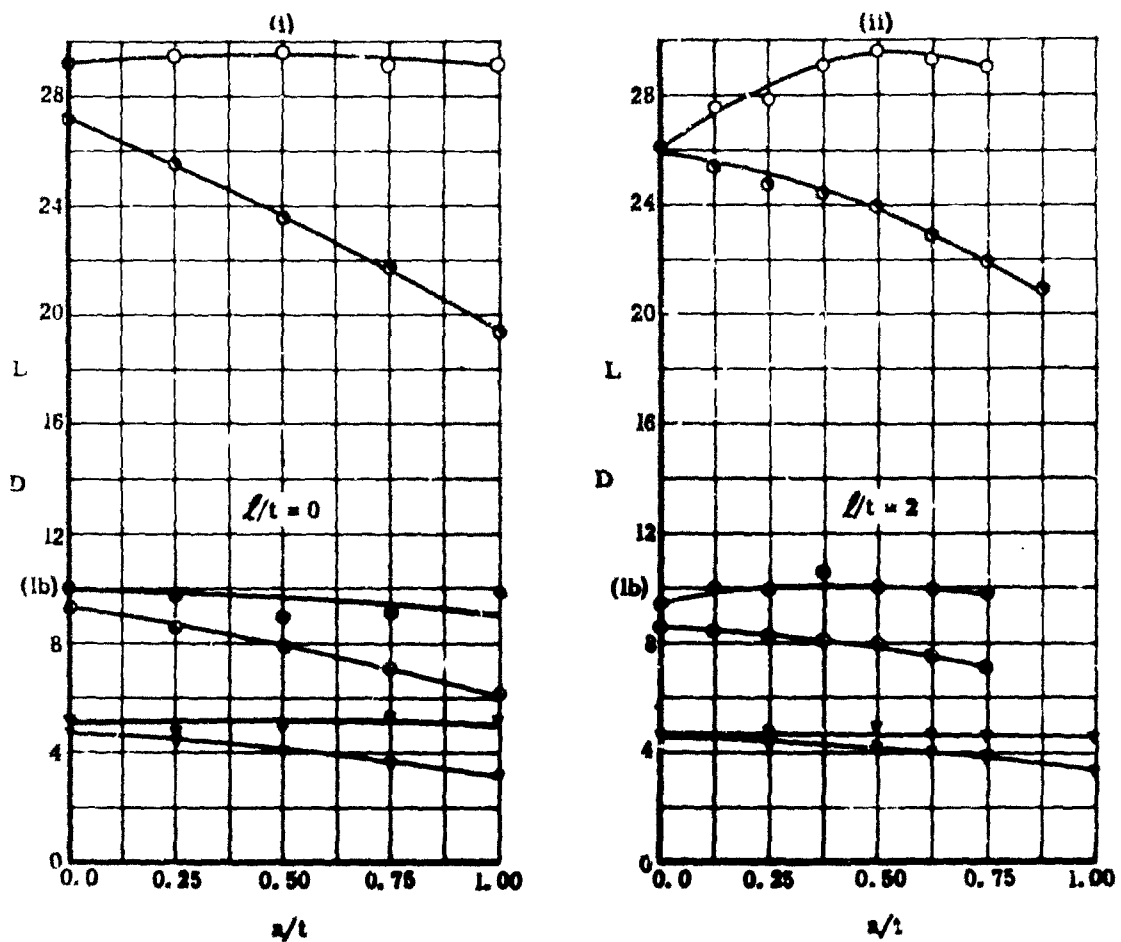


FIGURE 23a. EFFECT OF THE VERTICAL GAP SIZE ON THE MEASURED LIFT AND DRAG FORCES ACTING ON THE DEFLECTION SURFACE AT VARIOUS NOZZLE PRESSURE RATIOS.

$$t/4 = F/4 = R_0 3.0$$

P. R. \approx L.1 ∇ ∇
 L.2 \bullet \bullet
 L.7 \circ \bullet

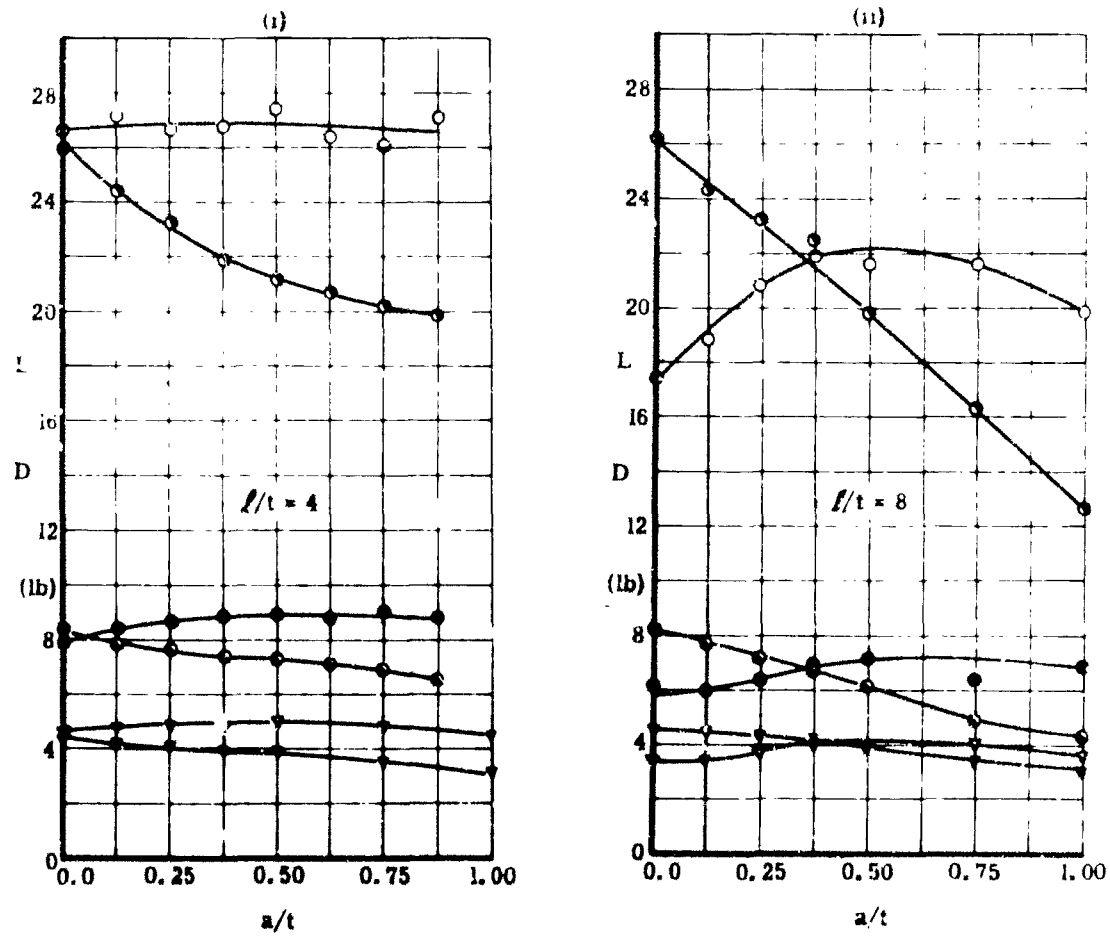
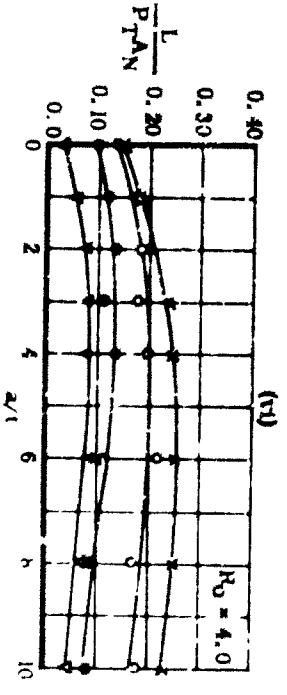
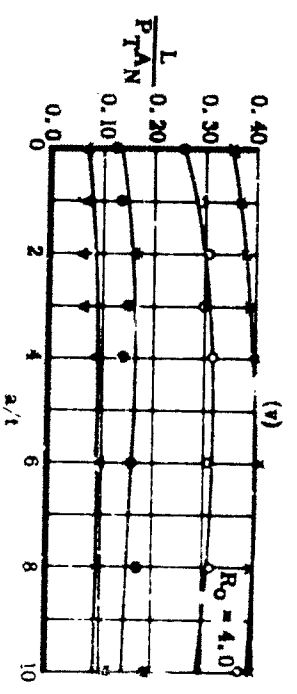
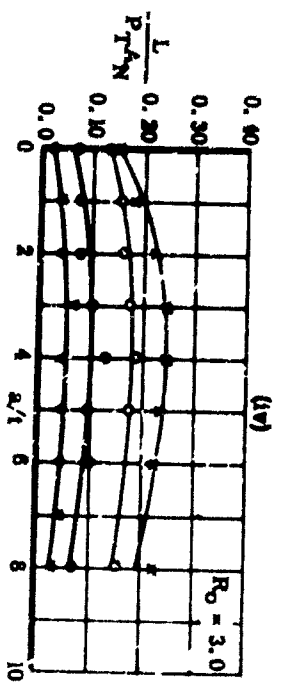
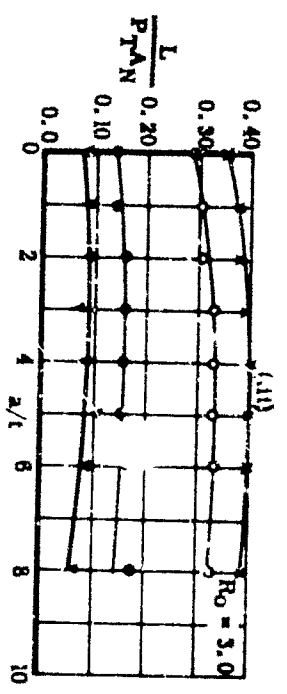
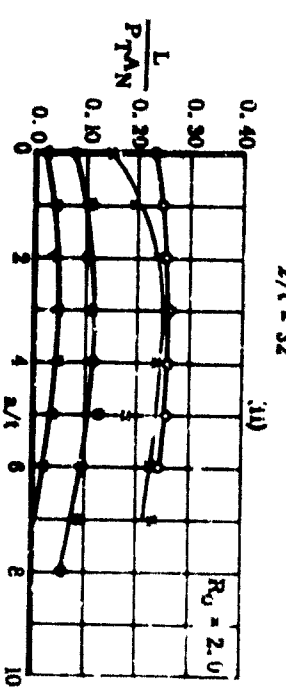
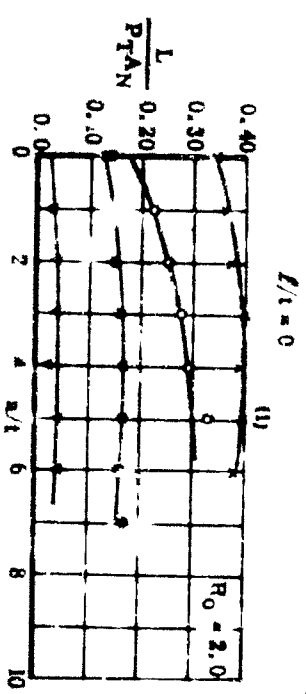


FIGURE 23b. EFFECT OF THE VERTICAL GAP SIZE ON THE MEASURED LIFT AND DRAG FORCES ACTING ON THE DEFLECTION SURFACE AT VARIOUS NOZZLE PRESSURE RATIOS.

P.R. ≈ L1 *
 L2 ●
 L7 ○
 2.2 x

$$\frac{L}{l} = \frac{P}{U} - R_0 \chi$$



53

FIGURE 24.

EFFECT OF THE HORIZONTAL AND VERTICAL GAP SIZES ON THE NON-DIMENSIONAL LIFT FORCE AT VARIOUS NOZZLE PRESSURE RATIOS AND DEFLECTION SURFACE RADII

$$L/l = 0 \quad F/L = R_0 \chi$$

P.R. ≈ 1.1 ▽
 1.2 ●
 1.7 ○

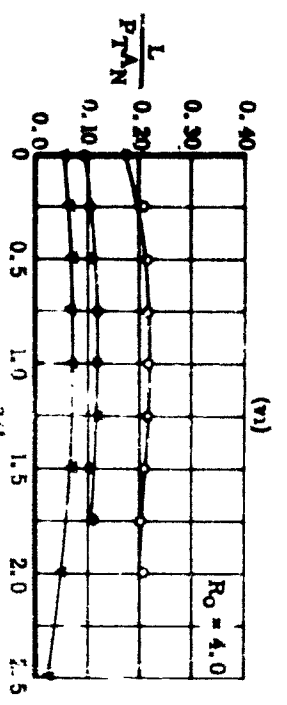
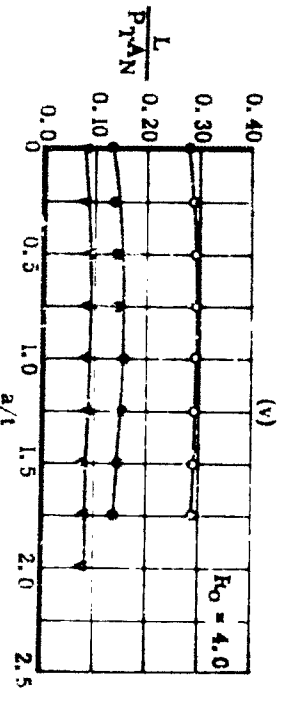
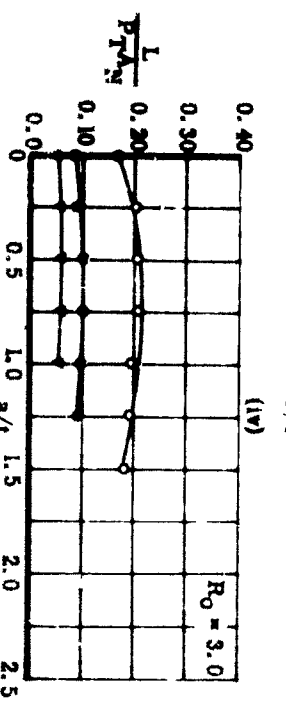
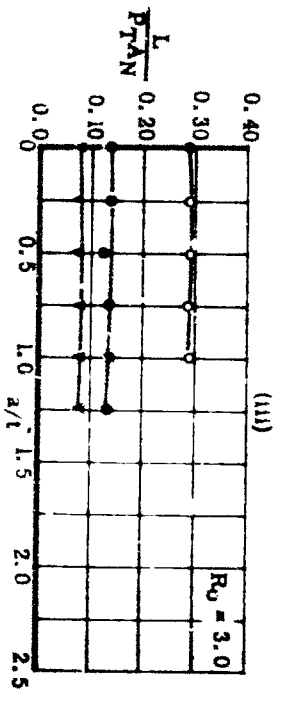
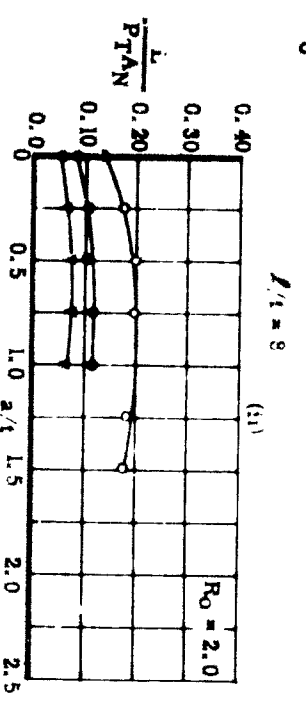
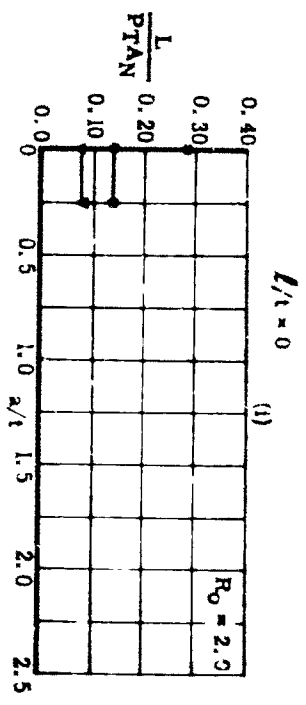


FIGURE 25. EFFECT OF THE HORIZONTAL, AND VERTICAL GAP SIZES ON THE NON-DIMENSIONAL LIFT FORCE AT VARIOUS NOZZLE PRESSURE RATIOS AND DEFLECTION SURFACE RADII.

$$l/16 - Fl/4 - R_0 \lambda$$

$$P.R. \approx 1.1 \nabla$$

$$1.2 \bullet$$

$$1.7 \circ$$

$$2.2 \times$$

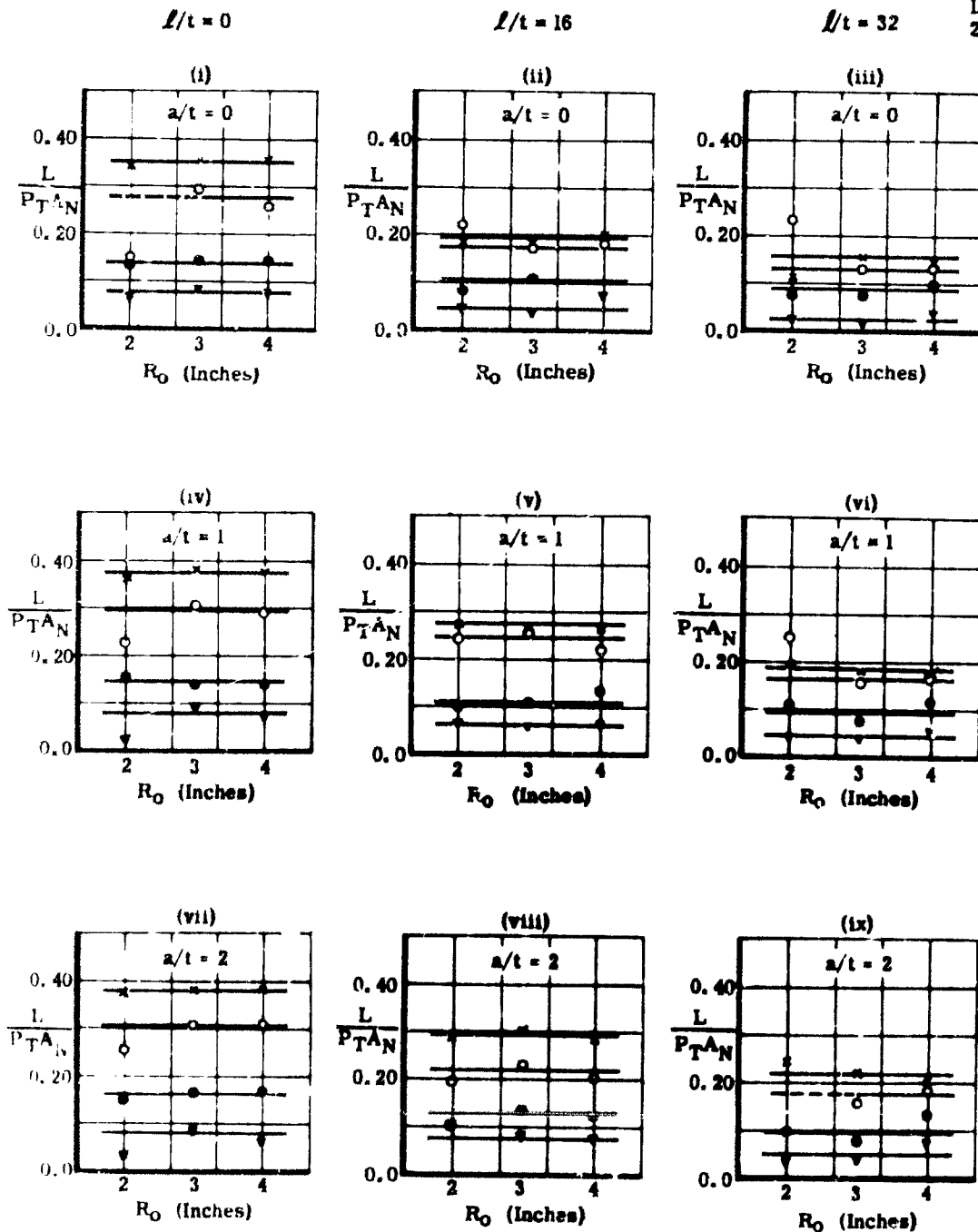


FIGURE 28a. EFFECT OF DEFLECTION SURFACE RADII ON THE NON-DIMENSIONAL LIFT FORCE FOR VARIOUS HORIZONTAL AND VERTICAL GAP SIZES AND NOZZLE PRESSURE RATIOS.

$$t/16 = Fl/4 - R_0 \chi$$

$$P.R. = L1 \nabla$$

$$L2 \circ$$

$$L7 \bullet$$

$$2.2 \times$$

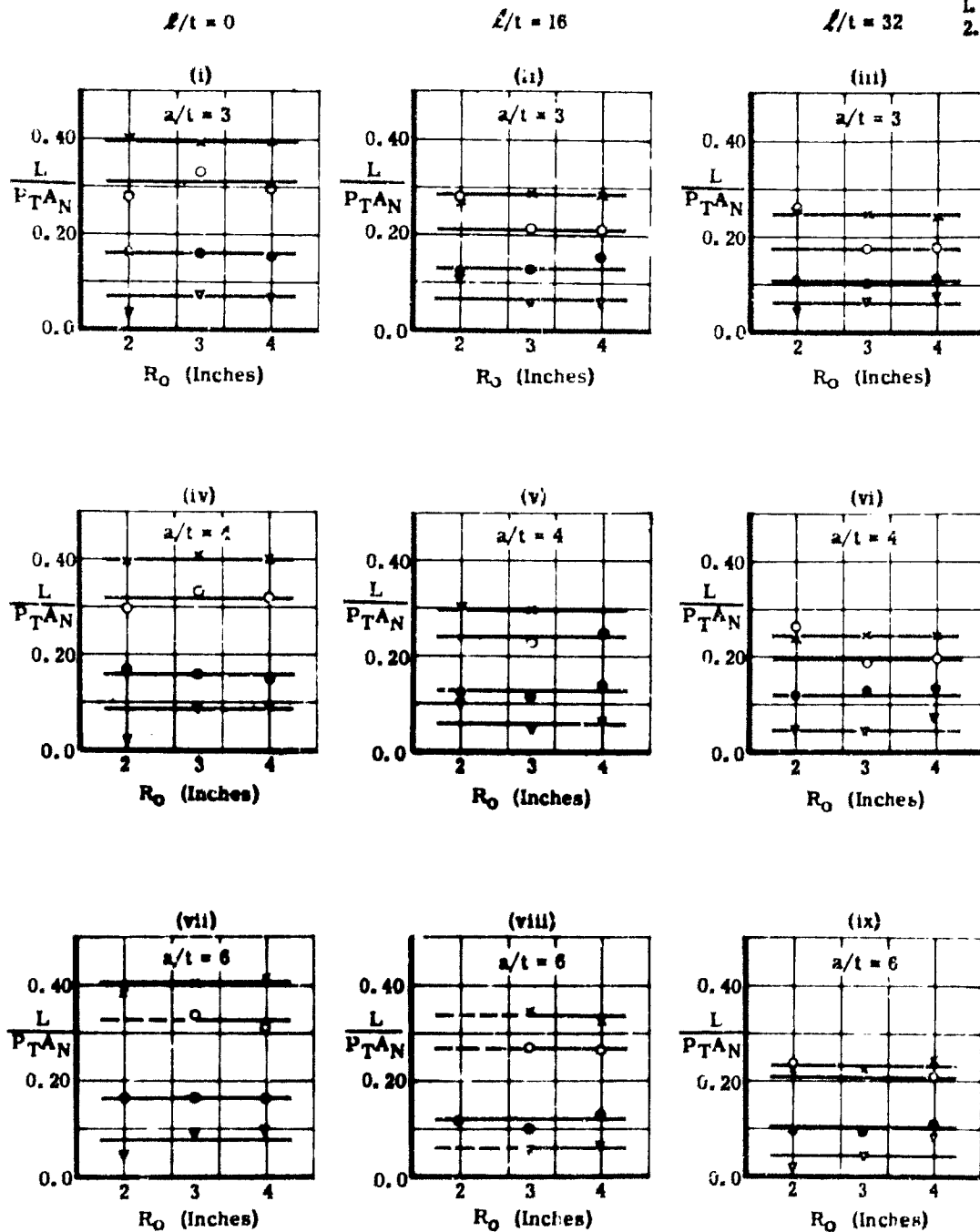


FIGURE 26b. EFFECT OF DEFLECTION SURFACE RADII ON THE NON-DIMENSIONAL LIFT FORCE FOR VARIOUS HORIZONTAL AND VERTICAL GAP SIZES AND NOZZLE PRESSURE RATIOS.

$$11/4 - F1/4 - R_0 \chi$$

$$P.R. \approx 1.1 \nabla$$

$$1.2 \bullet$$

$$1.7 \circ$$

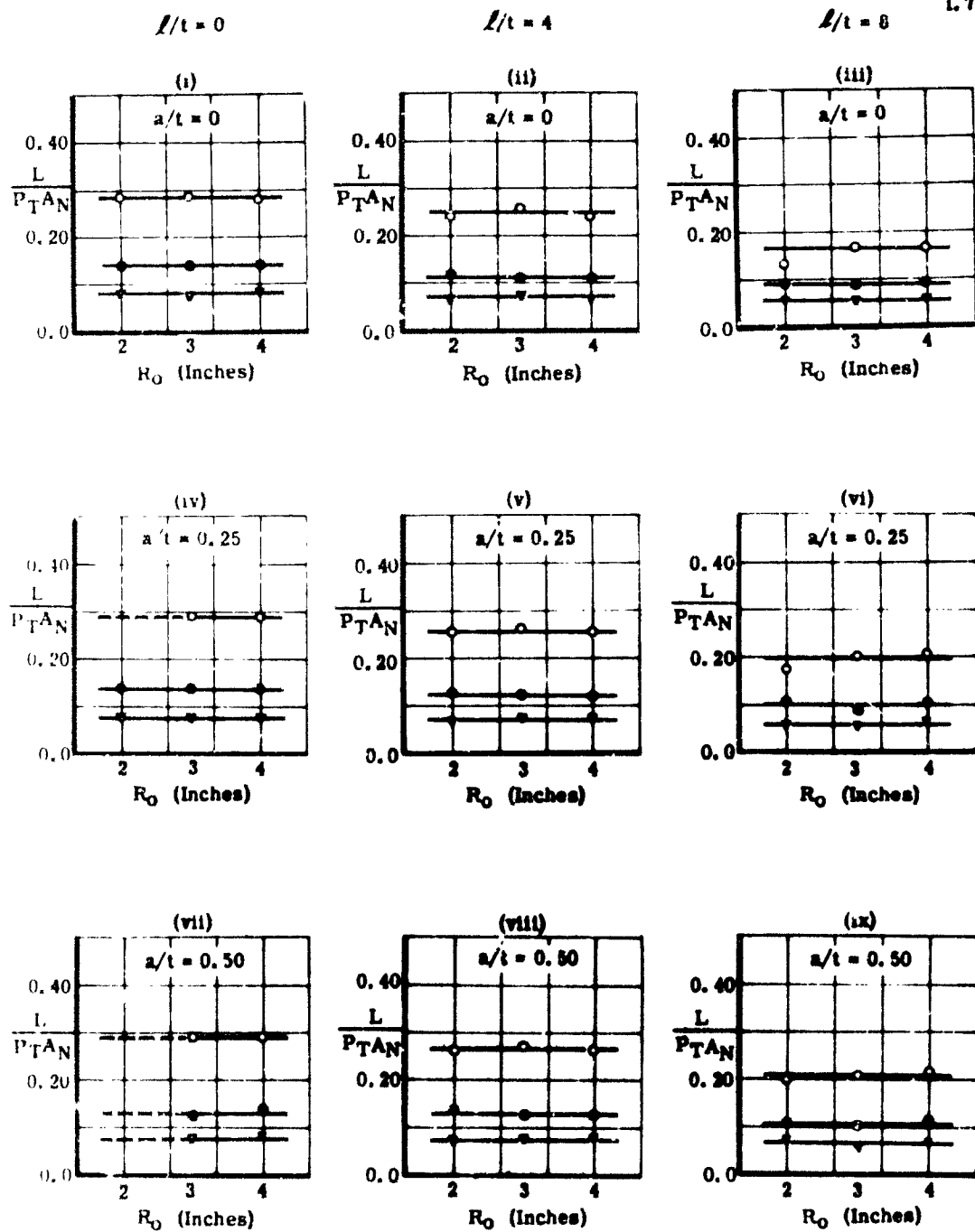


FIGURE 27a. EFFECT OF DEFLECTION SURFACE RADII ON THE NON-DIMENSIONAL LIFT FORCE FOR VARIOUS HORIZONTAL AND VERTICAL GAP SIZES AND NOZZLE PRESSURE RATIOS.

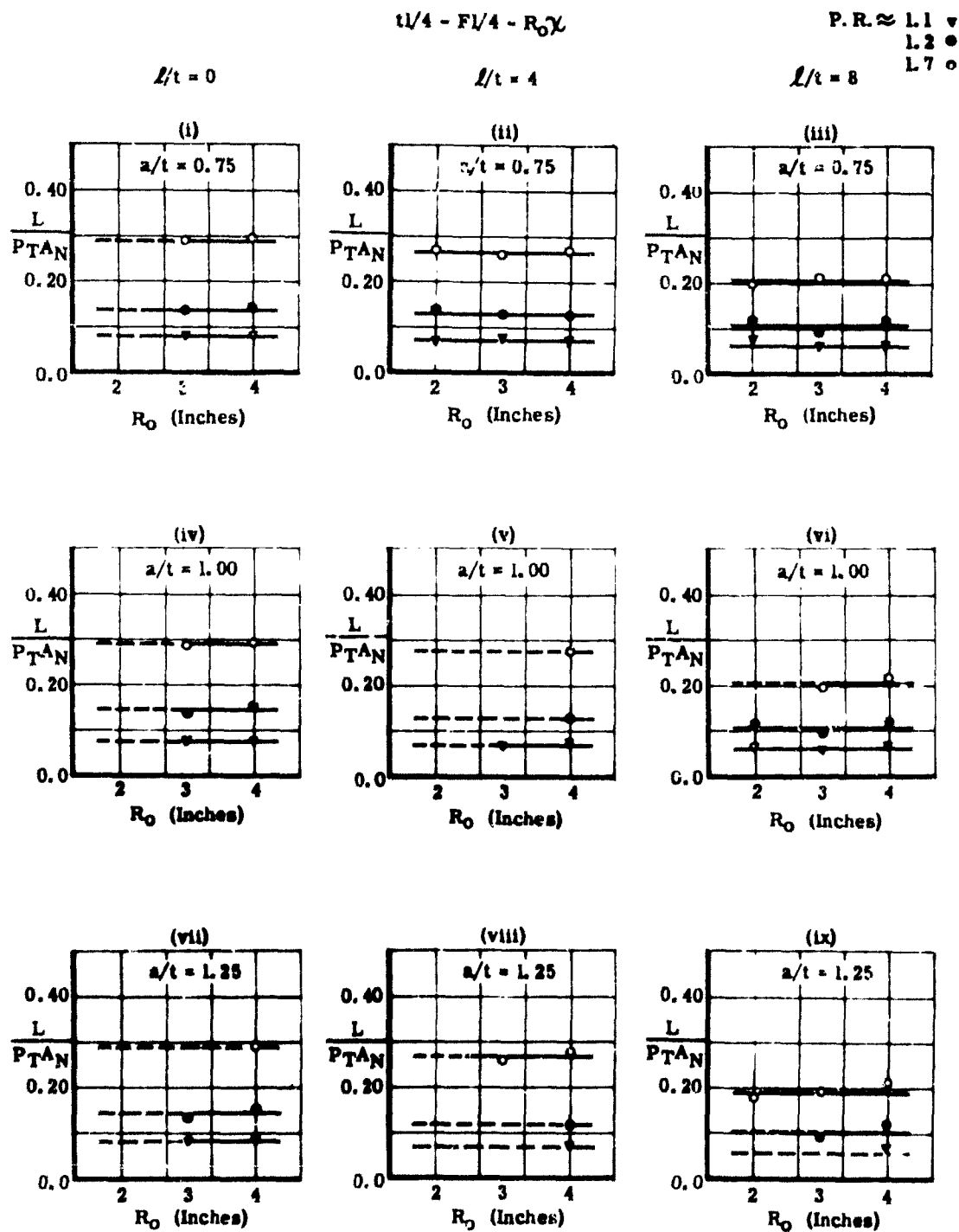
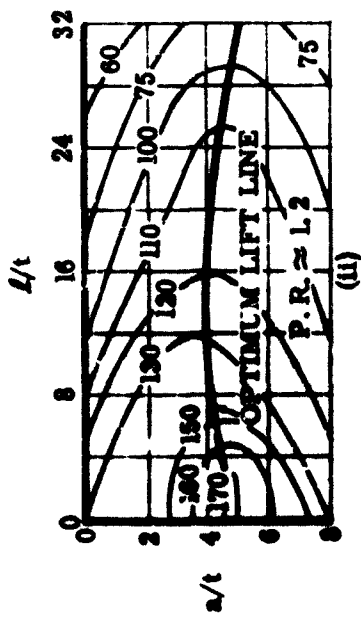
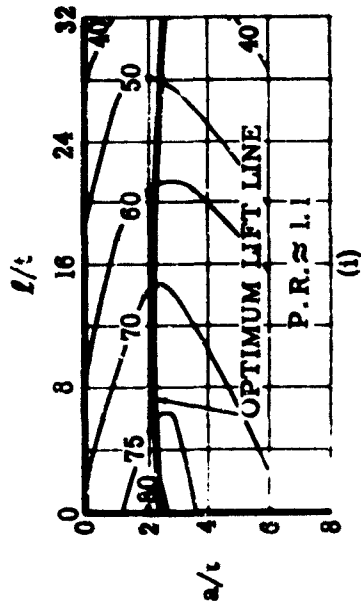


FIGURE 27b. EFFECT OF DEFLECTION SURFACE RADII ON THE NON-DIMENSIONAL LIFT FORCE FOR VARIOUS HORIZONTAL AND VERTICAL GAP SIZES AND NOZZLE PRESSURE RATIOS.

t1/16 - FL/4 - R₀2.0



NON-DIMENSIONAL LIFT = $\frac{L}{P_0 A N}$

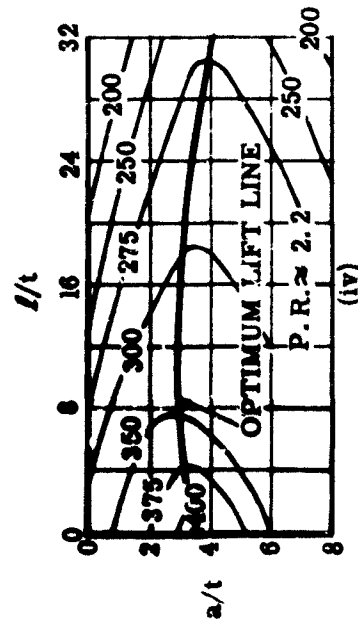
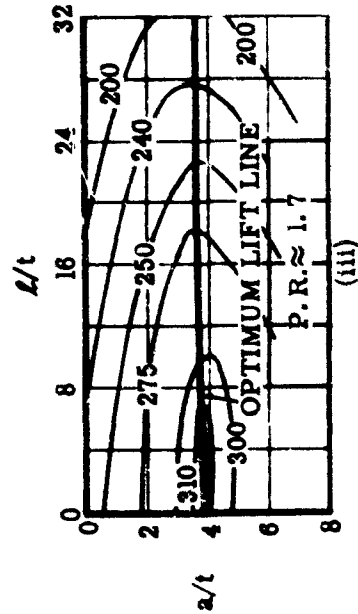
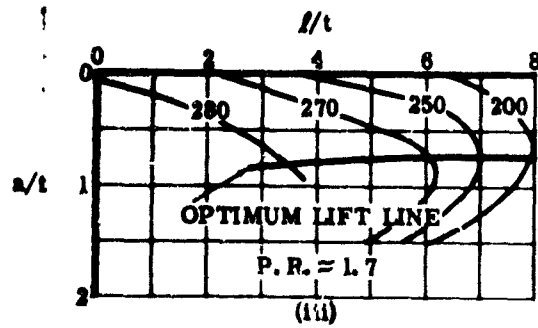
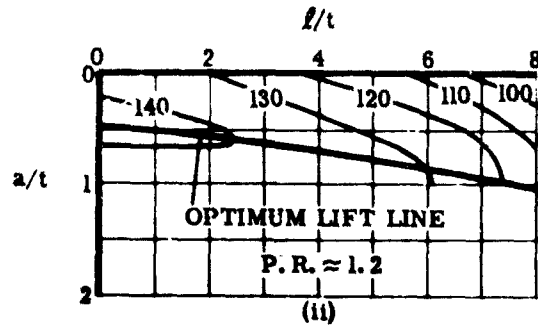
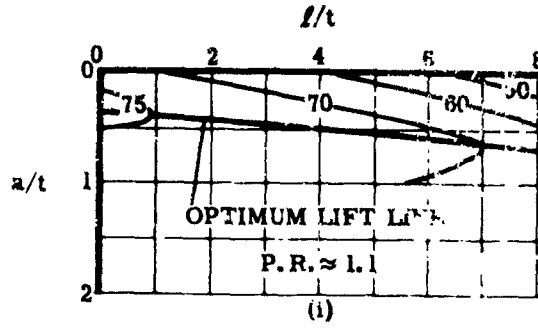


FIGURE 28. CONTOURS OF CONSTANT NON-DIMENSIONAL LIFT FOR VARIOUS HORIZONTAL AND VERTICAL GAP SIZES AND NOZZLE PRESSURE RATIOS.

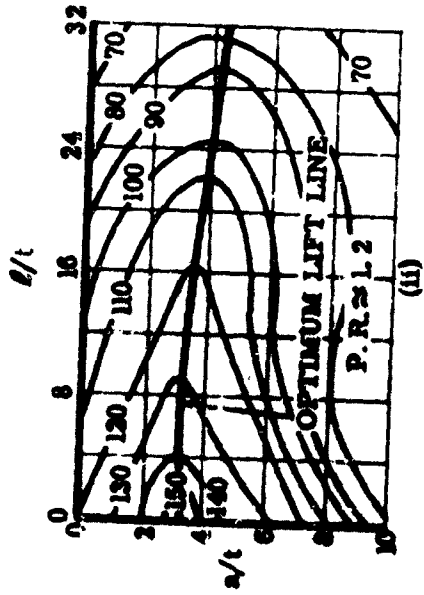
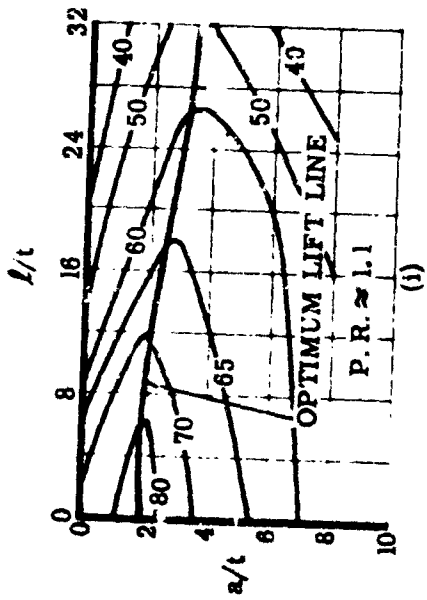
$tl/4 - F/4 - R_0 2.0$



$$\text{NON-DIMENSIONAL LIFT} = \frac{L}{P_T A_N}$$

FIGURE 29. CONTOURS OF CONSTANT NON-DIMENSIONAL LIFT FOR VARIOUS HORIZONTAL AND VERTICAL GAP SIZES AND NOZZLE PRESSURE RATIOS.

t1/16 - F1/4 - R₀3.0



71

NON-DIMENSIONAL LIFT = $\frac{L}{\rho V^2 A N}$

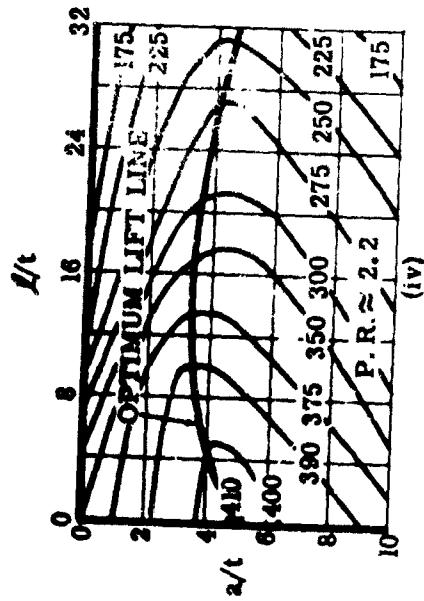
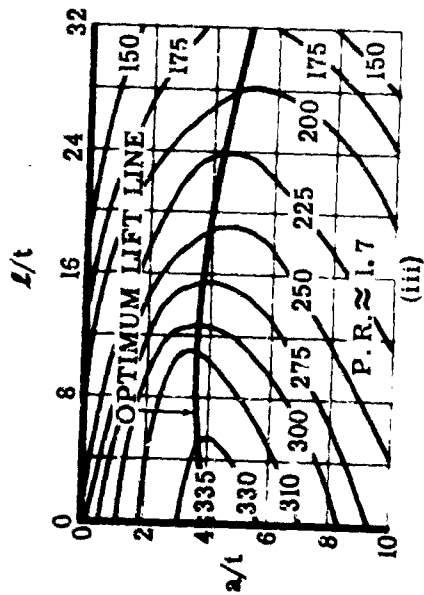
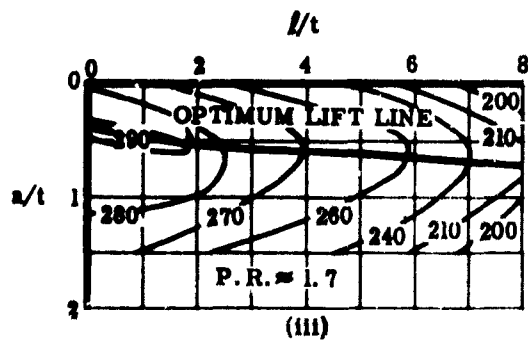
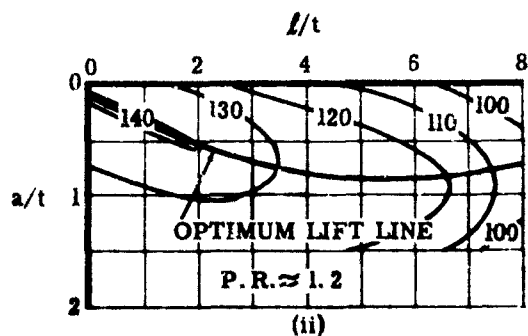
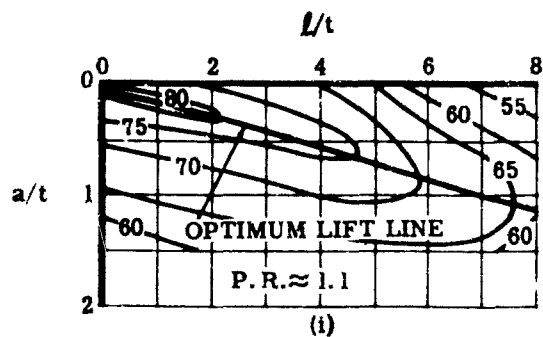


FIGURE 30. CONTOURS OF CONSTANT NON-DIMENSIONAL LIFT FOR VARIOUS HORIZONTAL AND VERTICAL GAP SIZES AND NOZZLE PRESSURE RATIOS.

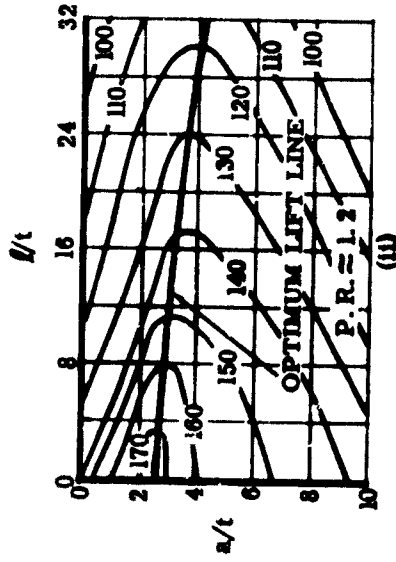
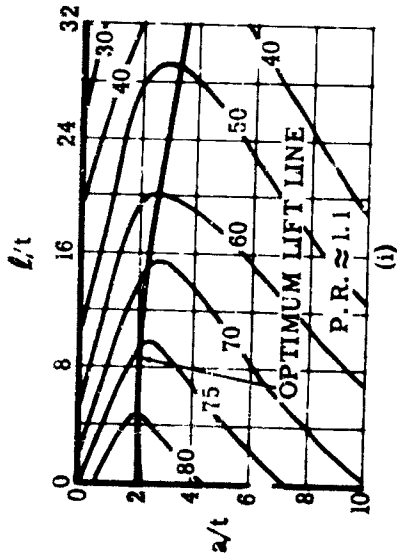
$$t_1/4 - F_1/4 - R_0 3.0$$



$$\text{NON-DIMENSIONAL LIFT} = \frac{L}{P_{TAN}}$$

FIGURE 31. CONTOURS OF CONSTANT NON-DIMENSIONAL LIFT FOR VARIOUS HORIZONTAL AND VERTICAL GAP SIZES AND NOZZLE PRESSURE RATIOS.

$tL/16 - F1/4 - R_0 4.0$



NON-DIMENSIONAL LIFT = $\frac{L}{P_T \Delta N}$

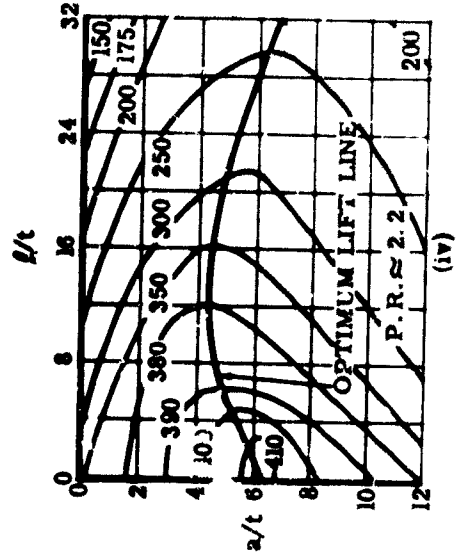
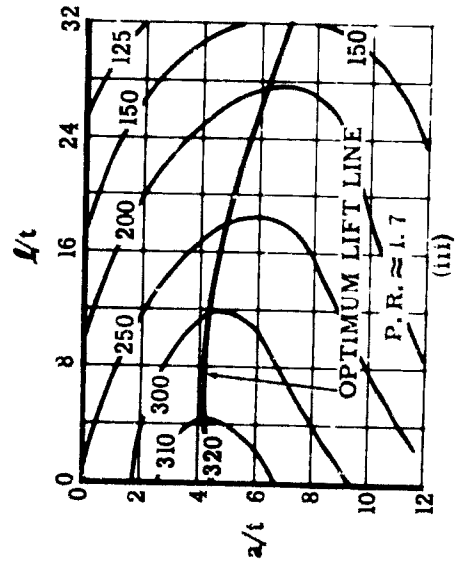
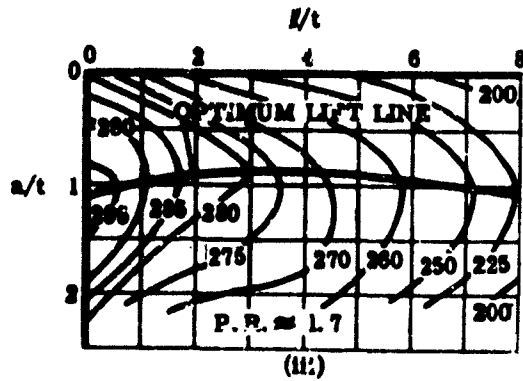
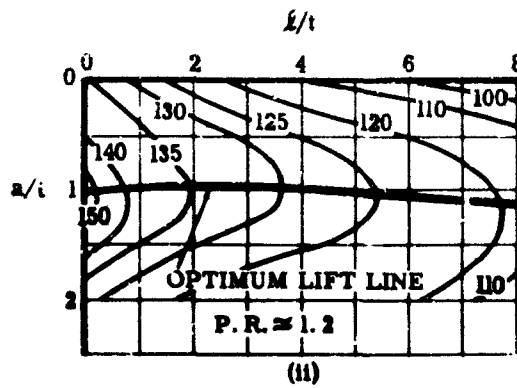
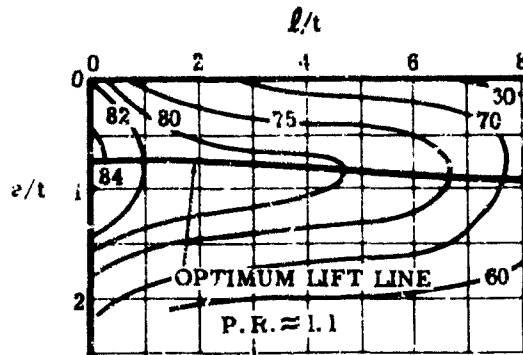


FIGURE 32.

CONTOURS OF CONSTANT NON-DIMENSIONAL LIFT FOR VARIOUS HORIZONTAL AND VERTICAL GAP SIZES AND NOTCH WIDTHS

$$t/4 - F/4 - R_0 = 1.0$$



$$\text{NON-DIMENSIONAL LIFT} = \frac{L}{P_{TAN}}$$

FIGURE 33. CONTOURS OF CONSTANT NON-DIMENSIONAL LIFT FOR VARIOUS HORIZONTAL AND VERTICAL GAP SIZES AND NOZZLE PRESSURE RATIOS.

BIBLIOGRAPHY

1. Bailey, A. B., Use of the Coanda Effect for the Deflection of Jet Sheets Over Smoothly Curved Surfaces, Part I, University of Toronto, Institute of Aerophysics, Technical Note No. 49, August 1961.
2. Bailey, A. B., and Gariand, D. B., "Development of a Compressed Air Facility", Bulletin and Annual Progress Report 1958, University of Toronto, Institute of Aerophysics, October 1959, pp. 42-43.
3. Korbacher, G. K., "The Coanda Effect at Deflection Surfaces Detached from the Jet Nozzle", Canadian Aeronautics and Space Journal, Volume 8, Number 1, January 1962, pp. 1-6.
4. Palouste 500 Series, Technical Data, Issue 1, Publication No. E. 1003, Blackburn-Turbomeca, Blackburn & General Aircraft Ltd., Engine Division, Brough, E. Yorks, England, November 1957.
5. Roderick, W. E. B., Use of the Coanda Effect for the Deflection of Jet Sheets Over Smoothly Curved Surfaces, Part II, University of Toronto, Institute of Aerophysics, Technical Note No. 51, September 1961.

DISTRIBUTION

US Army Materiel Command	3
US Army Mobility Command	2
US Army Aviation Materiel Command	5
Chief of R&D, DA	1
US Army Transportation Research Command	30
USATRECOM Liaison Officer, US Army R&D Group (Europe)	1
US Army Engineer R&D Laboratories	2
Army Research Office-Durham	2
US Army Research Support Group	1
US Army Aviation School	1
US Army General Equipment Test Activity	1
Air Force Systems Command, Wright-Patterson AFB	2
Air Proving Ground Center, Eglin AFB	1
Air University Library, Maxwell AFB	1
Chief of Naval Operations	1
Bureau of Naval Weapons	5
US Naval Postgraduate School	1
US Naval Ordnance Test Station	1
David Taylor Model Basin	1
Marine Corps Liaison Officer, US Army Transportation School	1
Ames Research Center, NASA	1
NASA-LRC, Langley Station	1
Lewis Research Center, NASA	1
NASA Representative, Scientific and Technical Information Facility	2
Research Analysis Corporation	1
National Aviation Facilities Experimental Center	1
US Army Standardization Group, Canada	1
Canadian Liaison Officer, US Army Transportation School	1
British Army Staff, British Embassy, Washington	1
US Army Standardization Group, U. K.	1
Defense Documentation Center	20
US Government Printing Office	1

APPENDIX I

EXACT PRESSURE RATIOS FOR PRESSURE DISTRIBUTIONS,
PRESSURE COEFFICIENTS, AND MEASURED FORCES ACTING
ON THE DEFLECTION SURFACES AS IN FIGURES 5 to 33 INCLUSIVE

t (inch)	R_o (inch)	l ** (inch)	P_T / P_a (1. 1)*	P_T / P_a (1. 2)*	P_T / P_a (1. 7)*	P_T / P_a (2. 2)*
1/16	2	0.0	1.10	1.20	1.71	2.22
		0.5	1.10	1.20	1.71	2.20
		1.0	1.10	1.20	1.71	2.19
		2.0	1.10	1.20	1.71	2.25
1/16	3	0.0	1.10	1.20	1.71	2.21
		0.5	1.10	1.20	1.72	2.24
		1.0	1.10	1.20	1.73	2.20
		2.0	1.10	1.19	1.70	2.22
1/16	4	0.0	1.10	1.21	1.71	2.22
		0.5	1.11	1.21	1.71	2.28
		1.0	1.10	1.21	1.71	2.17
		2.0	1.10	1.20	1.71	2.22
1/4	2	0.0	1.10	1.20	1.71	N
		0.5	1.10	1.20	1.71	
		1.0	1.10	1.20	1.71	O
		2.0	1.10	1.20	1.70	
1/4	3	0.0	1.10	1.20	1.70	
		0.5	1.10	1.21	1.70	D
		1.0	1.10	1.20	1.70	
		2.0	1.10	1.20	1.72	A
1/4	4	0.0	1.10	1.20	1.72	T
		0.5	1.10	1.20	1.69	
		1.0	1.10	1.19	1.72	A
		2.0	1.10	1.20	1.71	

* Nominal pressure ratio.

** Pressure ratios shown in the Figures are average values during a test run; i. e., $a = 0$ to flow detachment from the deflection surface.

COMPARISON OF MEASURED AND INTEGRATED RESULTANT FORCES
ACTING ON A DEFLECTION SURFACE

$tX - F1/4 - R_0 4.0$									
t (inch)	P. R.	a (inch)	ℓ (inch)	$\int \Delta P ds$ (pounds per inch)	F_{Fi} (lb.)	L (lb.)	D (lb.)	$L^2 + D^2$ (lb. 2)	$\sqrt{L^2 + D^2} = F_{r m}$ (lb.)
1/16	1.2	0.000	0.5	0.304	2.4	2.3	2.1	9.4	3.1
		0.625	0.5	0.490	3.9	2.3	0.9	5.0	2.4
		0.000	2.0	0.206	1.6	1.9	2.4	9.3	3.1
		0.625	2.0	0.314	2.5	1.5	0.3	2.2	1.5
1/16	1.7	0.000	0.5	1.020	8.2	5.3	6.4	68.6	8.3
		0.625	0.5	1.070	8.6	6.7	2.7	51.5	7.2
		0.000	2.0	0.894	7.2	3.6	7.0	61.8	7.9
		0.625	2.0	0.629	5.0	4.8	0.9	23.3	4.8
1/4	1.2	0.000	0.5	1.520	12.2	8.8	8.6	150.7	12.3
		0.4375	0.5	1.490	11.9	8.7	4.7	97.3	9.9
		0.000	2.0	1.325	10.6	6.7	7.2	95.6	9.8
		0.500	2.0	1.080	8.6	7.2	3.2	61.6	7.9
1/4	1.7	0.000	0.5	4.600	36.8	26.0	26.9	1398.0	37.4
		0.4375	0.5	4.075	32.6	27.4	15.6	993.0	31.5
		0.000	2.0	3.540	28.2	17.1	23.8	857.0	29.3
		0.4375	2.0	3.740	29.9	20.6	9.9	523.0	22.9

APPENDIX II

Unclassified

Security Classification

DOCUMENT CONTROL DATA - R&D		
<i>(Security classification of title, body of abstract and indexing annotation must be entered when the overall report is classified)</i>		
1 ORIGINATING ACTIVITY (Corporate author) Institute for Aerospace Studies University of Toronto Toronto, Canada		2a REPORT SECURITY CLASSIFICATION Unclassified
		2b GROUP N/A
3 REPORT TITLE THE COANDA EFFECT AT DEFLECTION SURFACES WIDELY SEPARATED FROM THE JET NOZZLE		
4 DESCRIPTIVE NOTES (Type of report and inclusive dates) None		
5 AUTHOR(S) (Last name, first name, initial) Benner, S. D.		
6 REPORT DATE December 1964	7a TOTAL NO OF PAGES 78	7b NO OF REFS 5
8a CONTRACT OR GRANT NO	8c ORIGINATOR'S REPORT NUMBER(S) USATRECOM 64-70	
8b PROJECT NO Task ID121401A14203	8d OTHER REPORT NO(S) (Any other numbers that may be assigned) N/A UFIXS Tech. Note No. 78	
10 AVAILABILITY LIMITATION NOTICES Qualified requesters may obtain copies of this report from DDC. This report has been furnished to the Department of Commerce for sale to the public.		
11 SUPPLEMENTARY NOTES None	12 SPONSORING MILITARY ACTIVITY U.S. Army Transportation Research Command Fort Eustis, Virginia	
13 ABSTRACT The flow phenomenon in both liquids and gases of the adherence of a jet or jet sheet to a solid surface has been named the Coanda Effect. This report discusses an experimental investigation, which has again shown that the Coanda Effect is not limited to attached deflection surfaces or to inclined single or multiple flat-plate surfaces. The horizontally ejected subsonic and overchoked jet sheets successfully bridged horizontal and vertical gaps of 32 and 10 times the nominal jet sheet thickness ($t = 1/16$ inch) respectively; for $t = 1/4$ inch, the corresponding ratios were eight and two. The vertical gap was increased until the flow detached from the deflection surface. Vertical and horizontal forces acting on three different deflection surfaces were measured with a strain gauge balance. The configurations were tested at nominal pressure ratios of 1.1, 1.2, 1.7, and 2.2, and the surface pressures were recorded.		

DD FORM 1473

Unclassified

Security Classification

14 KEY WORDS	LINK A		LINK B		LINK C	
	ROLE	WT	ROLE	WT	ROLE	WT

INSTRUCTIONS

1. ORIGINATING ACTIVITY: Enter the name and address of the contractor, subcontractor, grantee, Department of Defense activity or other organization (corporate author) issuing the report.

2a. REPORT SECURITY CLASSIFICATION: Enter the overall security classification of the report. Indicate whether "Restricted Data" is included. Marking is to be in accordance with appropriate security regulations.

2b. GROUP: Automatic downgrading is specified in DoD Directive 5200.10 and Armed Forces Industrial Manual. Enter the group number. Also, when applicable, show that optional markings have been used for Group 3 and Group 4 as authorized.

3. REPORT TITLE: Enter the complete report title in all capital letters. Titles in all cases should be unclassified. If a meaningful title cannot be selected without classification, show title classification in all capitals in parentheses immediately following the title.

4. DESCRIPTIVE NOTES: If appropriate, enter the type of report, e.g., interim, progress, summary, annual, or final. Give the inclusive dates when a specific reporting period is covered.

5. AUTHOR(S): Enter the name(s) of author(s) as shown on or in the report. Enter last name, first name, middle initial. If military, show rank and branch of service. The name of the principal author is an absolute minimum requirement.

6. REPORT DATE: Enter the date of the report as day, month, year, or month, year. If more than one date appears on the report, use date of publication.

7a. TOTAL NUMBER OF PAGES: The total page count should follow normal pagination procedures, i.e., enter the number of pages containing information.

7b. NUMBER OF REFERENCES: Enter the total number of references cited in the report.

8a. CONTRACT OR GRANT NUMBER: If appropriate, enter the applicable number of the contract or grant under which the report was written.

8b, c, & 8d. PROJECT NUMBER: Enter the appropriate military department identification, such as project number, subproject number, system numbers, task number, etc.

9a. ORIGINATOR'S REPORT NUMBER(S): Enter the official report number by which the document will be identified and controlled by the originating activity. This number must be unique to this report.

9b. OTHER REPORT NUMBER(S): If the report has been assigned any other report numbers (either by the originator or by the sponsor), also enter this number(s).

10. A. AVAILABILITY LIMITATION NOTICES: Enter any limitations on further dissemination of the report, other than those imposed by security classification, using standard statements such as:

- (1) "Qualified requesters may obtain copies of this report from DDC."
- (2) "Foreign announcement and dissemination of this report by DDC is not authorized."
- (3) "U. S. Government agencies may obtain copies of this report directly from DDC. Other qualified DDC users shall request through _____."
- (4) "U. S. military agencies may obtain copies of this report directly from DDC. Other qualified users shall request through _____."
- (5) "All distribution of this report is controlled. Qualified DDC users shall request through _____."

If the report has been furnished to the Office of Technical Services, Department of Commerce, for sale to the public, indicate this fact and enter the price, if known.

11. SUPPLEMENTARY NOTES: Use for additional explanatory notes.

12. SPONSORING MILITARY ACTIVITY: Enter the name of the departmental project office or laboratory sponsoring (paying for) the research and development. Include address.

13. ABSTRACT: Enter an abstract giving a brief and factual summary of the document indicative of the report, even though it may also appear elsewhere in the body of the technical report. If additional space is required, a continuation sheet shall be attached.

It is highly desirable that the abstract of classified reports be unclassified. Each paragraph of the abstract shall end with an indication of the military security classification of the information in the paragraph, represented as (TS), (S), (C), or (U).

There is no limitation on the length of the abstract. However, the suggested length is from 150 to 225 words.

14. KEY WORDS: Key words are technically meaningful terms or short phrases that characterize a report and may be used as index entries for cataloging the report. Key words must be selected so that no security classification is required. Identifiers, such as equipment model designation, trade name, military project code name, geographic location, may be used as key words but will be followed by an indication of technical context. The assignment of links, rules, and weights is optional.